臺灣地區110年地震前兆監測資料彙整及分析

子計畫一

地震前兆監測-三分量地磁資料分析

顏宏元[1] 陳俊榕[2] 羅祐宗[1]

[1]中央大學地球科學系

[2]工業技術研究院綠能研究所

摘要

九二一大地震後，經檢視全臺磁力連續觀測資料發現，位於車籠埔斷層兩端的磁力站—鯉魚潭站及灣丘站，都觀測到磁力異常訊號，這些異常訊號與地震的發生有時間上的巧合。一般認為，當岩層受到應力作用而產生裂隙，地層內所含的帶磁礦物會散發在空間中，造成地磁場的變化。本計畫分析新建置的全臺三分量地磁連續觀測網資料，以了解地磁場強度改變與地震活動的關聯性。

關鍵詞：地磁、地震活動

Abstract

After 921Chi-Chi earthquake, numerous magnetic anomaly signals were observed in the northern and southern parts of the Chelungpu fault, and it is coincided with the time of Chi-Chi earthquake occurred. It is generally believed that the magnetic minerals contained in the formation will be dispersed in space, causing changes in the geomagnetic field. This project analyzes the 3-components geomagnetic data of the re-establishment observation network to understand the associated with seismicity and changed in tectonic stress.

Key Words: Geomagnetic, seismicity

壹、前言及研究目的

在 1999 年九二一集集大地震後，我們發現距車籠埔斷層北端 8 公里的鯉魚潭磁力站，地磁總強度在地震發生前一個多月就紀錄到擾動的訊號，振幅達到 180 nT，這些擾動訊號的振幅逐漸變小且在同年 10 月 22 日嘉義大地震發生的同時，這些擾動訊號就沒有被偵測到，這些巧合讓我們認為地磁場強度異常應該和大地震的發生有關；另外，位於臺南的灣丘地磁觀測站，似乎也紀錄到一些擾動的訊號，研判與嘉義大地震有關(Yen et al., 2004)。

臺灣地磁連續觀測網，大致上可以分為三個時期：

（1）1988~2001 年由中央研究院地球科學研究所建置的臺灣地區地磁連續觀測網，除了崙坪(LP)參考站位在地震活動不頻繁的地區外，其他分別為鯉魚潭(LY)、灣丘(TW)、恆春(HC)、臺東(TT)、玉里(YL)、花蓮(HL)和內城(NC)等 7 個地磁觀測站，均在地震活動頻繁或活動構造地區。站內安裝 G-856 可攜式質子進動磁力儀(Proton-Procession magnetometer, G856)，地磁資料存於儀器的硬碟中，每兩個月由技術人員前往各站下載資料。

（2）2002~2006 年中央大學除了將原有 8 個地磁觀測站的儀器汰換外，還增加了 3 個新的觀測站，包含桃園爺亨(YH)觀測站，中部山區的南投雙龍(SL)觀測站，以及南部山區的屏東瑪家(PT)觀測站，選定金門(KM)的磁力站為本觀測網的參考基準站。所使用的儀器為加拿大 GEM 公司所生產之 GSM90F 型磁力儀。該儀器的解析度為 0.1nT，精確度為 0.2nT，量測範圍 20000 ~ 120000nT，取樣率為 1Hz，最小達每秒 1 次，記錄資料傳送至中央大學的記錄中心。

（3）2007 年後，中央大學將所建置的「臺灣地區地磁場連續觀測網」移轉給中央氣象局。2014 年起為了加強對池上斷層的監測，於池上玉蟾園增設了池上(CS)站。2016 年由於舊有的屏東瑪家站屢遭破壞，於是將瑪家地磁觀測站遷移至馬仕部落而更名為馬仕(MS)站。

由於儀器老舊，地磁連續觀測網陸續有多個測站出現了資料中斷的現象，或觀測站附近環境改變而影響資料品質。中央氣象局從 2018 年來開始，陸續進行地磁觀測儀器更新，將原量測全磁場的儀器汰換為三分量磁力儀(圖一)，此儀器由日本 TIERRA TECNICA 公司所製造，取樣率為 1Hz，包含接收器、前置放大器、主機和 GPS，以網路將所觀測的資料即時傳輸到紀錄中心。花蓮(HL)和金門(KM)分別尋找新設站地點。原花蓮（HL）站周圍因鐵路電氣化且增設高壓電塔，嚴重影響觀測站的資料品質，加上原放置感應器附近的坡度陡峭而不宜建置三分量地磁觀測儀器，花蓮新的三分量磁力觀測站位在新城(XC)鄉大漢技術學術校園一隅。原臺東(TT)和雙龍(SL)兩個站，因為地形較為崎嶇而無法安裝三分量磁力儀，所以分別尋找新的設站地點，臺東地區新的三分量磁力觀測站位在臺東大學知本校區(TT)地球科學園區一隅；原雙龍（SL）站因風災影響造成道路中斷，傳輸訊號又極為不穩定，新的地磁觀測站則設置在中央氣象局日月潭測候站(SM)一隅。另新增了馬祖(MT)及蘭嶼兩個地磁觀測站。地震活動相對低的馬祖地區，尋覓一適當地點做為新建三分量地磁觀測站，可與金門站一起當作中央氣象局「臺灣地區三分量地磁觀測網」的基準參考站。最新測站位置分布如圖二所示。

今年計畫主要為檢視新的三分量地磁連續觀測網之地磁觀測網資料品質，並

了解地磁場強度改變與幾個規模較顯著地震事件的關聯性。

貳、研究方法

地球磁場的變化（微脈動）是和地震活動、洋流及電離層潮汐等有關，臺灣是研究地磁場微脈動的最佳地區。 Zeng et al. (2002) 利用單個地磁觀測站的日變化關係進行分析，發現有一些地磁異常似乎與地震發生有關聯，但不能很明確對即將發生地震的時間、地點、規模，做較為明確的估計。理論上，磁力的日變化主要受到太陽風與地磁層的影響，在小區域中變化量理論上應該相似，因此各測站與參考站的比值應該大致上接近於 1。換言之，此法扣除各個觀測站日變化的效應，如果比值有偏移的現象，則可能是因地下應力累積所造成地磁站附近的地磁強度的改變。Liu et al. (2006) 改進 Zeng et al. (2002) 的分析方法，以兩個地磁觀測站進行比例數的計算，並加入地震發生與觀測站之間距離的考量，期望在地震發生與地磁關連的時間、規模、地點，能有較佳的預估。該方法就是計算各磁力觀測站每日磁力值最大與最小值進行相減，得到各站之日變化振幅，並將各磁力站與參考站之日變化振幅相除。以 1999 年集集地震為例，選取地震前後 15 天的資料作圖，發現 LY 與 TW (靠近車籠埔斷層南北端的兩個測站) 比值的分佈有明顯的偏離背景分佈(圖三)。Liu et al. (2006) 認為這個偏移情形來自於孕震區的導電性改變或產生電流進而影響磁場。

日本在研究地震前兆的發生大多使用超低頻法 (Ultra-Low-Frequency, ULF)，此方法是將在時間域所得到的三分量磁力資料，經過 FFT 轉換成頻率域，再選擇頻率域中的 0.001~0.003Hz 為研究範圍。研究發現地震對地磁的影響在 Z 方向最為明顯 (Hattori et al., 2004)。由於地震對地磁的影響在 Z 方向最為明顯，而 H 向分量大多維持不便，所以將三分量的地磁觀測資料之 Z 方向分量除以 H 方向分量，根據比值改變趨勢探討與發生地震的關聯性。中央氣象局自 2018 年開始，將臺灣地區地磁觀測站原量測全磁場的儀器汰換為三分量磁力儀。有了地磁場三分量的資料，本計畫嘗試利用超低頻法 (Ultra-Low-Frequency, ULF)，就今年幾個地震事件進行分析。

參、具體成果

中央氣象局「臺灣地區地磁連續觀測網」建置完成後，各測站所觀測到地磁三分量的資料(圖四) 都能正常且穩定的傳送回紀錄中心。僅有日月潭測站於 7 月中旬有資料傳輸中斷的情形，雖然在 9 月中有恢復資料資料傳送，但到 9 月底因雷擊導致無法觀測。在地震中心同仁辛勤維護，所記錄到的地磁資料品質相當地不錯，並將所回傳資料建置臺灣地區地磁資料庫，提供使用者正確且完善的地磁資料。

2021 年有多個較顯著規模的地震發生，計畫考量到分析方法及三分量地磁紀錄的時段，選擇了：

（1）4 月 18 日發生在花蓮壽豐的地震（M=6.2），震源深度為 13.9 公里，在壽豐鄉水璉村記錄到最大的加速度為 723.59 gal，餘震持續將近一個月。

（2）7 月上半個月發生在花蓮壽豐和吉安兩個地區，超過 70 個地震的群震，最大規模為 5.4。

（3）8 月 6 日晚上在花蓮富里發生規模 5.4 的地震，震源深度只有 7.2 公里。之後又連續發生 8 起餘震，造成 9 戶國宅受損。

（4）9 月 13 日傍晚在南投縣仁愛鄉發生規模 5.6 的地震，深度達 47 公里，蠻特別的地震事件。

本計畫利用三分量地磁觀測站所記錄到的資料，分別採用日變化比值法 (Liu et al. 2006) 和超低頻法 (Hattori et al., 2004) 兩種方法，探討可能的前兆異常。

A. 日變化比值法

(a) 0418 花蓮壽豐的地震

選擇馬祖(MT)做為參考站，以 2021 年 1-10 月的資料當作背景值，以 20 天為一窗格計算，每次移動窗格 1 天。選擇東部新城(XC)及池上(CS)兩個測站；西部選了日月潭(SM)和鯉魚潭(LY)兩個測站相互比較。新城測站與馬祖的日變化比值於地震前 20 天左右，開始出現比值超過一個標準差以上，此比值偏離情形在地震後 30 天仍有出現超過一個標準差的情形(圖五)，比值偏離的現象於地震前後都持續不斷的發生，可能與這次地震持續近 1 個月的餘震有關或是其他因素影響所致，則需更進一步的研究來釐清。另比值偏離現象於日月潭測站中卻沒有出現，且其與馬祖站日變化比值的中位數接近於 1 (圖五)。圖六分別是東部的池上站及西部的鯉魚潭站，這兩個地磁站離 0418 壽豐地震較遠，池上站日變化比值之振幅有些微的增大情形，但超過 1 個標準差的情況不多，應該與 0418 壽豐地震無關；位於西部的鯉魚潭站，與馬祖站日變化比值的中位數接近於 1，標準偏差比較小，代表該站的資料品質佳，雖然在地震前後有比值超過 1 個標準偏差的情形，但比值都在 0.7 以內。

(b) 7 月花蓮壽豐和吉安地區的群震

7 月初在海岸山脈北段（即壽豐和吉安兩個地區）接連發生多起有感地震。7 月 7 日發生規模 5.4 的地震，1 天內共有 13 個餘震發生；7 月 14 日在花蓮吉安發生規模 5.2 的地震，接著 1 天內發生 38 起餘震。同樣選擇馬祖(MT)做為參考站，以 2021 年 1-10 月的資料當作背景值，以 20 天為一窗格計算，每次移動窗格 1 天，分析 7 月 14 日前後 60 天的比值變化。選擇東部新城(XC)及池上(CS)兩個測站；西部選了日月潭(SM)和鯉魚潭(LY)兩個測站相互比較。新城測站與馬祖的日變化比值的中位數為 0.7，於地震前 30 天左右，開始出現比值超過一個標準差以上，但此比值偏離情形在地震後就幾乎沒有出現 (圖七)，反而在離發生群震較遠的池上站，有明顯比值超過一個標準差的偏離情形(圖七)，是否為 8 月 6 日富里地震的前兆訊號，值得加以探討。圖八是分別位於南投的日月潭站及苗栗的鯉魚潭站。雖然日月潭站的資料並不完整，但與馬祖站日變化比值的中位數接近於 1，且比值大都在一個標準偏差內。鯉魚潭站與馬祖站日變化比值的中位數接近於 1，雖然在地震前後仍有比值超過 1 個標準偏差的情形，但比值都在 0.7 以內。

(c) 0806 富里的地震

分析方式和參考站均和前兩個地震事件相同。選擇東部池上(CS)及新城(XC)兩個測站；西部選了日月潭(SM)和鯉魚潭(LY)兩個測站相互比較。近震央的池上地磁站，在富里地震前 60 天及地震後 30 天，都有比值超過一個標準差以上的情形(圖九)；新城測站與馬祖的日變化比值於地震前靠近 60 天開始出現比值超過一個標準差以上，但在地震前 5 天及地震發生後，比值偏離情形就沒有出現(圖九)。圖十則是位於臺灣西部的鯉魚潭(LY)和日月潭(SM)兩個測站，鯉魚潭站的日變化比值的分布與前兩個地震事件相同；雖然日月潭站的資料並不完整，但與馬祖站日變化比值的中位數接近於 1，且比值大都在一個標準偏差內。

(d) 0913 南投的地震

因位於最近震央的日月潭站，於 7 月中旬有資料傳輸中斷的情形，雖然在 9 月中有恢復資料資料傳送，但到 9 月底無法正常傳輸資料。在西部測站除了日月潭觀測站外，也選了鯉魚潭(LY)及爺亨(YH) 兩個地磁站，東部則選擇較近這個地震的新城(XC)測站來進行分析，整個分析仍然以馬祖站為參考站。因觀測資料中斷而造成計算背景的資料長度不足，但仍企圖想看看此特殊的地震事件是否有前兆現象，擷取 9 月 13 日（地震發生當天）前 60 天及後 30 天的資料進行分析。新城測站與馬祖的日變化比值的中位數為 0.7（圖十一），與前三個地震事件比較，新城站偏離一個標準差的情形變少，反而 9 月 13 日前 30 天開始，馬祖參考站的日變化量大於新城站，顯然此次地震事件並沒有造成新城站的地磁異常的改變。這段期間新城站日變化比值大於 1 個標準偏差的情況相對少出現的現象，或許是因為花蓮地區地震發生的個數減少。此次地震事件震央附近的日月潭站，可惜該測站的記錄中斷而無法分析是否有地震磁異常前兆行為。圖十二是分別位於苗栗的鯉魚潭站及桃園的爺亨站。這兩個站與馬祖站日變化比值的中位數接近於 1，且比值大都在一個標準偏差內。不過有發現馬祖參考站的日變化量，於這段時間內都有大於鯉魚潭站及爺亨站的情形。這兩個站為「臺灣地區地磁場連續觀測網」的觀測站，在全磁場觀測時的資料品質都不錯，有必要再確定馬祖站的資料是否受到干擾而造成較大的日變化？

B. 超低頻法

本計畫選擇 3 個地磁觀測站，分別是新城(XC)、池上(CS)及日月潭(SM)站，並以馬祖(MT)為參考對比站。將在時間域所得到的三分量磁力資料，經過 FFT 轉換成頻率域中的 0.01Hz，再將三分量的地磁觀測資料之 Z 方向分量除以 H 方向分量，即求得 0.01Hz 時之垂直與水平改變量的比值，看看是否有極化指標出現明顯改變 (Hattori et al., 2004)。圖十三(A)至(D)依序是馬祖站、新城站、池上站及日月潭站所記錄到三分量地磁資料，選取 0.01Hz 之垂直與水平改變量的比值，圖中黑色線為每日的比值；藍色線則為一週比值的平均值（週均值）。

馬祖站垂直與水平改變量的比值，1-10 月週均值在 0.8 至 1.0 之間變化（圖十三（A）），比值改變的情況平穩，沒有特別突跳的現象。圖十三（B）是新城站 1-9 月垂直與水平改變量的比值，該站週均值是在 0.7 至 0.9 之間跳動，於 4 月底的週均值增大至 1.2，2 週後又回復到 0.8，此一突跳的現象在其他三個站並沒有發現，可以很確定不是磁暴作用所造成改變，至於造成比值為 0.4 變化的原因，是測站受

干擾或是與 7 月花蓮壽豐和吉安地區的群震有關，會再配合其他觀測資料來探討。圖十三（C）是池上站 1-9 月垂直與水平改變量的比值，該站週均值是在 1.2 至 0.8 之間變動。該站週均值從今年初開始緩慢變小，到 3 月底的週均值降到 0.85。從 4 月份開始，期間有 0418 花蓮壽豐的地震、7 月花蓮壽豐和吉安地區的群震、0806 富里的地震及 0913 南投的地震發生，週均值都在 0.8 至 1.1 之間上下震盪變化，即使靠近池上觀測站所發生的 0806 富里地震，似乎沒有看到比值異常的情形。日月潭站是這個方法在西部的觀測站，該站在 7 月中旬的紀錄有中斷的情形，到了 9 月初訊號傳輸恢復正常，可惜在 0913 南投地震後的訊號傳輸又再度中斷（圖十三（D））。日月潭站週均值是在 1.0 至 0.7 之間改變，相較新城和池上兩個站的變化情況，日月潭站相對的平緩，與馬祖參考站的變化情形相似。雖然在圖十三（D）中可以看到，於訊號中斷前週均值有明顯的上升，在 9 月初訊號傳輸恢復正常時的週均值下降，但因為資料有中斷的情形，週均值的上升和下降，實在無法判斷是否與 0913 南投地震有關？

肆、結果與討論

中央氣象局「臺灣地區三分量地磁連續觀測網」已經建置完成，各測站所觀測到的資料都能正常的傳輸到地震測報中心，將所回傳資料建置臺灣地區三分量地磁資料庫，提供使用者正確且完善的地磁資料。

今年度的計畫是利用三分量地磁資料，採用日變化比值法及超低頻法兩種方法，就今年 4 個較顯著規模的地震進行分析研究，探討可能的前兆異常。日變化比值法初步的結果：

1. 位於東部的新城(XC)站和池上(CS)站與馬祖的日變化比值的中位數為 0.7 和 0.8，標準偏差相對西部測站小；位於西半部的日月潭站、鯉魚潭(LY)站及爺亨(YH)站，與馬祖的日變化比值的中位數接近 1，標準偏差依測站位置而有所不同，但比值大於 1 個標準差的現象相對東部的觀測站比較少。
2. 0418 花蓮壽豐的地震、7 月花蓮壽豐和吉安地區的群震及 0806 富里的地震，位於西半部的日月潭站、鯉魚潭(LY)站及爺亨(YH)站，與馬祖的日變化比值偏離 1 個標準差的現象較少；但在新城和池上兩個觀測站，於地震前、後都有大於 1 個標準差的情形，沒有一致的比值偏離方向且分布較為離散。
3. 位於東西部的地磁站之日變化比值有明顯的差異，這些差異是否與地震活動有關，或是觀測站訊號受到干擾，將進一步的釐清。

利用三分量地磁資料，採用超低頻法來探討可能的地震前兆異常。本計畫選擇 3 個地磁觀測站，分別是新城(XC)、池上(CS)及日月潭(SM)站，並以馬祖(MT)為參考對比站。以今年 1-10 月份的資料來看，新城和池上兩個站的週均值高低變化較日月潭站和馬祖站明顯，表示東、西部的地磁站在低頻訊號也有著差異，這種差異的原因也是值得再深入的探討。

伍、誌謝

本計畫由中央氣象局提供經費，地球物理課同仁協助測站會勘、維護及資料彙整，在此深表感謝。

參考文獻

Hattori, K., 2004. ULF Geomagnetic Changes Associated with Large Earthquakes. TAO, Vol. 15, No. 3, 329-360.

Liu, J. Y., C. H. Chen, Y. I. Chen, H. Y. Yen, K. Hattori, K. Yumoto (2006). Seismo-geomagnetic anomalies and M>= 5.0 earthquakes observed in Taiwan during 1988–2001. Physics and Chemistry of the Earth, 31, 215–222.

Yen, H. Y., C. H. Chen, Y. H. Yeh, J. Y. Liu, C. J. Lin and Y. B. Tsai (2004). Geomagnetic fluctuations during the Chi-Chi, Taiwan earthquake, *Earth, Planets and Space*, 56, 39-45.

Zeng, X., J.Y. Liu, Y. Lin and C. Xu (2002). The evolution of dynamic imagines of geomagnetic field and strong earthquake. *J. Atmo. Elec.*, 22, 191-205.

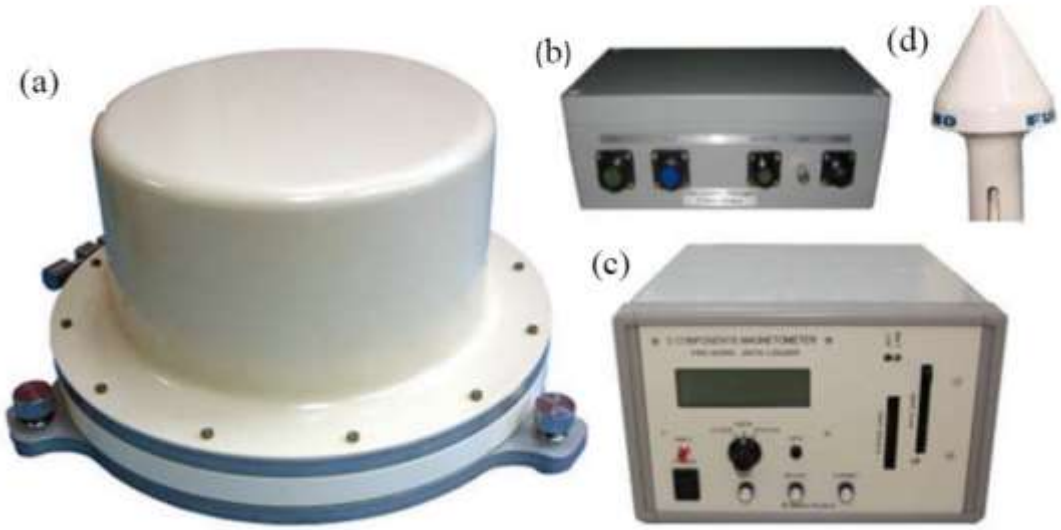

圖一、本研究所使用之三分量磁力儀，(a)磁力儀、(b)前置放大器、(c)主機和(d)GPS (http://www.tierra.co.jp/products/FRG-604RC.pdf) 。

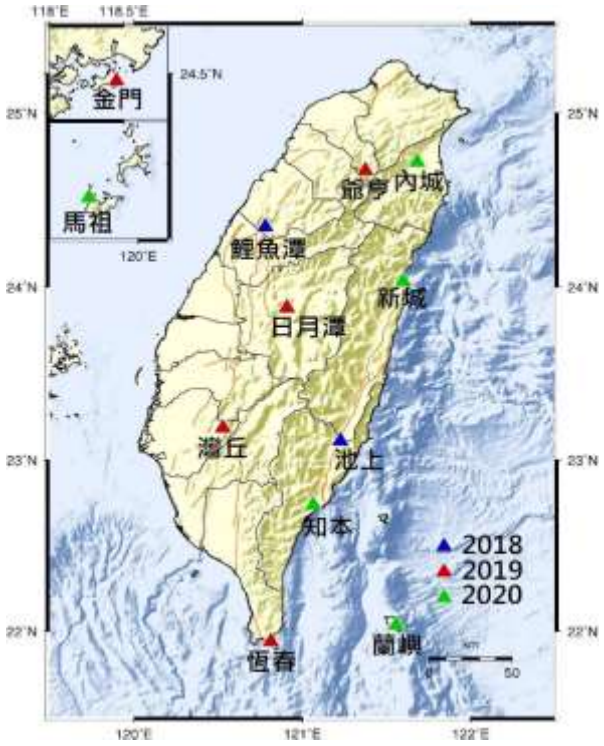

圖二、中央氣象局「臺灣地區三分量地磁觀測網」測站分布圖。

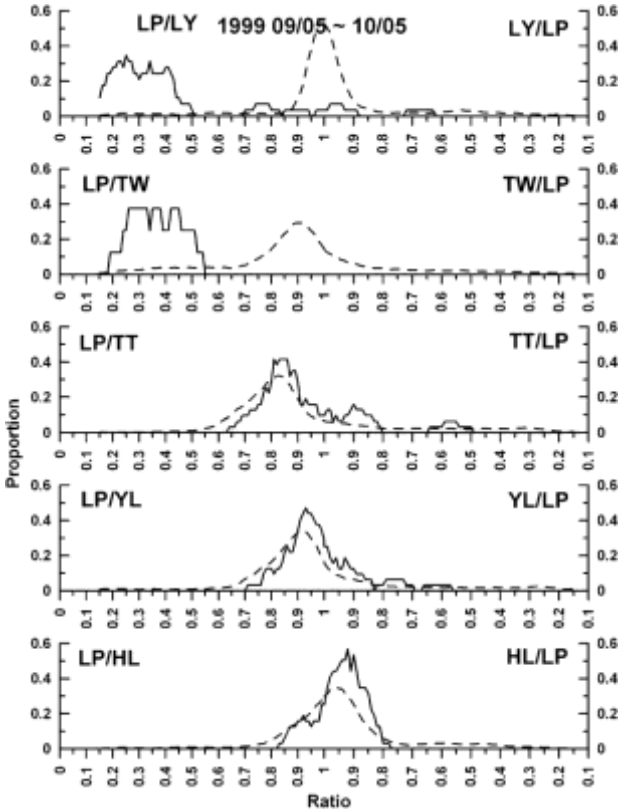

圖三、集集地震前後各月（前後 15 天）各磁力計監測分佈圖 縱軸是比值的數量分佈，橫軸代表參考站除上觀測站和觀測站除上參考站的比值。背景分佈和監測分佈分別用虛線和實線表示。

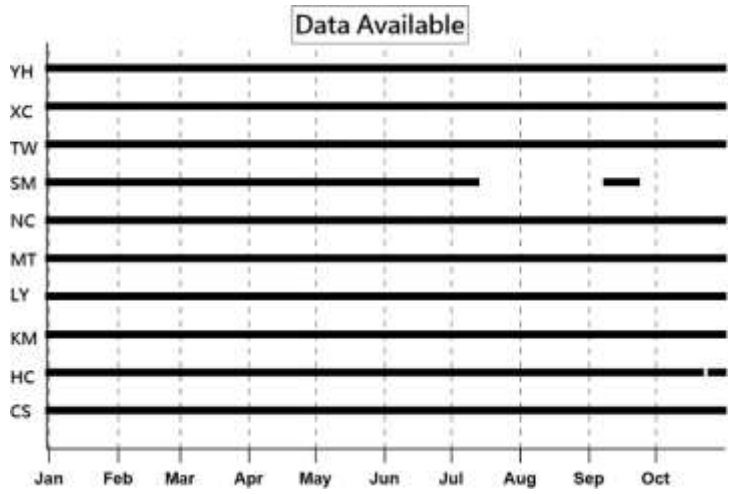

圖四、檢視今年度各地磁站的資料回傳情形，除了日月潭站的資料有中斷的情形外，其他各測站的資料都有完整的紀錄。(測站代號：CS 池上、HC 恆春、KM 金門、LY 鯉魚潭、MT 馬祖、NC 內城、SM 日月潭、TW 灣丘、XC 新城、YH 爺亨)

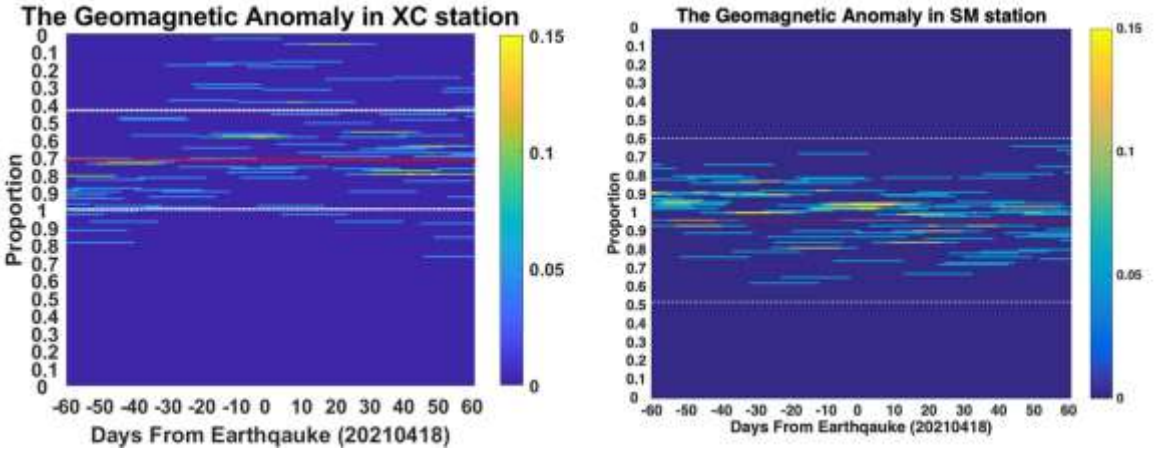

圖五、0418 花蓮壽豐的地震選擇東部新城(XC)及池上(CS)兩個測站；西部選了日月潭(SM)和鯉魚潭(LY)兩個測站相互比較。(左)新城站與馬祖站的日變化比值。(右)日月潭站與馬祖站的日變化比值，所有變化都沒有超過 1 個標準偏差範圍，比值中位數接近 1。(紅色虛線為比值分佈中位數，白色虛線為一個標準差範圍。)

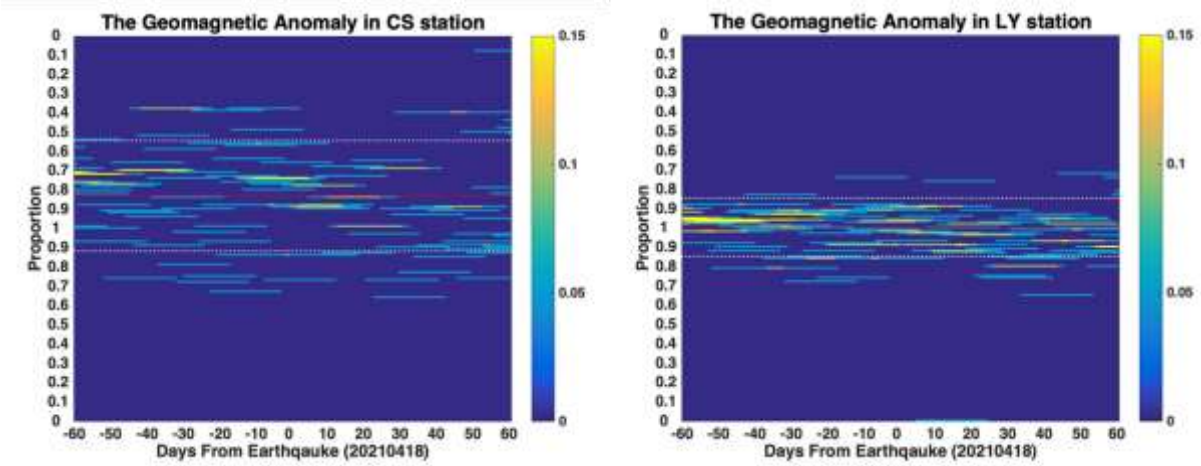

圖六、0418 花蓮壽豐的地震選擇東部新城(XC)及池上(CS)兩個測站；西部選了日月潭(SM)和鯉魚潭(LY)兩個測站相互比較。(左)池上站與馬祖站的日變化比值。(右)鯉魚潭站與馬祖站的日變化比值，比值中位數接近 1。(紅色虛線為比值分佈中位數，白色虛線為一個標準差範圍。)

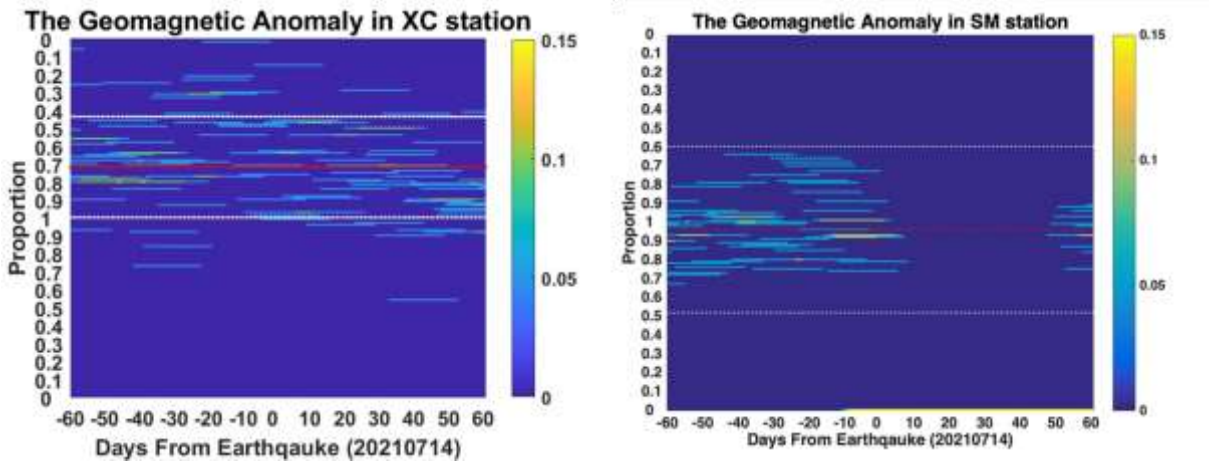

圖七、7 月花蓮壽豐和吉安地區的群震選擇東部新城(XC)及池上(CS)兩個測站；西部選了日月潭(SM)和鯉魚潭(LY)兩個測站相互比較。(左)新城站與馬祖站的日變化比值。 (右)池上站與馬祖站的日變化比值。(紅色虛線為比值分佈中位數，白色虛線為一個標準差範圍。)

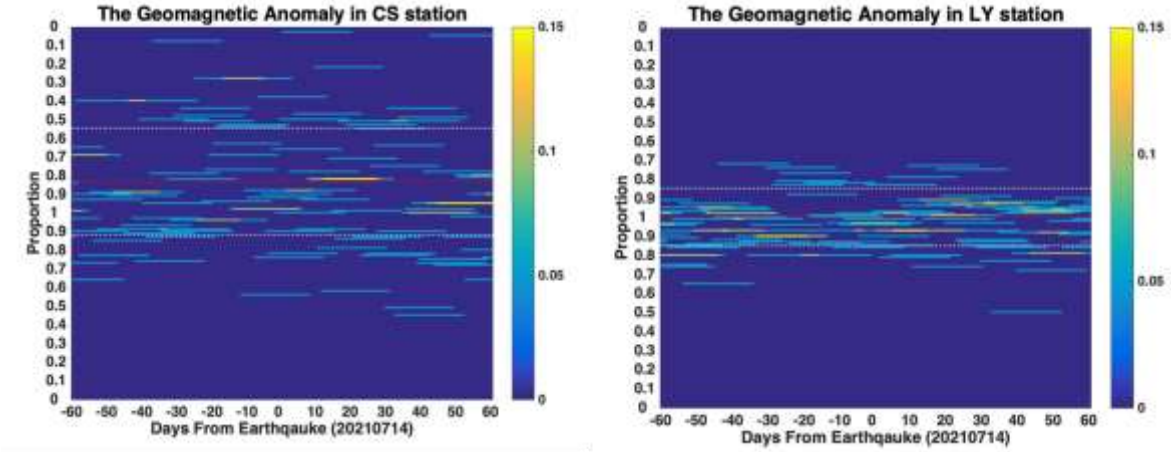

圖八、7 月花蓮壽豐和吉安地區的群震選擇東部新城(XC)及池上(CS)兩個測站；西部選了日月潭(SM)和鯉魚潭(LY)兩個測站相互比較。(左)日月潭站與馬祖站的日變化比值，7 月初日月潭站發生問題而沒有資料。 (右)鯉魚潭站與馬祖站的日變化比值。這兩個西部觀測站與馬祖站的比值中位數都接近 1。(紅色虛線為比值分佈中位數，白色虛線為一個標準差範圍。)

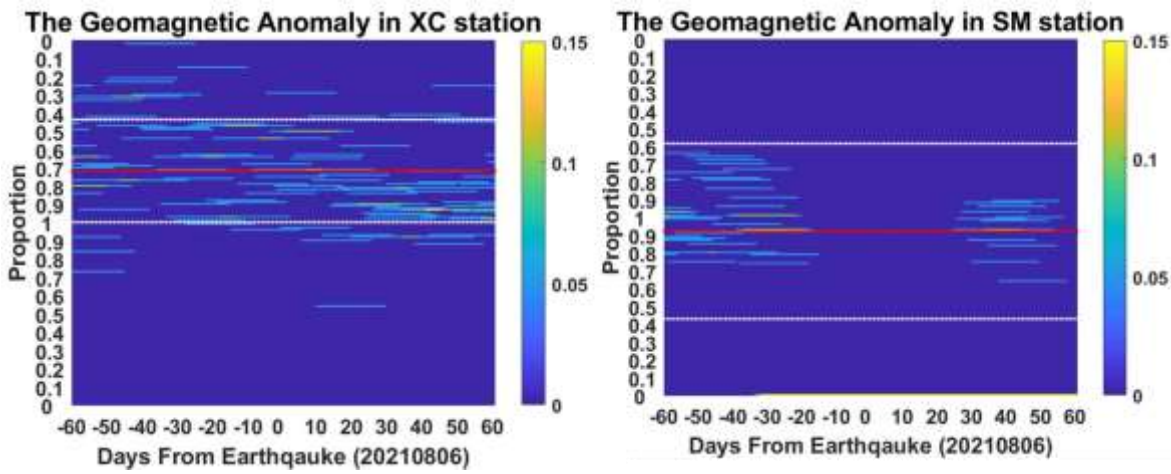

圖九、0806 富里的地震選擇東部池上(CS)及新城(XC) 兩個測站；西部選了日月潭(SM)和鯉魚潭(LY)兩個測站相互比較。(左)臺東池上站與馬祖站的日變化比值。(右)新城站與馬祖站的日變化比值。(紅色虛線為比值分佈中位數，白色虛線為一個標準差範圍。)

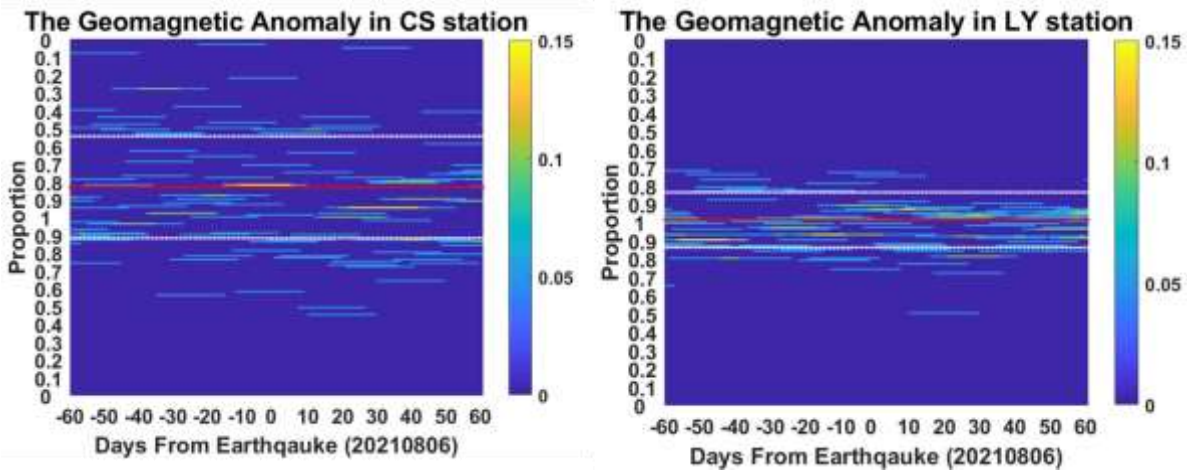

圖十、0806 富里的地震選擇東部池上(CS)及新城(XC)兩個測站；西部選了日月潭(SM)和鯉魚潭(LY)兩個測站相互比較。(左)鯉魚潭站與馬祖站的日變化比值。 (右)日月潭站（有資料中斷的情形）與馬祖站的日變化比值。這兩個西部觀測站與馬祖站的比值中位數都接近 1。(紅色虛線為比值分佈中位數，白色虛線為一個標準差範圍。)

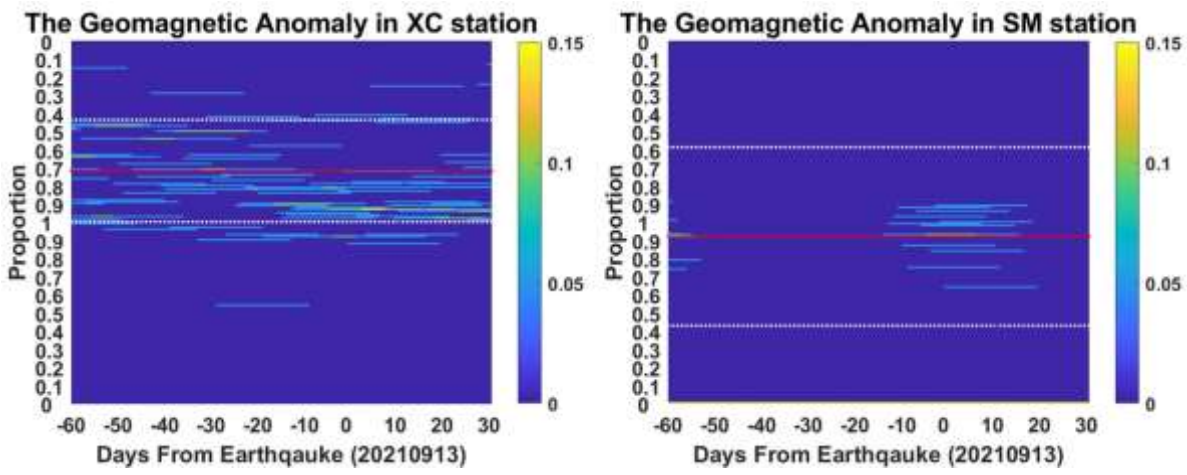

圖十一、0913 南投的地震在西部測站除了日月潭觀測站外，也選了鯉魚潭(LY)及爺亨(YH) 兩個地磁站，東部則選擇較近這個地震的新城(XC)測站來進行分析。(左)新城站與馬祖站的日變化比值。 (右)日月潭站（有資料中斷的情形）與馬祖站的日變化比值。新城站偏離一個標準差的情形變少，反而馬祖參考站的日變化量大於新城站。(紅色虛線為比值分佈中位數，白色虛線為一個標準差範圍。)

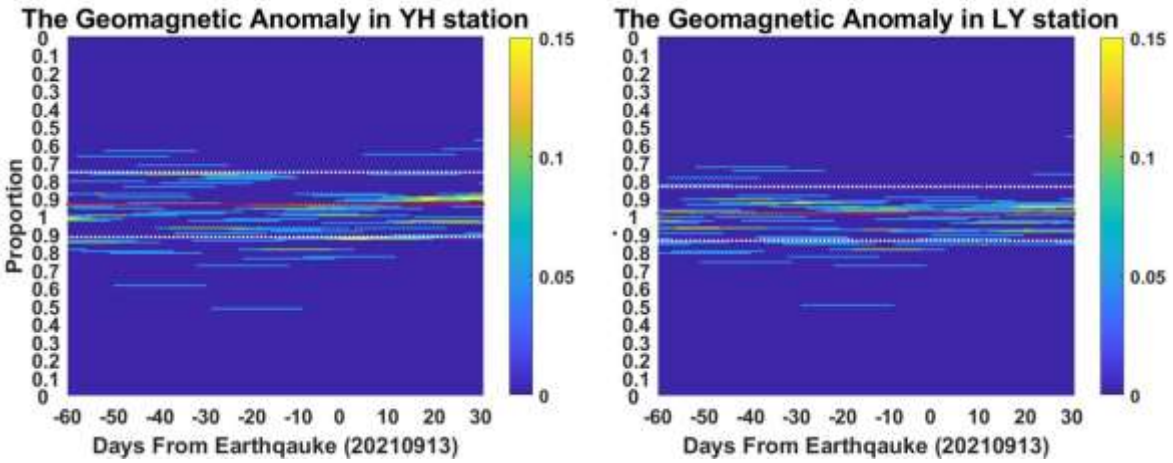

圖十二、0913 南投的地震在西部測站除了日月潭觀測站外，也選了鯉魚潭(LY)及爺亨(YH) 兩個地磁站，東部則選擇較近這個地震的新城(XC)測站來進行分析。(左)鯉魚潭站與馬祖站的日變化比值。 (右)爺亨站與馬祖站的日變化比值。這兩個西部觀測站與馬祖站的比值中位數都接近 1。(紅色虛線為比值分佈中位數，白色虛線為一個標準差範圍。)

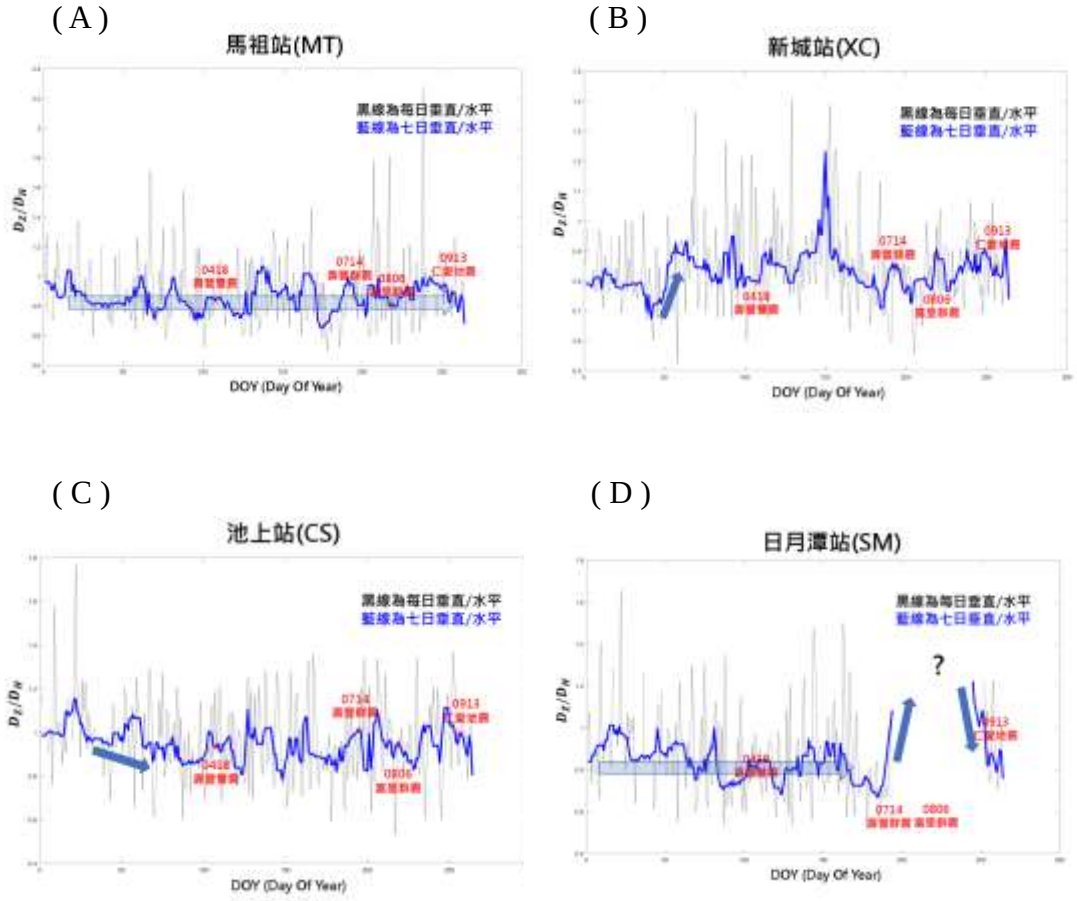

圖十三、分別是 (A)馬祖站，(B)新城站，(C)池上站及(D)日月潭站所記錄到三分量地磁資料，選取 0.01Hz 之垂直與水平改變量的比值。黑色線為每日的比值；藍色線則為一周平均的比值。

臺灣地區 110 年地震前兆監測資料彙整及分析

子計畫二

多變量 MagTIP 預報系統之研究

陳建志 吳宗義 陳宏嘉

國立中央大學地球科學系

摘要

對於大部分的 TIP (Time of Increased Probability) 演算法以至於本研究室所開發之 MagTIP、GEMSTIP 系統，輸入變數數量或資料通道數須固定才能確保所產生的參數模型具備一致的形式；一旦更動，參數模型必須重新訓練才能應用於新的預報階段。也就是說，三分量地磁場必須被轉換為全磁場才能延續舊有模式進行預報，而這麼做卻使更豐富的資訊被浪費。另一方面，若要改用三分量地磁場進行模型最佳化，則需等待額外一段訓練期(例如 7 年)才能開始進行有意義的預報。地下動力系統的變化涵蓋之時間尺度通常是巨大的，因此長時間累積的觀測資料具有寶貴的價值。為了能充分發揮新硬體設備所提供之內涵豐富的紀錄，同時不浪費珍貴的舊測站資料，我們預計發展多變量的 TIP 預報模式。本年度計畫發展之多變量的 MagTIP 系統支援三分量地磁紀錄輸入、全場－三分量混合訓練與預報、多重日統計量之計算，且容許更多時間序列(例如地磁導出量或地磁以外的物理量)參與訓練與預報。此系統預計將為通用多變量 TIP 系統之原型，為未來發展整合地磁與其他可能與地震相關的時間序列用於 TIP 預報模式之第一步。

關鍵字：地磁場異常、地震前兆

Abstract

For most TIP (Time of Increased Probability) algorithms, including our lab's MagTIP and GEMSTIP systems, the input number of variables or data channels has to be consistent; otherwise, re-optimization of the model parameters is required. Which means in the phase transiting from the previous full-field geomagnetic observation system to the new three-component one, a dimensionality reduction on the new data is required if we attempt to have a forecast basing on the model parameters that were trained basing on the old data. On the other way around, an extra period (e.g. 7 years) is required in order to collect sufficient new data to ensure model parameters were effectively optimized. The time scale of the evolution of the underground dynamical system is generally thought to be large, hence data collected from old instruments are also valuable. Aiming for

maximumly utilizing both the data from the most modern instruments and the old ones, we developed the multivariate MagTIP forecasting system. The multivariate MagTIP forecasting system is capable of accepting three-component and one-component geomagnetic data from different stations at once. It is potent in the scenario where both types of data were involved for either training and forecasting, and allows additional earthquake-relevant time series to be involved in the calculation of TIP. This system is going to serve as the corner stone for the integration of TIP predictions of various types.

keyword: geomagnetic anomalies, earthquake precursor

壹、前言

(一)背景與研究概述

在 2019 年,我們根據 GEMSTIP[1–3] 開發了基於中央氣象局磁力觀測系統之 TIP (Time of Increased Probability)演算法(簡稱 MagTIP)、得到全資料期間個別地磁測站最佳模型參數,並據此計算全體測站所涵蓋之時空範圍(簡稱聯合測站)的TIP 函數。結果顯示，基於地磁資料所計算之單站或聯合測站 TIP 與真實地震的發生呈現具統計顯著性的關聯性。2020 年計畫延續第一年的基礎優化演算法並發展 MagTIP 地震機率預報模式。藉由探討不同訓練期/預報期長度下特定預報期之預報表現，我們得以決定適當的訓練期時間窗寬度以及最佳化參數更新頻率，進而建立滾動式的地震機率預報系統並進行後驗式的預報實作。截至目前為止涵蓋多個資料區間的研究結果顯示，在訓練期根據地磁異常所得到的地震機率增加的時間(TIP)與目標地震(EQK)之擬合程度(Fitting Degree)普遍能以 95%以上的機率拒絕虛無假設；在預報期，TIP 命中目標地震的情況也通常優於隨機猜測。因此，我們可以更有信心的說地下動力系統擁有普適性，能同時影響地震動、地電與地磁系統。

對於地震活動這種涵蓋廣大時間尺度的目標事件來說，大規模且長時間的資料累積是非常重要的。儀器升級/變更導致的物理量型態及數量之改變、乃至於測站位置之變更，為難以避免之情事。例如，正在進行的以三分量地磁場紀錄儀替換舊有的全磁場紀錄儀計畫將陸續新增測站以及升級舊有儀器，以提供更高品質的地磁場資料。然而，對於傳統固定變量之 TIP 方法，物理量型態與數量之改變會造成在新舊資料之間取捨的兩難。以全場(1 通道)升級為三分量(3 通道)為例，三分量地磁場必須被轉換為全磁場才能延續舊有模式進行預報，而這麼做卻使更豐富的資訊被浪費。另一方面，若要改用三分量地磁場進行模型最佳化，則需等待額外一段訓練期(例如 7 年)才能開始進行有意義的預報。

為了因應全場－三分量地磁紀錄方式之改變，本年度計畫擬發展多變量 MagTIP 系統，並將預報時間尺度設為可變動之模型參數。可自動最佳化預報時間尺度之多變量 MagTIP 系統將為未來地磁場導出量以及預報時間尺度相關之研究做好準備。

貳、資料與方法

(一)地磁測站、資料與地震目錄

本期計畫使用與整理了 2006 年 11 月 15 日至 2021 年 5 月 25 日(在文中以「資料期間」代稱)中央氣象局磁力觀測系統 18 測站所紀錄之全場/三分量地磁場連續觀測資料。測站地理位置與名稱代號請見表 1 與圖 1。地磁測站安裝精度 0.1nT 的全磁場強度磁力儀或精度為 0.01nT 的三分量磁力儀，取樣率皆為每秒記錄一個觀測值。各測站所記錄之資料的缺值一覽如圖 2，其中每日紀錄到之資料點數占一日總秒數之比例以色階標示，而完全無資料的日子呈現白色。

(二)MagTIP 演算法與機率預報系統之概述

MagTIP 的核心概念是「機率增加的時間」(TIP, Time of Increased Probability)：如果某物理量與目標事件具有關聯性，在該物理量的特定統計指標呈現異常高/低值之時間區段中，「目標事件」的發生機率應會跟著提高。在本研究中，目標事件即為符合條件之地震事件(下稱"EQK")，而地震機率增加的時間(下稱"TIP=1")即為經由特定地磁場統計指標所指示之異常時間區段。

在 TIP 的相關研究及演算法中，如何設定判斷物理量在一段期間內是否屬異常之準則為問題的關鍵。為避免人為主觀的參數調整，MagTIP 演算法會根據過去一段期間(下稱「訓練期」)所觀測到的物理量紀錄以及已發生之事件，調整與最佳化定義異常之準則。此準則涵蓋一系列與異常指標定義、異常時間區段定義以及目標地震定義相關的參數(下稱「參數模型」，列於表 2。更詳細的說明請見 2019 年計畫)。根據訓練期地震機率增加之時間中實際發生地震之機率以及最佳參數模型，MagTIP 可以根據最近的地磁觀測計算未來一段期間(下稱「預報期」)內目標地震發生之機率。

MagTIP 目前預設採用的統計指標為反映地磁紀錄值分布不均程度之偏度 S(skewness)與反映資料分布集中程度之峰度 K(kurtosis)。其中，偏度與峰度的定義如式(1)、(2)所示；其數學上的特性以及用於研究地震前兆的優勢已於 2019 年計畫中說明。

$$S(x) = \text{skewness}(x) = \frac{\frac{1}{N}\sum_{i=1}^{N}(x_i-\mu)^3}{\left(\sqrt{\frac{1}{N}\sum_{i=1}^{N}(x_i-\mu)^2}\right)^3} \quad (1)$$

$$K(x) = \text{kurtosis}(x) = \frac{\frac{1}{N}\sum_{i=1}^{N}(x_i-\mu)^4}{\left(\frac{1}{N}\sum_{i=1}^{N}(x_i-\mu)^2\right)^2} \quad (2)$$

參、多變量 MagTIP 系統

地下動力系統的變化涵蓋之時間尺度通常是巨大的，因此長時間累積的觀測資料具有寶貴的價值。多變量 MagTIP 演算法是為了能充分發揮新硬體設備所提供之內涵豐富的紀錄，同時不浪費珍貴的舊測站資料而生。這裡的「變量」指地磁紀錄在一指定時間單位內的統計指標，例如前述之峰度或偏度，而變量的數量則是資料通道數量×統計指標數量。本年度計畫(預計)發展之多變量系統，除了能自動根據不同的資料通道數量調整變量數量以維持一致的訓練/預報結果，更允許使用者以參數輸入的方式變更/新增統計指標(程式碼範例見圖 5)。

(一)資料轉換與對全場/三分量地磁資料混用場景之支援

多變量 MagTIP 的主要開發目的/任務為極大化地同時利用新/舊測站所觀測的資料，並期望在全場/三分量儀器交接之過渡階段也能無縫接軌。在方法上，新系統會根據選定的期間範圍，自動掃描地磁資料並判斷種類(全場或三分量)、調整輸出變數數量，並調整定義異常日的數量門檻設定。圖 3 展示了全場/三分量資料混用場景下相關模組對資料與變量所進行的操作示意圖。圖 4 更進一步展示從全場過渡至三分量期間，異常日定義準則的自動調整示意圖。

另外，由於某些舊測站場址已不適宜進行地磁場觀測，故一些新三分量測站被設在鄰近場址。為了充分利用長期間累積觀測的全場地磁資料，若新測站資料觀測時間過短不足以產生最佳化參數模型，演算法會自動抓取 15 公里內鄰近測站的最佳化參數模型進行預報。

最後，目前原始地磁觀測資料存在多種形式([全場、三分量]×[1 小時、1 天 1 個檔案]，共 4 種)。新系統能自動將不同格式的檔案歸類並轉換成標準格式，並且具備錯誤檢查與新舊資料比對的機能，將有效減少耗費於資料前期處理之人力。

(二)速度與易用性的提升

多變量 MagTIP 系統包含 4 個主要模組與數個工具。主要模組為統計指標計算模組(statind)、異常指標數量計算模組(anomalyind)、TIP 計算模組(molscore 與 molscore3)。新系統在設計上希望能盡可能極小化因人工設定參數而造成錯誤或衝突的可能性。因此，在運行與操作上，各步驟的輸入皆依賴前一步驟輸出檔案之資料夾或變數，而各步驟的自訂選項統一使用鍵值對(name-value pair)的輸入方式進行設定。這樣的做法讓 MagTIP 演算法有著與 Matlab® 之官方套件一致的使用體驗、大幅度地避免因人為修改腳本變數而造成錯誤的可能，並使程式碼易於維護。

圖 6 展示了完整執行 MagTIP 全部步驟的最小可行範例，其中我們可以看到只要設定好存放讀取/寫入變數的目標資料夾即可簡單地執行工作。值得一提的是，演算法會自動產生獨一無二的識別碼，而各步驟的模組會據此特定出相關的檔案、辨識前一階段的工作狀態，再讀取應輸入之變數。這樣的設計能很大程度地避免人為操作失誤對計算產生的意外影響：例如因為沒有適當地移除上一個被人為或錯誤所中斷的工作階段中產生的檔案，或者不小心更動資料夾結構或名稱等事件而導致程式對資料之不當存取。在最極端的例子中，使用者甚至可以不做任何整理，把所有資料(無論是原始/轉檔後的地磁資料、不同參數設定下的工作階段所產生之

中繼檔案等等)無序地混雜置放在同一個資料夾目錄及其子目錄下，新系統仍能夠自動找到所需的檔案並正確地演算、輸出結果。

新系統在平行計算方面也有著大幅的改進：我們對主要的耗時步驟[*]皆另外提供平行化版本。圖 7 展示了以平行化版本執行前述工作(圖 6)的程式碼。使用者僅需在原本的指令名稱上加上"_parfor"後綴(例如 statind(…)→statind_parfor(…))，資料與工作即會根據運行主機可用的 CPU 核心數量被切割與分派，並在最後將結果整合。平行化版本與普通版本共用相同的核心程式碼，故兩者產生的結果將會完全相同，並共享一樣的鍵值對輸入選項。

最後，圖 8 示範性地展示了其他以輸入鍵值對的方式進行各步驟的選項自訂。圖 9 展示了輸出機率預報圖的範例程式碼與繪圖結果；圖 10 展示了輸出 EQKTIP 時間序列圖的範例程式碼與繪圖結果。其中，各模組/工具所支援的鍵值對輸入選項展示於圖 11 至圖 16；各模組的輸出變數資料結構展示於圖 17 至圖 20。

肆、預報時間尺度的初步分析

本期計畫完成了與預報時間尺度有關之程式碼調整，現在新系統的參數模型可允許不同的預報時間窗(T_{pred})長度作為訓練參數。使用上，與設定格點搜尋法的模型參數組合相同，以鍵值對的方式設定"Tpred"參數(詳見說明文件中關於 modparam 的部分)即可在訓練步驟中將指定的預報時間窗尺度納入參數模型最佳化之過程[†]。

我們使用可自動最佳化預報時間尺度之多變量 MagTIP 系統產生 5 個不同預測時間窗(T_{pred})尺度下的滾動式 TIP 預報[‡]，並對不同濾波頻段、預測時間窗長度下之整體預報表現進行最簡單的分析與比較。這 5 個預測時間窗尺度分別為 1、2、5、10、30 日。具體作法是將多個預測時間窗尺度一併納入參數模型進行訓練，並分別以各預報時間窗表現最佳之參數模型組合進行三維(時間與二維空間)的 TIP 預報。各頻段、預測時間窗下的預報 TIP 對目標地震的擬合程度(D)展示於圖 21；前述預報 TIP 的預警區域佔整體有效區域比例(τ)，以及預報 TIP 對目標地震的遺漏比例(ν)以莫昌爾圖表法(Molchan Diagram)展示在圖 22；最後，預報 TIP 與目標地震的匹配圖(Matching Diagram)展示在圖 23 至圖 42。其中，預報 TIP 涵蓋期間為 2014 年 11 月 17 日至 2021 年 5 月 25 日，是基於 2007 年 11 月 16 日至 2020 年 11 月 16 日的地磁資料進行滾動式計算得到的最佳參數模型組合(係指各測站、各訓練期排名第一的模型參數組合[§])所定義之。圖 21 及圖 22 中的 95%信賴邊界(CB, Confidence Boundary)係 Zechar 等人[4]所提出之評估 TIP 預報表現的參考線，其意

[*] 主要耗時模組分別為統計指標計算模組(statind)以及 TIP 計算模組(molscore 及 molscore3)。各模組的功能簡述詳見圖說。

[†] 另外在預報步驟中，TIP 預警區域會自動隨著訓練期得到的最佳參數模型群中的預報時間窗長度而調整，因此無須額外設定。

[‡] 滾動式預報預設以 7 年長度為訓練期，1 年長度為預報期；此範例滾動式預報程序之步進長度為 1 年，即參數模型更新率為 1 年/次。

[§] 「排名第一」係指即各測站，指定訓練期長度的參數模型中，擬合程度最高的參數模型；此最佳參數會隨訓練期(training phase)/預報期(forecasting phase)時間窗的滾動而改變。

義近似於信賴水平(Confidence Level)。

從未濾波組別的結果來看，我們可以觀察到預報 TIP 對目標地震之擬合程度隨T_{pred}增加而下降，而這樣的趨勢在 ULF-B (0.001-0.01Hz)濾波段組別也可觀察到但相當不明顯。在 ULF-A (0.001-0.003Hz)濾波段組別，$T_{\mathrm{pred}} = 1$與$T_{\mathrm{pred}} = 10$(日)參數下的預報 TIP 有著與目標地震最佳的擬合程度。而在 ULF-C (0.001-0.1Hz)組別，擬合程度普遍不佳。從莫昌爾圖表以及預報 TIP 時序圖來看，可以發現 ULF-C 組別相較於其他濾波段通常有更高的預警比例，其所造成之高誤報率使得擬合程度普遍更低。此初步分析結果與先前計畫 [5,6] 中基於$T_{\mathrm{pred}} = 1$的擬合程度分析結果互相呼應：ULF-A 與 ULF-B 濾波組別通常有著較佳的預報表現，而未濾波與 ULF-C 組別的預報表現通常是所有組別中較差的。

然而，此初步分析結果(圖 21 至圖 42)使用之預報 TIP 僅為用於產生機率預報、總數 500 組的聯合測站預報 TIP 時間序列中的其中一個序列。先前的分析 [5,6] 顯示排名前十的最佳模型所定義之單站預報 TIP 與偵測半徑內目標地震的擬合程度常常相當接近，但聯合測站預報中總數 500 組的聯合測站預報 TIP 與目標地震的擬合程度上常存在明顯差異。因此，目前的結果僅能為我們在預測時間尺度方面帶來最初步的認識與了解。

伍、地震個案分析

利用多變量 MagTIP 演算法，我們計算了 2021 年 4 月花蓮地震(M_L6.2)以及 2020 年 12 月宜蘭地震(M_L6.7)事件前後之機率預報。其中，預報模型是根據 2013 年 2 月 28 日至 2020 年 2 月 28 日的地震與地磁資料訓練資料進行最佳化。兩個案地震皆不在任一測站模型定義之偵測半徑內，但分別與新城(XC)、內城(NC)站相當靠近。

於花蓮地震之個案分析中，新城站為新啟用之三分量測站，缺乏足夠的歷史資料；另一方面，鄰近的全場地磁站花蓮站(HL)已停止觀測。為了最大化利用兩者，多變量 MagTIP 演算法使用花蓮站之歷史地磁資料進行預報模型最佳化，並在預報期根據新城站的最新觀測計算預報 TIP。根據三分量地磁資料所計算之日統計指標[偏度(S)與峰度(K)]時間序列依不同頻段顯示於圖 43 至圖 45；機率預報與 TIP 預報顯示於圖 46 至圖 48。基於 ULF-A 濾波頻段的預報結果(圖 47)顯示，於地震發生前後離震央最近的新城站偵測半徑內之機率值皆明顯較高；另一方面，基於未濾波及 ULF-B 濾波頻段在該區域的預報機率(圖 46 及圖 48)皆不顯著。

於宜蘭地震之個案分析中，根據三分量地磁資料所計算之日統計指標[偏度(S)與峰度(K)]時間序列依不同頻段顯示於圖 49 圖 51；機率預報與 TIP 預報顯示於圖 52 至圖 54。基於 ULF-A 濾波頻段的預報結果(圖 53)顯示，離震央最近之內城站的偵測半徑內在地震發生前出現了相當高的機率值，且在地震結束後該區域的預報機率快速下降。需要注意的是，在地圖顯示上此個案地震震央位於內城站偵測半徑的圓圈內，但因其震源深度達 76.8 公里，實際上的震源並不在偵測半徑內。

陸、結論

本期計畫完成多變量的 MagTIP 系統。新系統支援三分量地磁紀錄輸入、全場－三分量混合訓練與預報、多重日統計量之計算、預測時間窗之最佳化，且容許更多時間序列(例如地磁導出量或地磁以外的物理量)參與訓練與預報。新系統提供與 Matlab® 官方內建函式一致的使用體驗，而且強大的檔案搜尋比對機能能有效減少錯誤與耗費於資料處理之人力。最後，我們在平行化計算所下的努力，不僅使得計算時間能被大幅縮短，更同時保有高度的使用者友善性。

多變量 MagTIP 系統(相較於先前系統)的主要新增功能一覽：

- 支援三分量地磁紀錄的輸入
- 支援在全場/三分量地磁資料混用場景下的訓練及預報
- 支援多重日統計量之計算方法
- 支援預測時間窗之最佳化
- 同時支援不同原始地磁資料格式
- 新增地磁資料自動比對與歸類的機能
- 改善使用便利性、提升速度與系統穩定性
- 預報時間窗改進為可變訓練參數

MagTIP 演算法研發迄今已三年，主程式架構已趨完善。根據在過往三年計畫中涵蓋 14 年的地震與地磁觀測紀錄之相關研究，我們認為地磁異常與地震間的關連性是明確存在的；然而，在預報與訓練上仍有許多待解決或改善之議題，例如：單一模型之 TIP 預報品質並不穩定，且評估方式並不完美；在模型最佳化部分，根據過少地磁與地震資料所訓練出的模型應被屏棄；在機率預報方面，需發展適當的檢驗方式評估預報之品質；在資料方面，由於地磁資料完整度以及測站覆蓋程度有限，我們期待未來能把更多與地震相關的觀測資料(例如地電場觀測)納入聯合測站機率預報計算。

前述待解決的問題以及未來可發展之方向簡列於以下清單：

- 根據背景地震、地磁資料的完備程度剔除低參考價值的最佳化模型
- 同時使用地電、地磁資料進行訓練與預報
- 發展機率預報品質評估方法
- 發展新的統計指標計算方式

參考文獻

1. Chen H.-J. 地電訊號異常與地震的關聯性研究. *http://ir.lib.ncu.edu.tw:88/thesis/view_etd.asp?URN=102682002* (2018).

2. Chen, H.-J., Chen, C.-C., Ouillon, G. & Sornette, D. Using geoelectric field skewness and kurtosis to forecast the 2016/2/6, ML 6.6 Meinong, Taiwan Earthquake. *Terrestrial, Atmospheric and Oceanic Sciences* **28**, 745–761 (2017).

3. Chen, H.-J. & Chen, C.-C. Testing the correlations between anomalies of statistical indexes of the geoelectric system and earthquakes. *Nat Hazards* **84**, 877–895 (2016).

4. Zechar, J. D. & Jordan, T. H. Testing alarm-based earthquake predictions. *Geophysical Journal International* **172**, 715–724 (2008).

5. 陳建志 & 吳宗義. 以 MagTIP 預報模型評估地磁場異常與地震的關連性 (計畫編號：MOTC-CWB-109-E-01). (2020).

6. 陳建志 & 吳宗義. 地磁場異常與地震的關連性研究 (計畫編號：MOTC-CWB-108-E-01). (2019).

圖表

表 1 地磁測站站名、代號、位置一覽表。

測站代號	測站名稱	經度	緯度	觀測起始時間	觀測終止時間
MS	馬仕	120.633	22.61089	20151113	20181012
TW	灣丘	120.5286	23.18502	20061101	20190904
TT	卑南	121.0799	22.81765	20061101	無資訊
YL	玉里	121.2973	23.3924	20070528	20190922
HC	恆春	120.8137	21.94015	20070509	20190916
HL	加灣	121.6048	24.08111	20070411	20190411
PT	瑪家	120.6531	22.70307	無資訊	20121203
YH	爺亨	121.3758	24.66952	20071102	20181205
SL	雙龍	120.9558	23.78878	20070409	20190301
LY	鯉魚潭	120.7802	24.34651	20060921	20190117
NC	內城	121.6829	24.71802	20070515	20190831
KM	金門	118.4527	24.44934	20151113	20190122
CS	池上	121.2264	23.1112	20140325	20190109
MT	馬祖	119.923	26.1697	20200910	無資訊
LN	蘭嶼	121.558	22.0375	20201010	無資訊
ZB	知本	121.0648	22.7398	20201006	無資訊
XC	新城	121.6095	24.0383	20201006	無資訊
SM	日月潭	120.9076	23.881	20191008	無資訊

表 2 MagTIP 演算法的模型參數向量$\boldsymbol{g}$ 數值範圍

參數	M_c	R_c	A_{thr}	N_{thr}	P_{thr}	T_{thr}	T_{obs}	T_{lead}	T_{pred}
數值範圍	5	20-100	1-10	1-n	0.1-0.5	$P_{thr} \times T_{obs}$	5-100	0-100	[1,2,5,10,30]
(單位)		(km)		n 為統計指標×最大通道數	(比例)	(days)	(days)	(days)	(days)

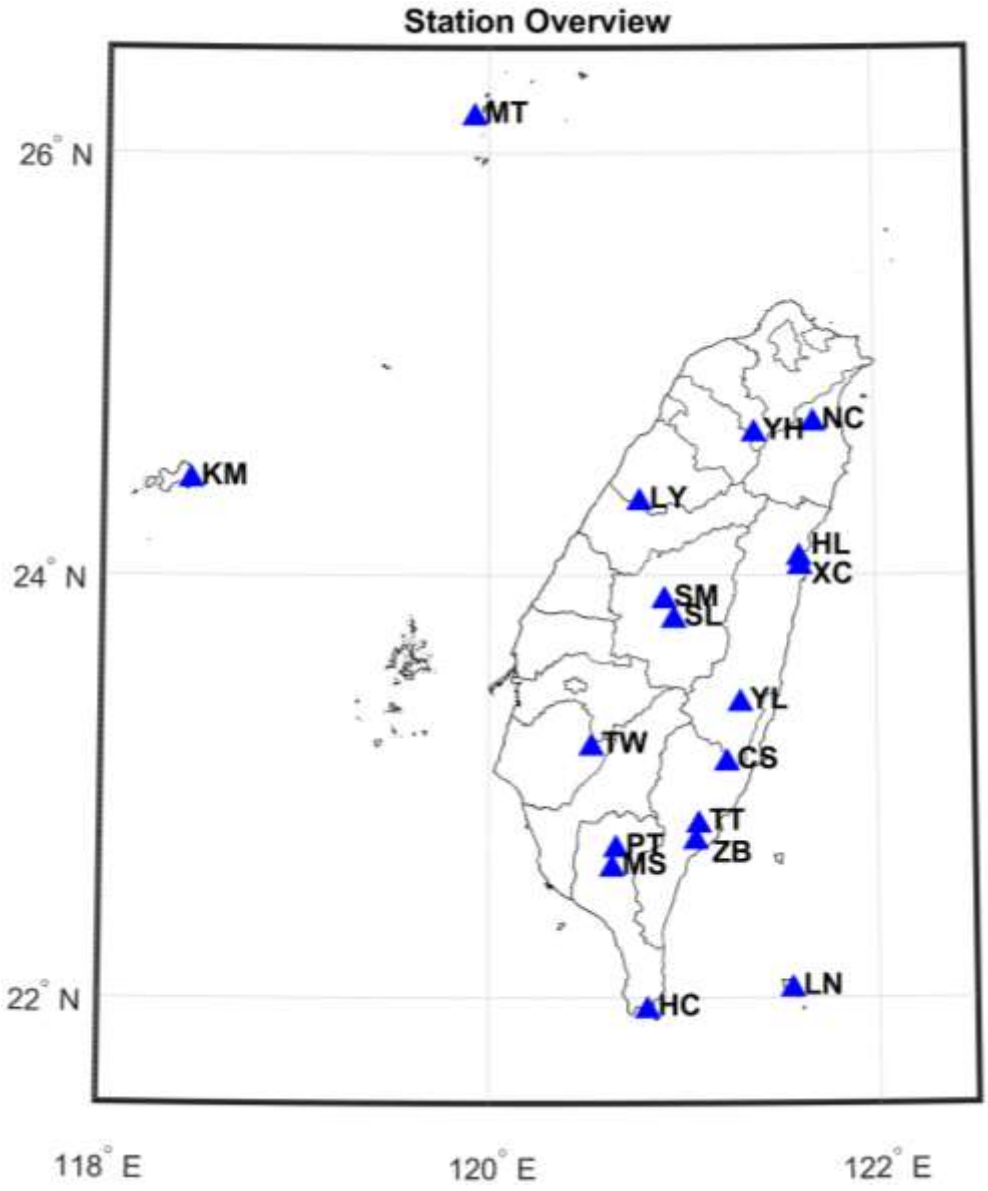

圖 1 中央氣象局地磁觀測站一覽圖。

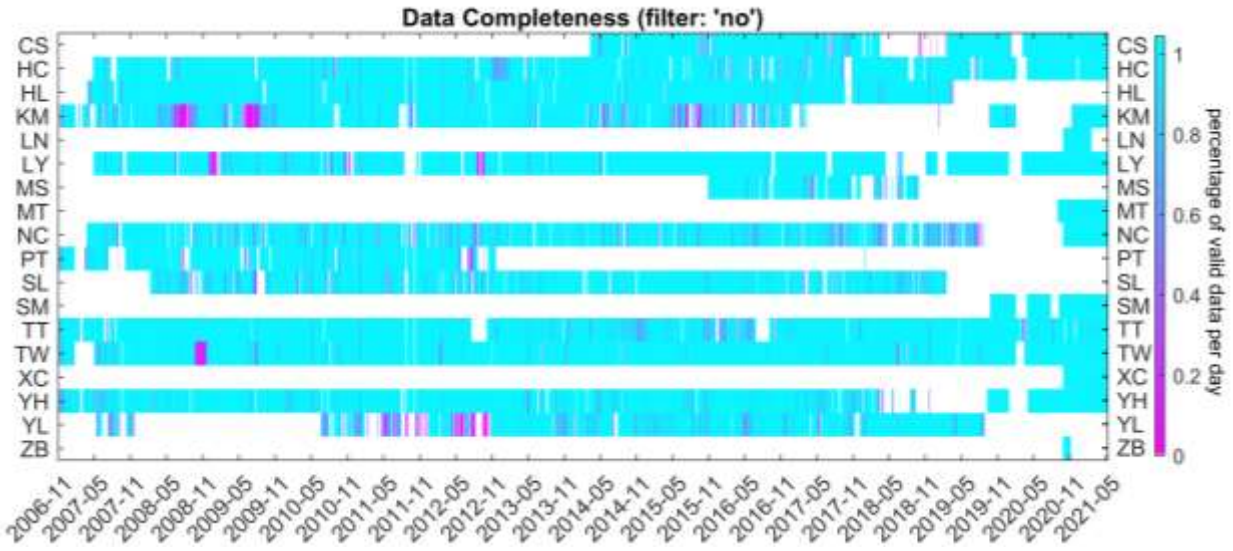

圖 2 使用之測站資料一覽。每日有效資料點數之比例以色階標示，完全無資料的日子呈現白色。

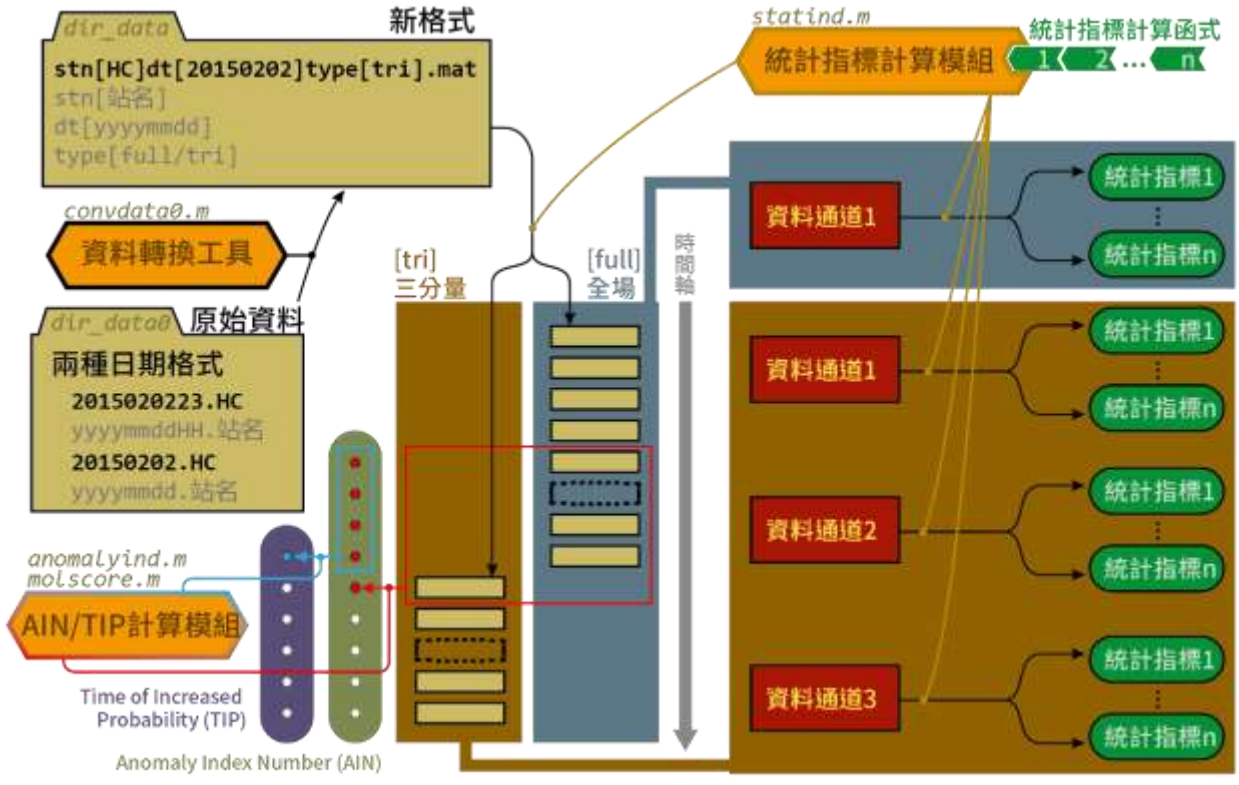

圖 3 多變量 MagTIP 的資料、變量分配以及 AIN、TIP 計算之示意圖。

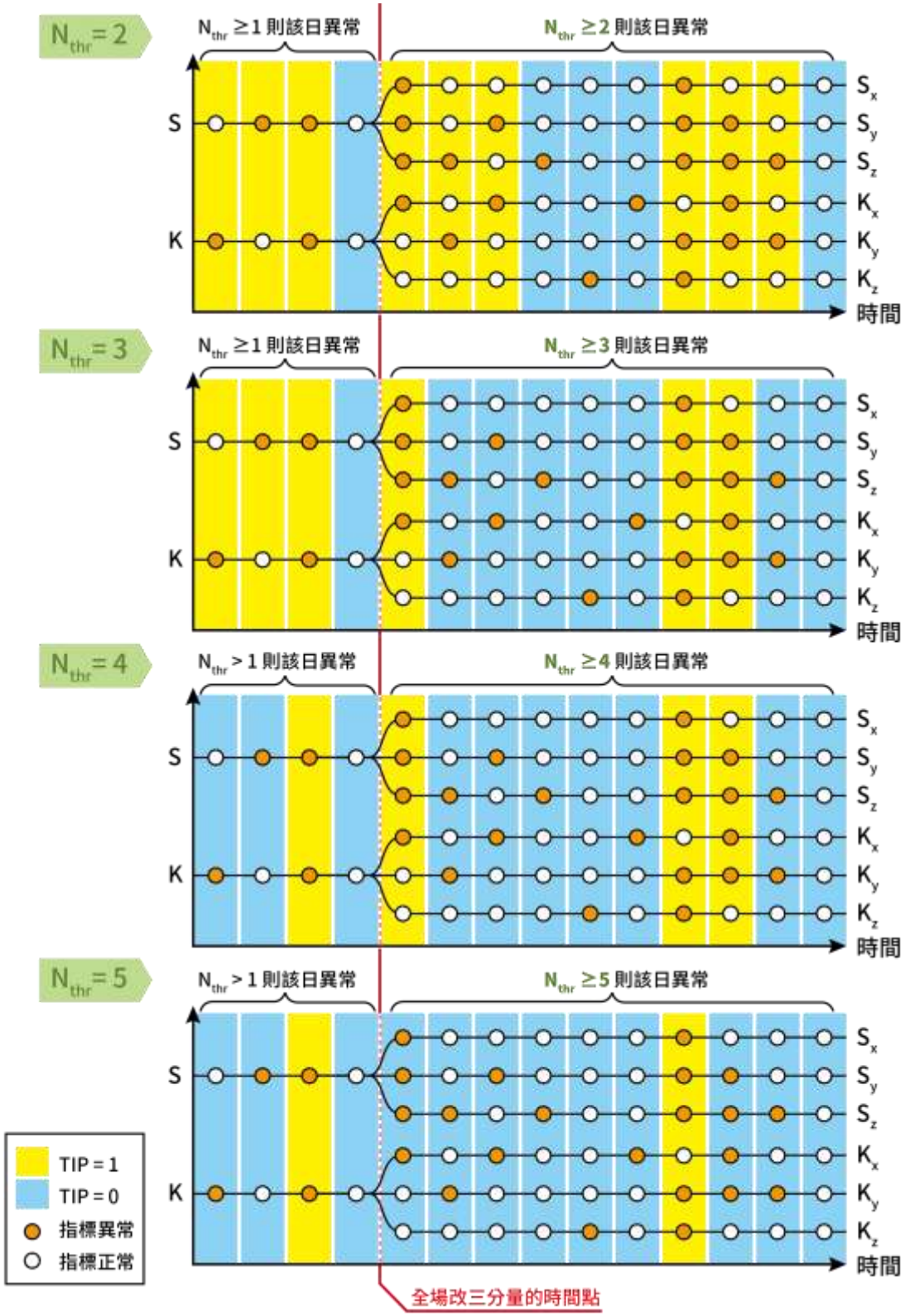

圖 4 全場過渡至三分量期間，異常日定義準則的自動調整示意圖。

```
statind(dir_data,dir_stat,...
        'StatName',{'M','V','S','K'},...
        'StatFunction',{@mean, @var, @skewness, @kurtosis});
```

圖 5 多變量 MagTIP 系統變更/新增統計變量計算方式的程式碼範例。其中，'StatName'用於設定變量的代稱，'StatFunction'用於設定計算日統計變量的方式。在此範例中，以 Matlab 內建的 mean、var、skewness、kurtosis 函式計算日磁場平均值、變異數、偏度與峰度，作為此次計算的統計指標。其他模組的計算會自動根據此階段的結果進行變數數量設定及調整。

```
convdata0(dir_data0, dir_data);
statind(dir_data,dir_stat);
anomalyind(dir_stat,dir_tsAIN);
molscore(dir_tsAIN,dir_catalog,dir_molchan);
molscore3(dir_tsAIN,dir_molchan,dir_catalog,dir_jointstation);
```

圖 6 執行整個 MagTIP 演算法流程的最小可行範例。convdata0 為資料轉換模組；其中，dir_data0 為存放原始地磁觀測資料的資料夾，dir_data 則是輸出資料夾。statind 為統計指標計算模組；其中，dir_stat 為存放統計指標的資料夾。anomalyind 為 AIN 計算模組；其中，dir_tsAIN 為存放異常指標數量的資料夾。molscore 以及 molscore3 屬 TIP 計算模組；其中，dir_catalog 為存放地震目錄、測站位置表格的資料夾，dir_molchan 是存放 Molchan score 的資料夾，dir_jointstation 是存放預報機率以及聯合測站相關變數的資料夾。

```
statind_parfor(dir_data,dir_stat);
anomalyind(dir_stat,dir_tsAIN);
molscore_parfor(dir_tsAIN,dir_catalog,dir_molchan);
molscore3_parfor(dir_tsAIN,dir_molchan,dir_catalog,dir_jointstation);
```

圖 7 同圖 6，但是在 statind、molscore 以及 molscore3 這三個步驟使用平行運算。statind_parfor、molscore_parfor 以及 molscore3_parfor 的輸入與輸出與無_parfor 後綴的普通版本完全一樣，並支援所有普通版本具有的功能。

```
trnphases =  [datetime(2008,1,2), datetime(2015,1,2)];
filters = {'ULF-A','ULF-B'};
statind_parfor(dir_data,dir_stat,'Filter',filters, 'SaveFilteredData', true);
anomalyind(dir_stat,dir_tsAIN);
molscore_parfor(dir_tsAIN,dir_catalog,dir_molchan,'TrainingPhase',trnphases);
molscore3_parfor(dir_tsAIN,dir_molchan,dir_catalog,dir_jointstation,...
                'ForecastingPhase', calyears(1), 'OverwriteFile', true);
```

圖 8 承圖 7，並透過鍵值對輸入的方式自訂選項：(statind)設定兩種濾波方式(ULF-A、ULF-B)並儲存濾波後的檔案。(molscore)指定訓練期從 2008 年 1 月 2 日至 2015 年 1 月 2 日。(molscore3)將聯合測站預報期設為 1 年且更改輸出檔案覆寫設定為

true。

```
dir_prob = fullfile(dir_jointstation,'png','prob');
dates2plot = datetime(2020,3,1):calmonths(6):datetime(2021,3,1);
dir_prob2 = plotProbability(dir_jointstation,dir_catalog,dir_prob,...
                            'TimeRange',dates2plot);
```

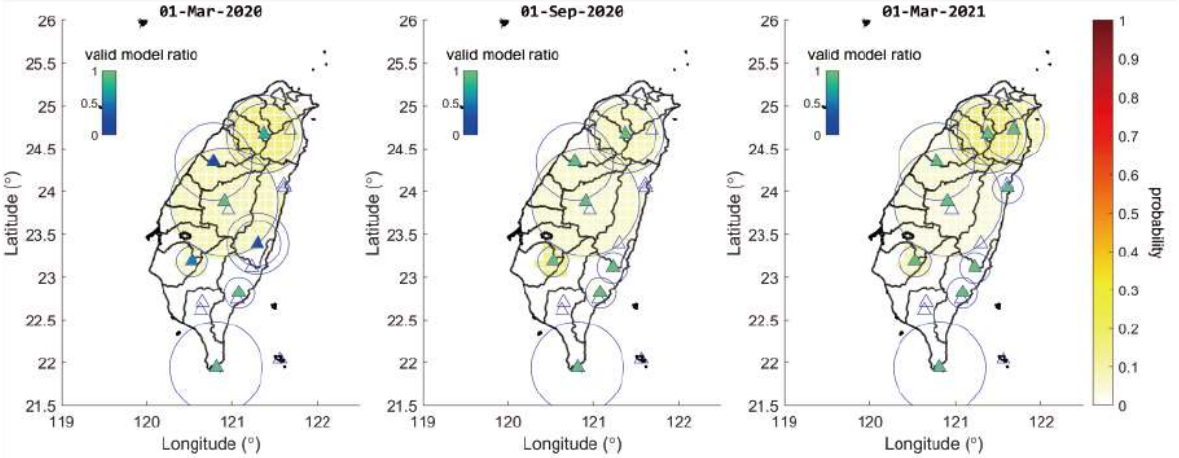

圖 9 輸出機率預報圖的範例程式碼與繪圖結果。其中的自訂選項說明請見圖 15。

```
dir_png = fullfile(dir_molchan,'png','EQKTIP');
plotEQKTIP1(dir_tsAIN,dir_molchan,dir_catalog,dir_png,...
            'ForecastingPhase',calyears(1),'ShowTrainingPhase',1,'Rank',1,...
            'ForceMagnitude',-0.5,'scatter',1);
```

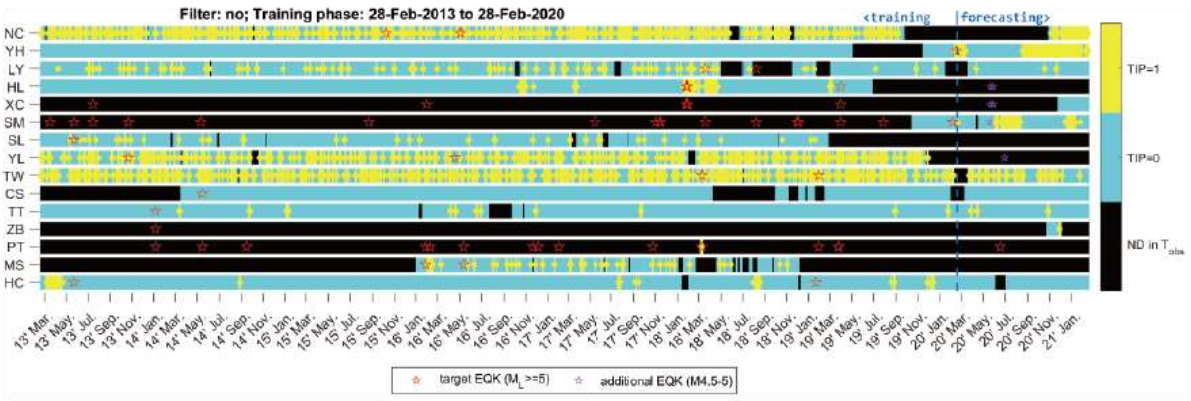

圖 10 輸出 EQKTIP 時間序列圖的範例程式碼與繪圖結果。其中的自訂選項說明請見圖 16。

`statind` takes the following optional name-value pair arguments:

- `'StatName'`
  - The abbreviations for the name of statistical indices. They can be arbitrarily defined but have to be the same number of elements as that of `'StatFunction'`.
  - Default is `{'S','K'}` (for Skewness and Kurtosis).
- `'StatFunction'`
  - The function handle for calculating statistical index.
  - It has to be of the same number of elements as that of `'StatName'`
  - Default is `{@skewness,@kurtosis}` for calling the `skewness.m` and `kurtosis.m` functions.
- `'Filter'`
  - Apply filter(s) to time series loaded from `dir_data`. Generally applying a filter very largely increase the computing time, so you may consider `'SaveFilteredData'`.
  - Default is `{'no'}`, where no filter will be applied.
  - Supported arguments are `'no'`, `'ULF-A'` (a band pass filter of frequency range `[0.001 0.003]` Hz), `'ULF-B'` (`[0.001 0.01]` Hz), and `'ULF-C'` (`[0.001 0.1]` Hz).
  - Also see `filterthedata.m`.
  - If multiple filters are applied, for example `{'no', 'ULF-A'}`, then two sets of result according to no-filter data and ULF-A band passed data are going to be produced.
- `'SaveFilteredData'`
  - Save the filtered data to an alternative folder. Their directory is parallel to that of no-filter data.
- `'FilterByDatetime'`
  - It should be a two element datetime array.
  - If applied, all files with date time tag not in the range will be ignored.
  - Default is `[datetime(0001,1,1), datetime(2999,12,31)]`, resulting in no data selection by date time tag.

圖 11 statind 所支援的自訂功能與選項。

`anomalyind` takes the following optional name-value pair arguments:

- `'AthrList'`
  - Default is `[1:10]`.
- `'MovingWindow'`
  - Default is `1000`.

圖 12 anomalyind 所支援的自訂功能與選項。

`molscore` takes the following optional name-value pair arguments:

- `'TrainingPhase'`
  - Assigns a (set of) training phase(s). It should be of type `'calendarDuration'`, `'duration'`, an N by 2 array of `'datetime'`, or an N by 2 cell array.
  - For example, it can be
    - an N by 2 `datetime` array such as `reshape(datetime(2009:2016,2,1),[],2)`.
    - an N by 2 cell array such as

      ```
      {calyears(7),datetime(2012,11,11);...
       calyears(7),datetime(2011,11,11);...
       calyears(7),datetime(2010,11,11)};
      ```

      , which specify the end day of the training phases as 2010-Nov-11, 2011-Nov-11 and 2012-Nov-11, all having a length of 7 year long training period (i.e. `calyears(7)`).
    - (N is the number of the training phases)
  - If given an N by 2 array specifying N training phases, then N sets of results will be produced separately, with output format `'[MolScore]stn[%x]ID[%s]filt[%s]dt[%s-%s].mat'`.
  - Default is `calyears(7)`. Which specify the end day of training phase the day before the last day of statistical indices or anomaly index number, with a length of 7 year period.
- `'modparam'`
  - Specify the model parameters for grid search. It should be a cell array; all elements in the cell array will be directly passed into `modparam.m` as input arguments.
  - For example, { `'Athr',[1:2:10],'Rc',[20, 30]` }.
  - Default is `{}`.
- `'AdditionalCheck'`
  - Apply some additional check and tests. This option is for developer.
  - Default is `false`.

圖 13 molscore 所支援的自訂功能與選項。

`molscore3` takes the following optional name-value pair arguments:

- `'ForecastingPhase'`
  - It should be `'calendarDuration'`, `'duration'`, or an N by 2 `'datetime'` array.
  - Notice that if it is an `'datetime'` array, its size should be identical as that of training phases (`Info.TrainingPhase` of the `[MolchanScore]Information.mat`)
  - Default is `calyears(1)`, where the forecasting phase starts from the next day of the end day of the training phases, with a length of one calendar year.

圖 14 molscore3 所支援的自訂功能與選項。

`plotProbability` takes the following optional name-value pair arguments:

- `'LongitudeLimit'`
  - Set the longitude range of the map to show.
  - It should be 1 by 2 numeric array.
  - Default is `[119 122.5]`.
- `'LatitudeLimit'`
  - Set the latitude range of the map to show.
  - It should be 1 by 2 numeric array.
  - Default is written in `fmt.m`.
- `'AdditionalCheck'`
  - Do additional check. If not passed, error will be raised.
  - It should be either `true` or `false`.
  - Default is `true`.
- `'Stacking'`
  - Stack the probabilities over a time range.
  - It should be `CalendarDuration`.
  - Default is `false`.
  - Example: with `...,'Stacking', calmonths(3)`, we have one plot every 3 months. In which the probability stacked in this interval is demonstrated. If `'PlotEpicenter'` is enabled, all target earthquakes will also be plotted at once in this time interval.
- `'PlotEpicenter'` (experimental)
  - Plot epicenter of target earthquakes (if there is).
  - Something may go wrong if `'Stacking'` is also enabled.

圖 15 plotProbability 所支援的自訂功能與選項。

`plotEQKTIP1` takes the following optional name-value pair arguments:

- `'ForecastingPhase'`
  - Set the time range for the forecasting phase
  - It has to be `calendarDuration`
  - Default is `calyears(1)`, which set forecasting phase(s) the succeeding one-year period right after the end of training phase(s).
- `'ShowTrainingPhase'`
  - Whether to also plot the EQK and TIP in the training phase or not.
  - Default is `false`.
- `'scatter'`
  - Plot TIP using the `scatter` function.
  - Default is `false`.
  - `'scatter'` and `'imagesc'` can both be `ture`.
- `'imagesc'`
  - Plot TIP using the `imagesc` function.
  - Default is `true`.
- `'Rank'`
  - Set which model in the best models to be applied for defining TIP.
  - Default is `1` (Plot TIP defined by the first-rank model).
- `'datetimeTickArguments'`
  - Customize the way to show time tick labels.
  - It takes the same input arguments as `datetime_ticks.m`
  - For example, `...'datetimeTickArguments', {"yy' mmm.", 1,'months'}` we have `datetime(2020,01,05)` demonstrated as `20' Jan` with `1` month interval.
- `'ShiftEQK2DateStart'`
  - Shift the exact time of an event to the beginning of the day.
  - Default is `false`.

圖 16 plotEQKTIP1 所支援的自訂功能與選項。

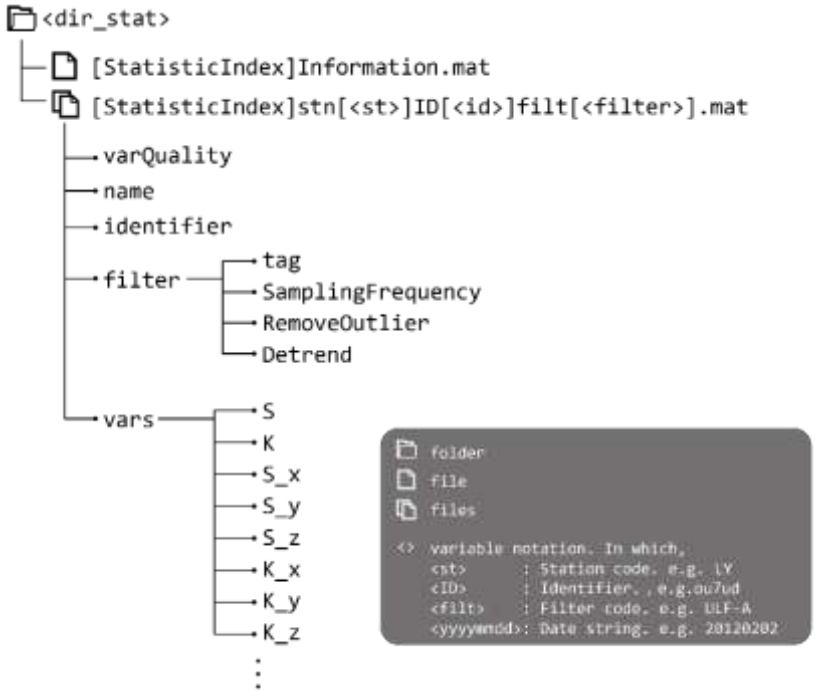

圖 17 statind 的輸出變數(StaticIndex)的資料結構。

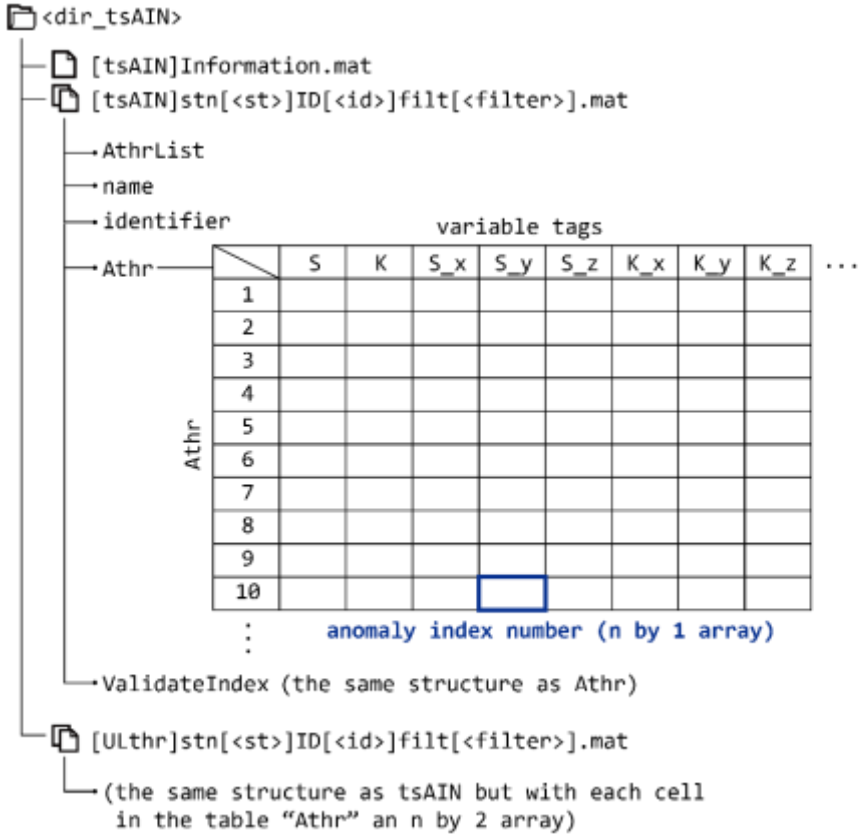

圖 18 anomalyind 的輸出變數(tsAIN)的資料結構。

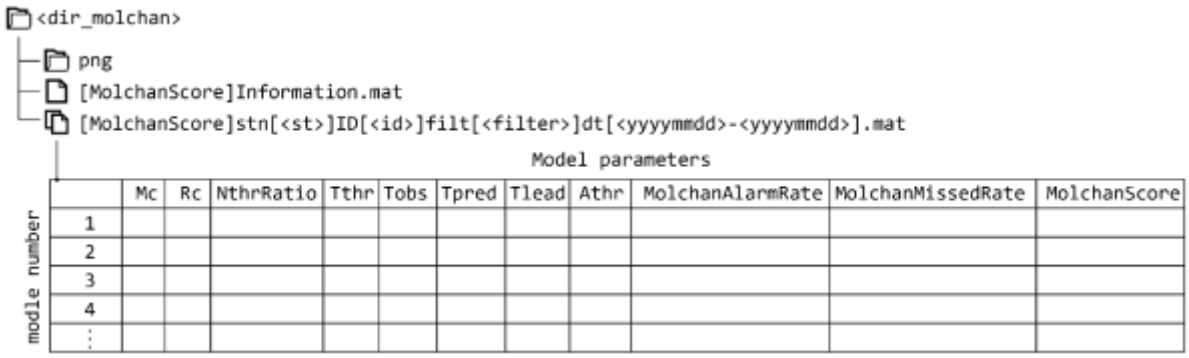

圖 19 molscore 的輸出變數(MolchanScore)的資料結構。

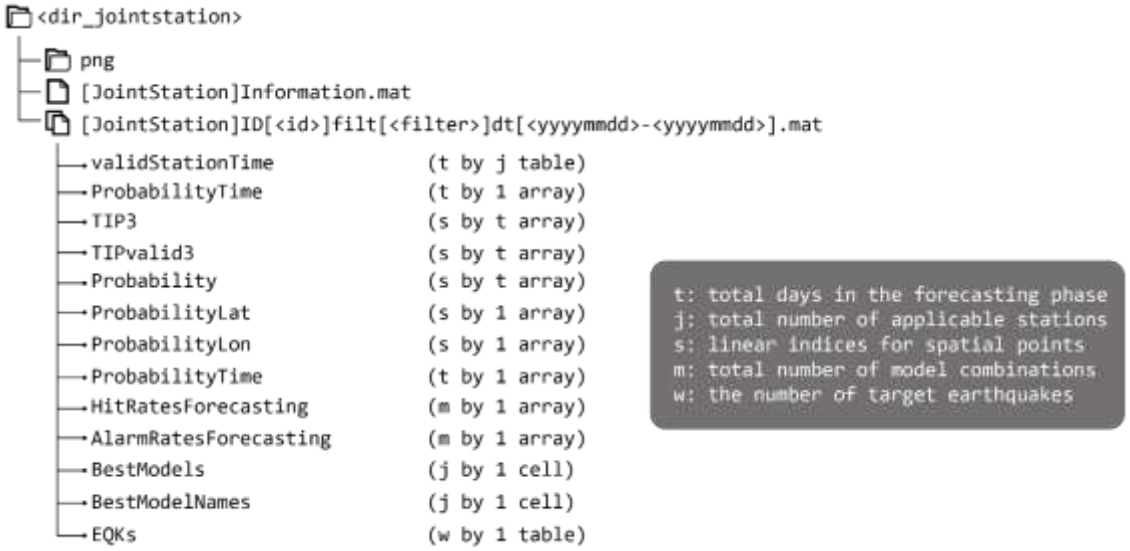

圖 20 molscore3 的輸出變數(JointStation)的資料結構。

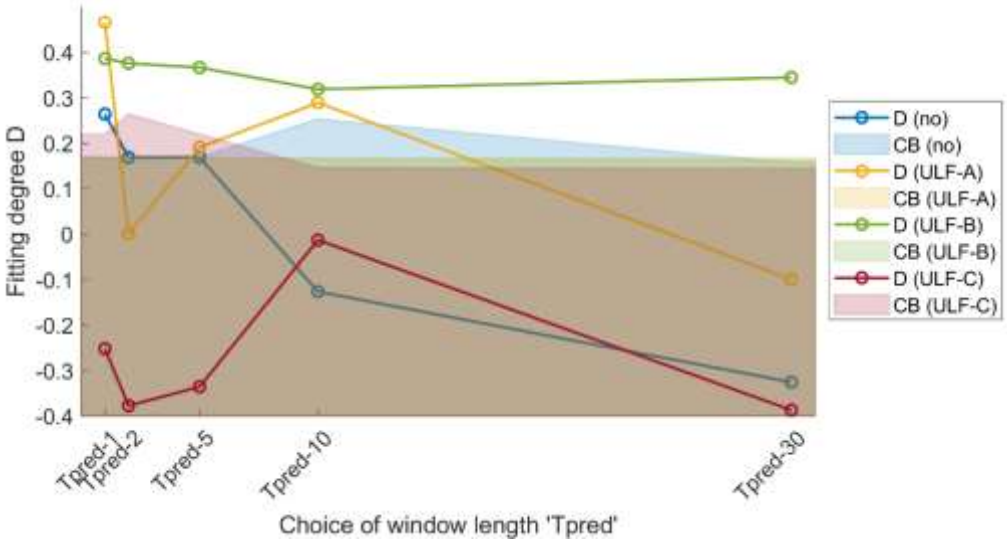

圖 21 各濾波頻段[未經濾波、0.001-0.003Hz(代號 ULF-A)、0.001-0.01Hz(代號 ULF-B)、0.001-0.1Hz(代號 ULF-C)]、五種預報期長度(Tpred=[1,2,5,10,30] days)下的擬合程度(Fitting Degree)值。擬合程度係指預報 TIP 與其涵蓋期間內的目標地震之擬合程度。預報 TIP 涵蓋 2014-Nov-17 至 2021-May-25，由滾動更新之最佳參數模型組合(係指各測站、各訓練期排名第一)所定義。模型最佳化根據 2007-Nov-16 至 2020-Nov-16 的地磁資料計算；其中，訓練期時間窗設為 7 年，最佳模型更新頻率為 1 年/次(即滾動時間窗步進長度為一年)。圖中半透明填色區塊為 95%信賴邊界；擬合程度(D 值)若落在邊界以上(外)，代表單靠隨機猜測而碰巧得到此數值的機率小於 5%。

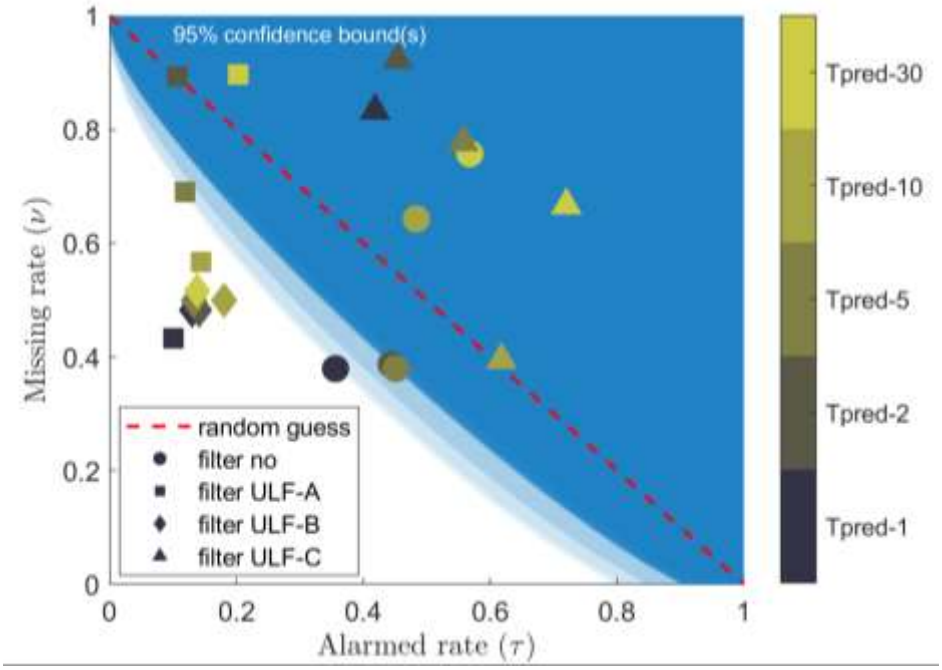

圖 22 各濾波頻段[未經濾波、0.001-0.003Hz(代號 ULF-A)、0.001-0.01Hz(代號 ULF-B)、0.001-0.1Hz(代號 ULF-C)]、五種預報期長度(Tpred=[1,2,5,10,30] days)下的預報 TIP 預警比例(Alarm rate τ)對目標地震遺漏率(Missing rate ν)。預報 TIP 涵蓋 2014-

Nov-17 至 2021-May-25，由滾動更新之最佳參數模型組合(係指各測站、各訓練期排名第一)所定義。模型最佳化根據 2007-Nov-16 至 2020-Nov-16 的地磁資料計算；其中，訓練期時間窗設為 7 年，最佳模型更新頻率為 1 年/次(即滾動時間窗步進長度為一年)。

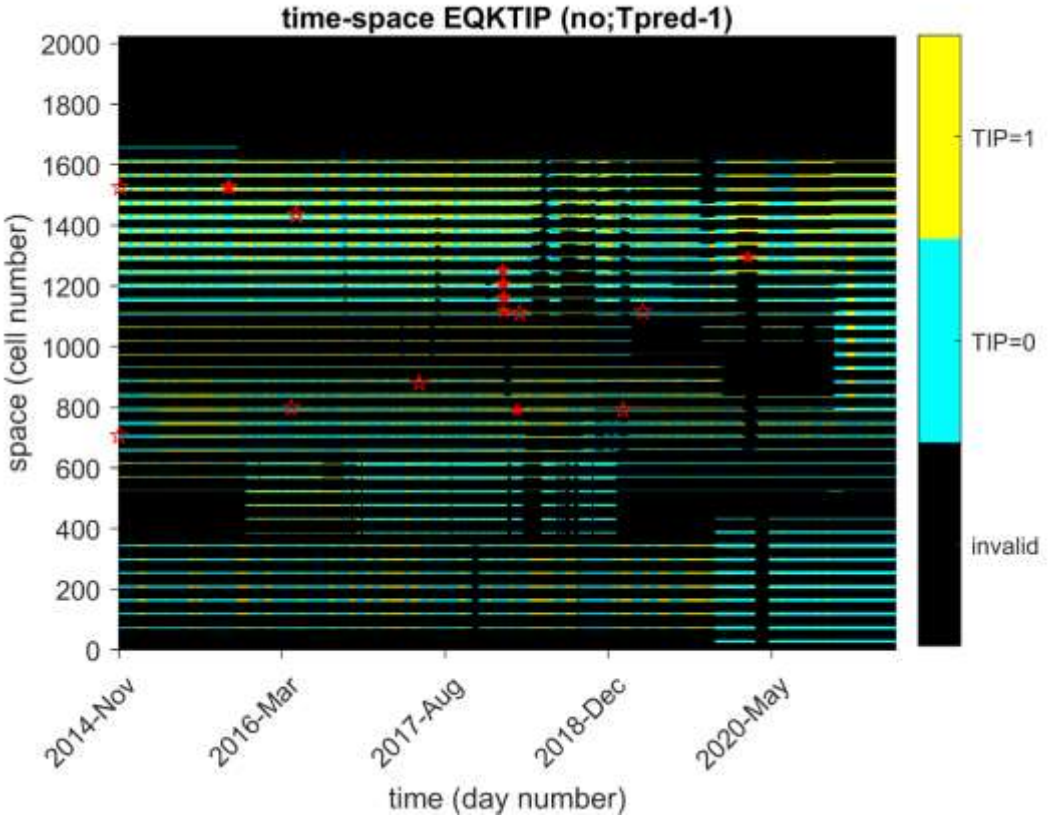

圖 23 承圖 21 及圖 22，預報 TIP 與目標地震一覽。

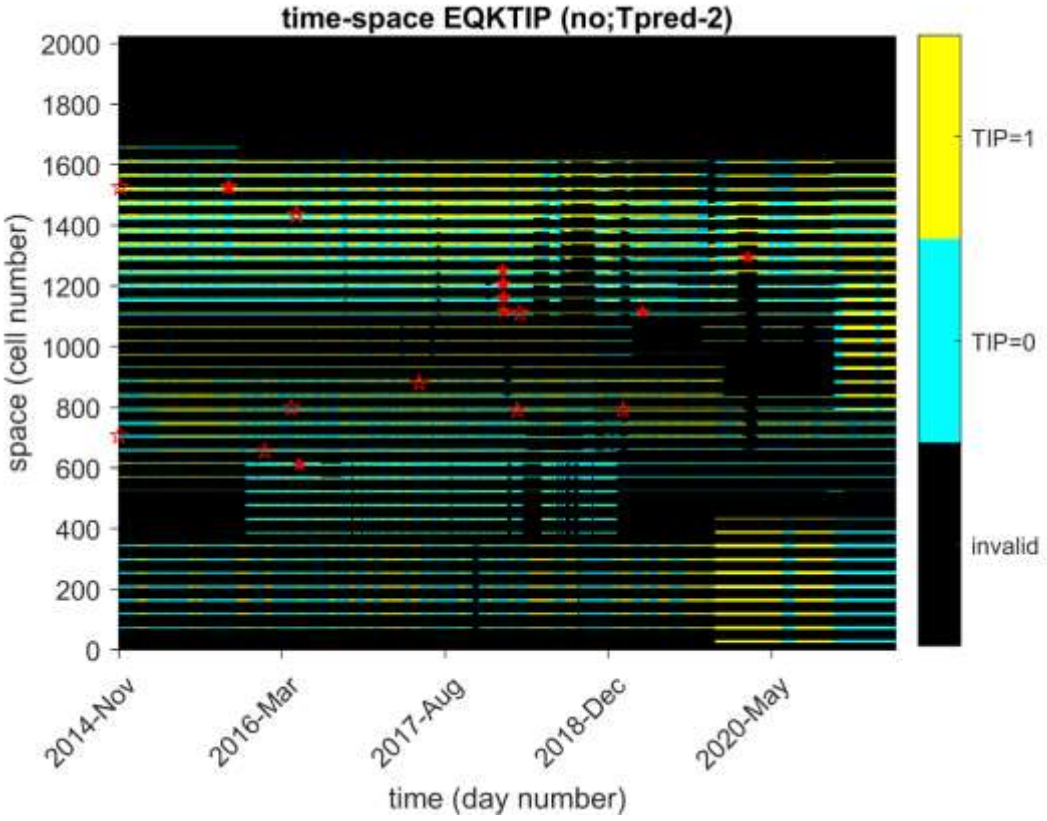

圖 24 承圖 21 及圖 22，預報 TIP 與目標地震一覽。

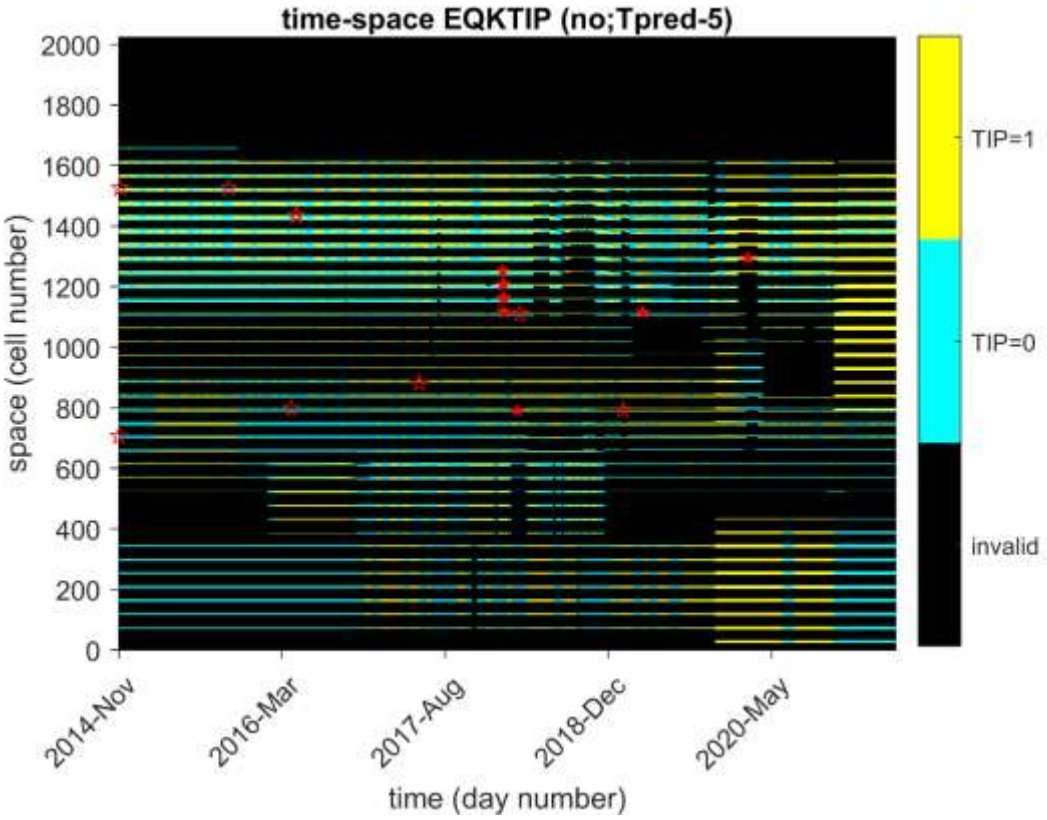

圖 25 承圖 21 及圖 22，預報 TIP 與目標地震一覽。

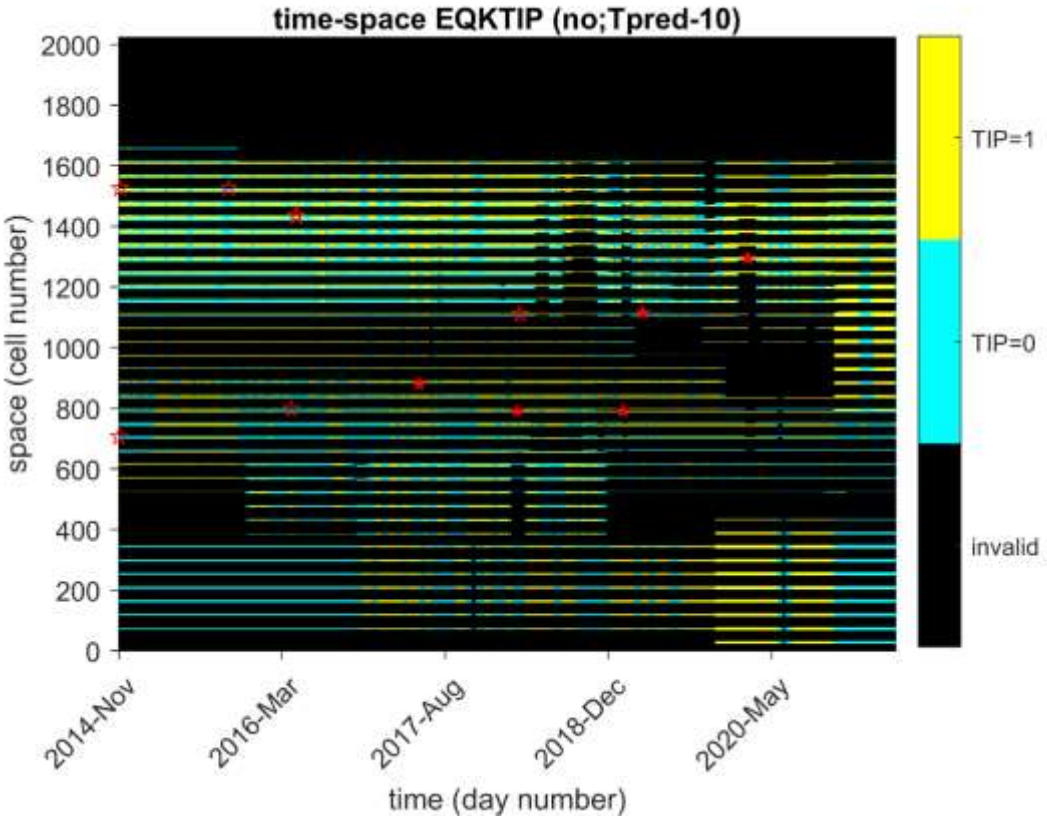

圖 26 承圖 21 及圖 22，預報 TIP 與目標地震一覽。

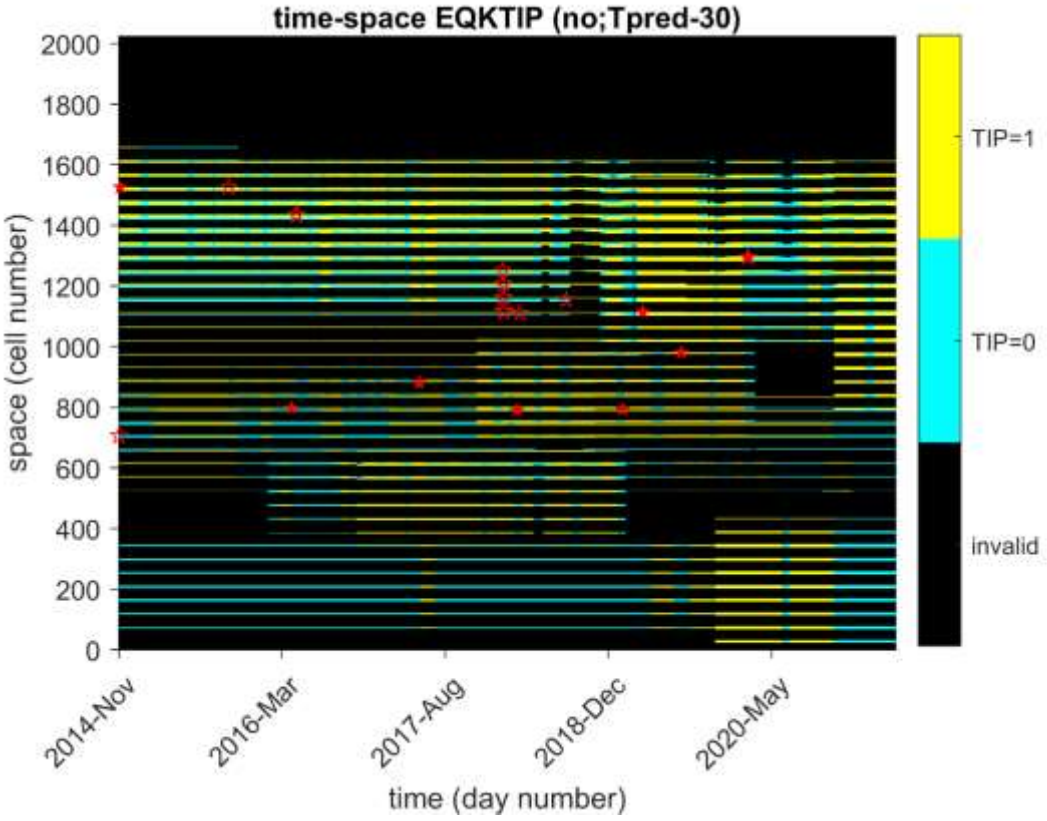

圖 27 承圖 21 及圖 22，預報 TIP 與目標地震一覽。

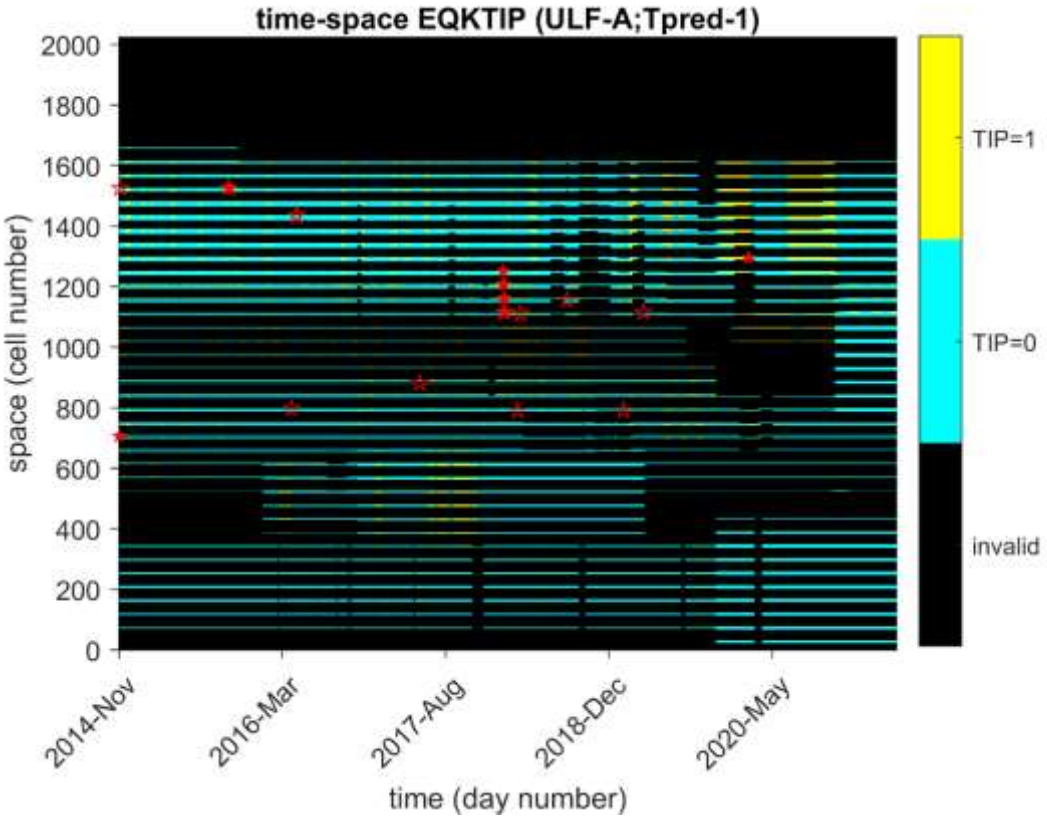

圖 28 承圖 21 及圖 22，預報 TIP 與目標地震一覽。

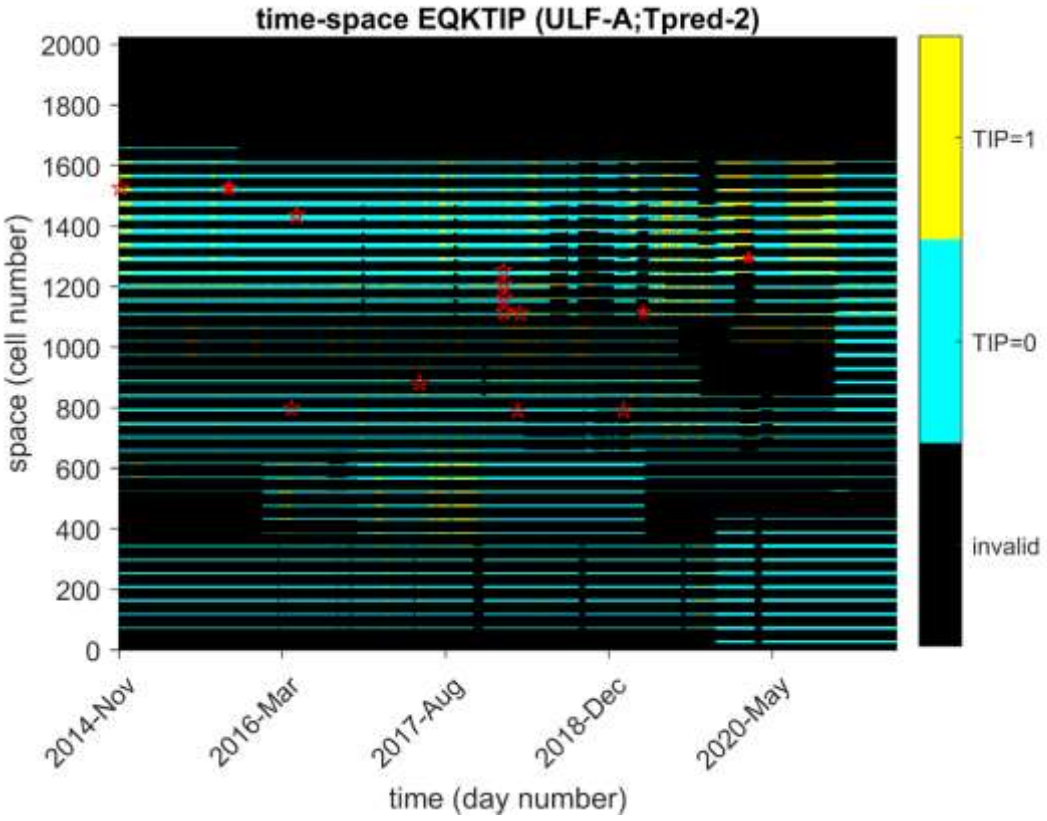

圖 29 承圖 21 及圖 22，預報 TIP 與目標地震一覽。

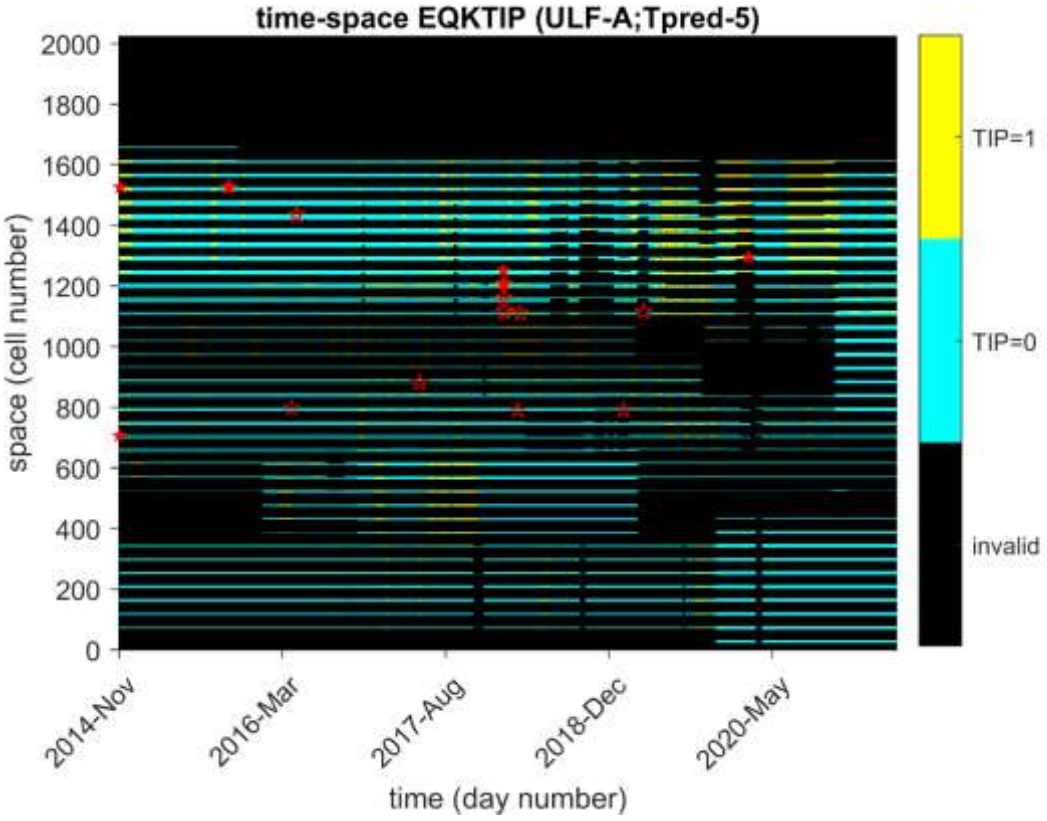

圖 30 承圖 21 及圖 22，預報 TIP 與目標地震一覽。

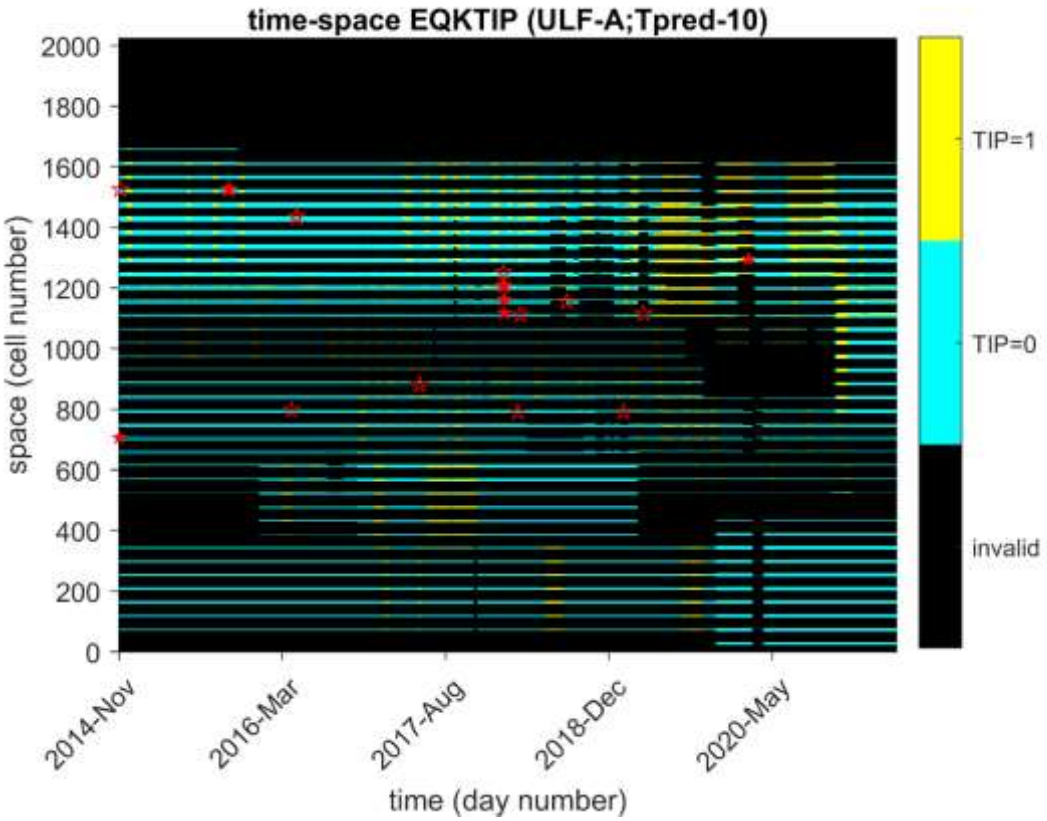

圖 31 承圖 21 及圖 22，預報 TIP 與目標地震一覽。

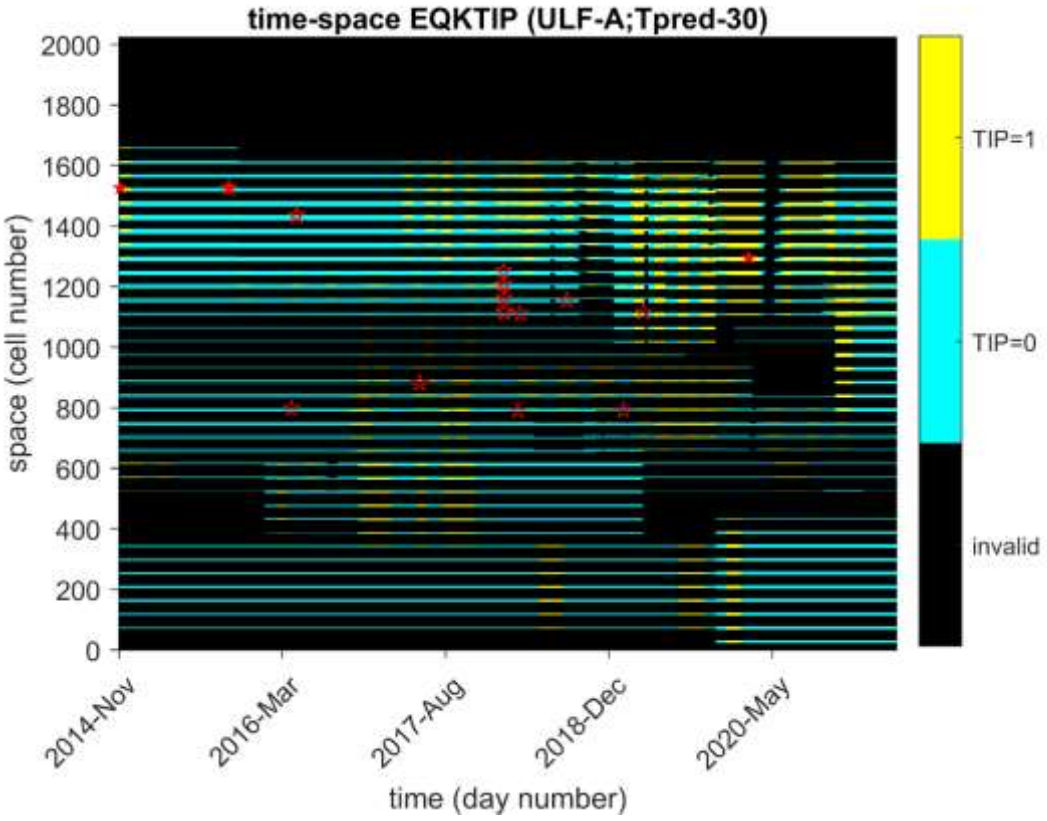

圖 32 承圖 21 及圖 22，預報 TIP 與目標地震一覽。

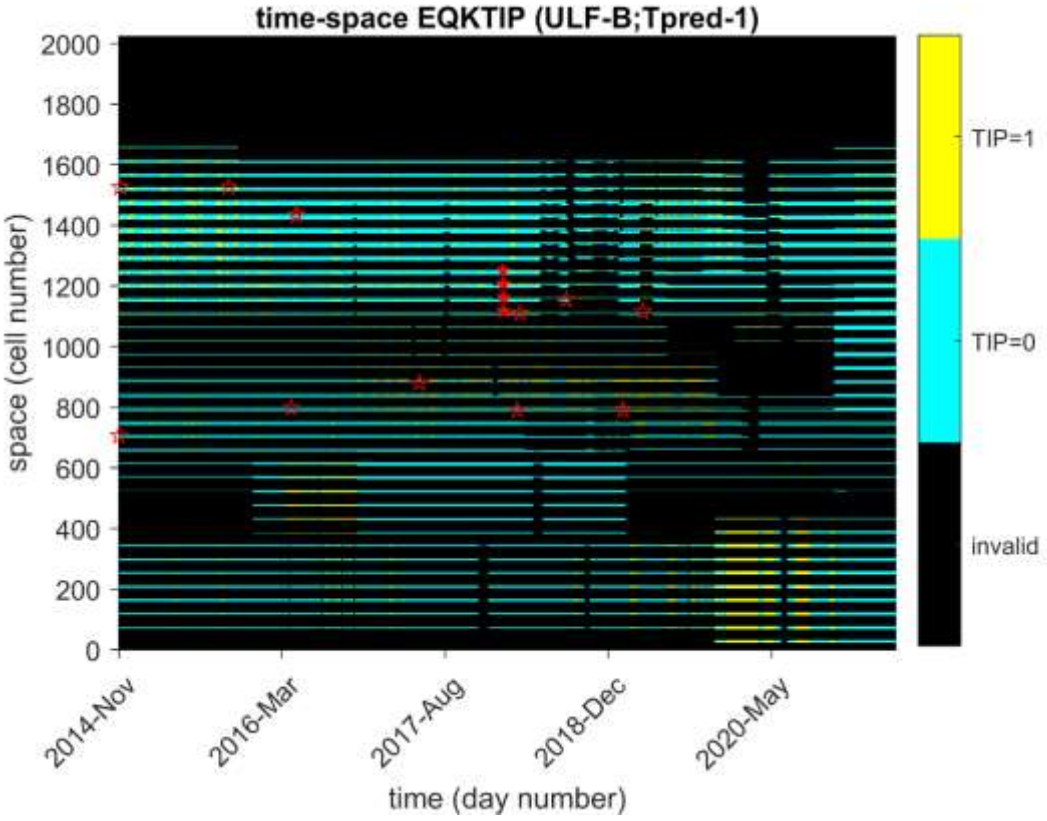

圖 33 承圖 21 及圖 22，預報 TIP 與目標地震一覽。

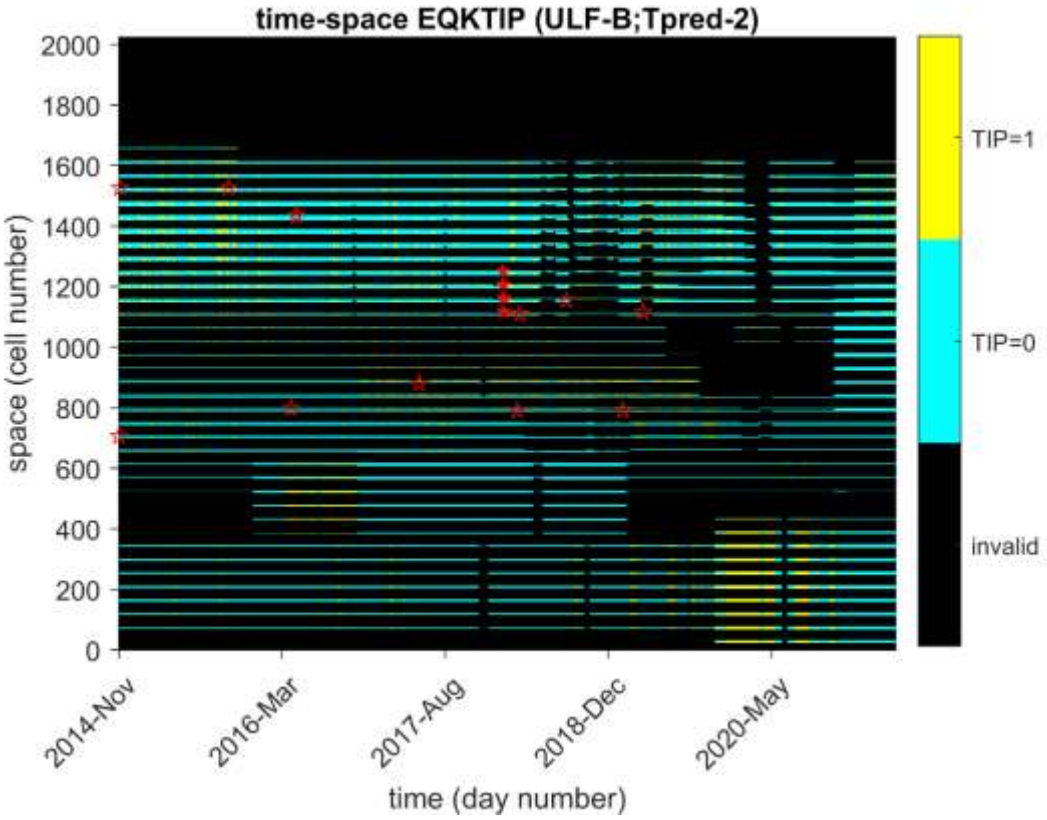

圖 34 承圖 21 及圖 22，預報 TIP 與目標地震一覽。

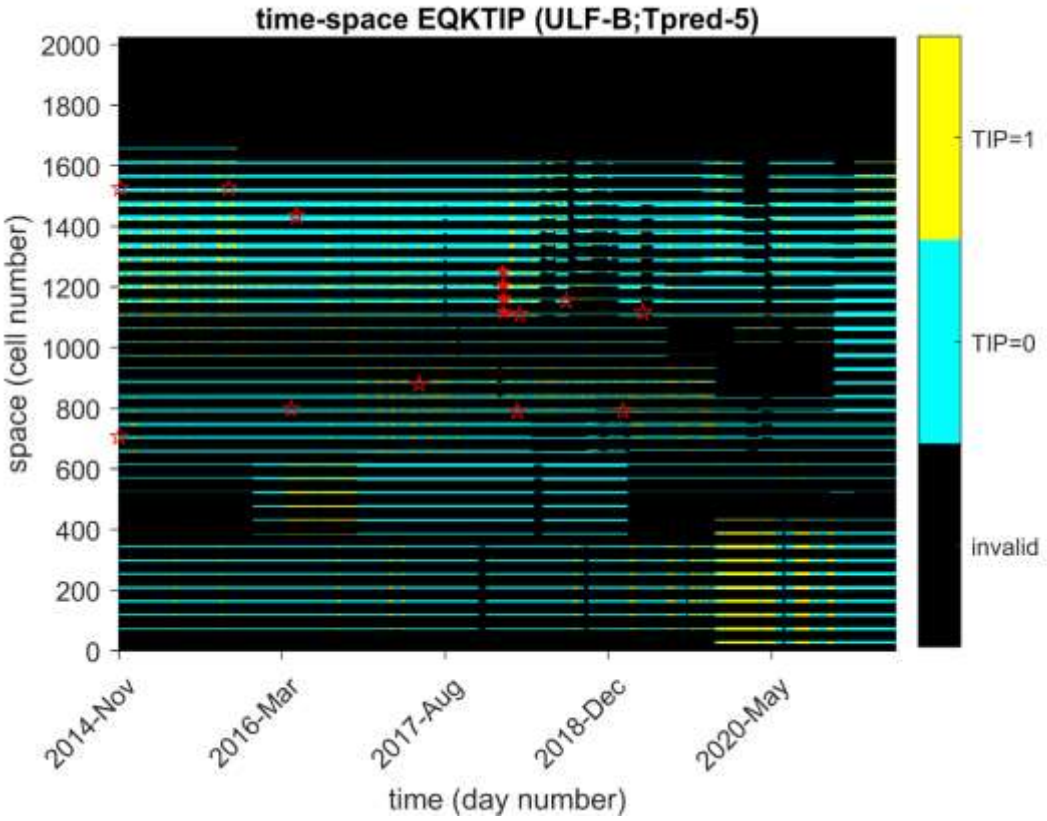

圖 35 承圖 21 及圖 22，預報 TIP 與目標地震一覽。

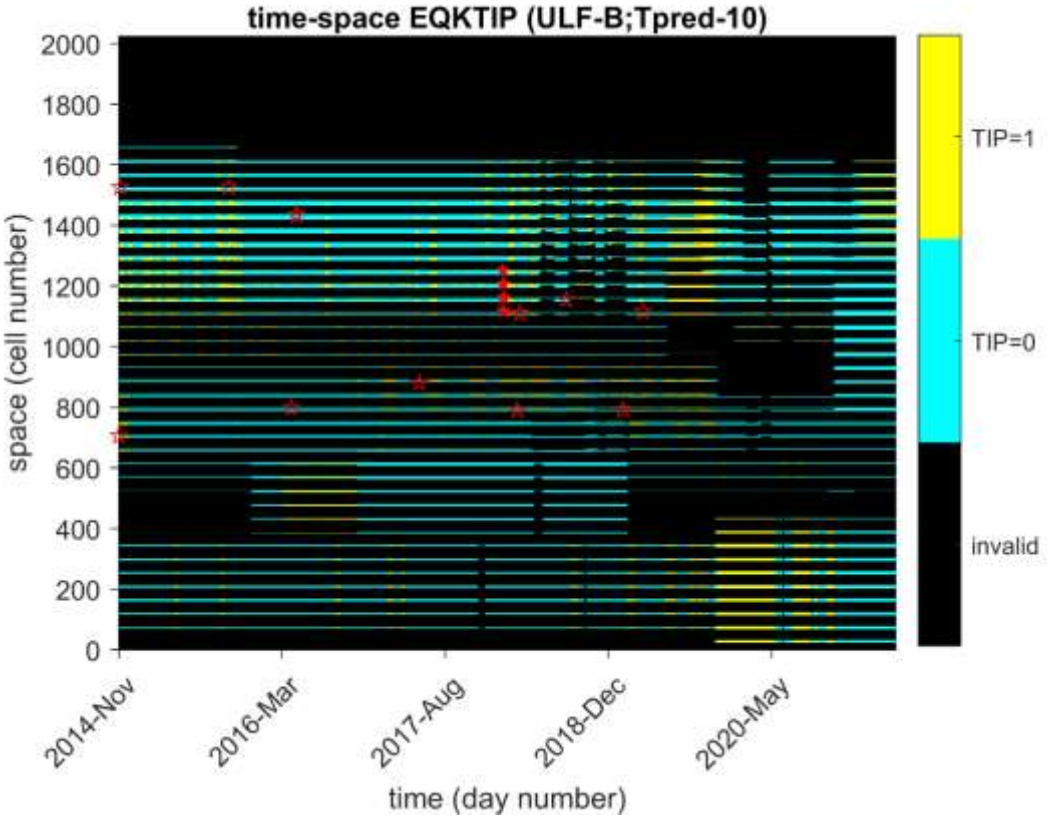

圖 36 承圖 21 及圖 22，預報 TIP 與目標地震一覽。

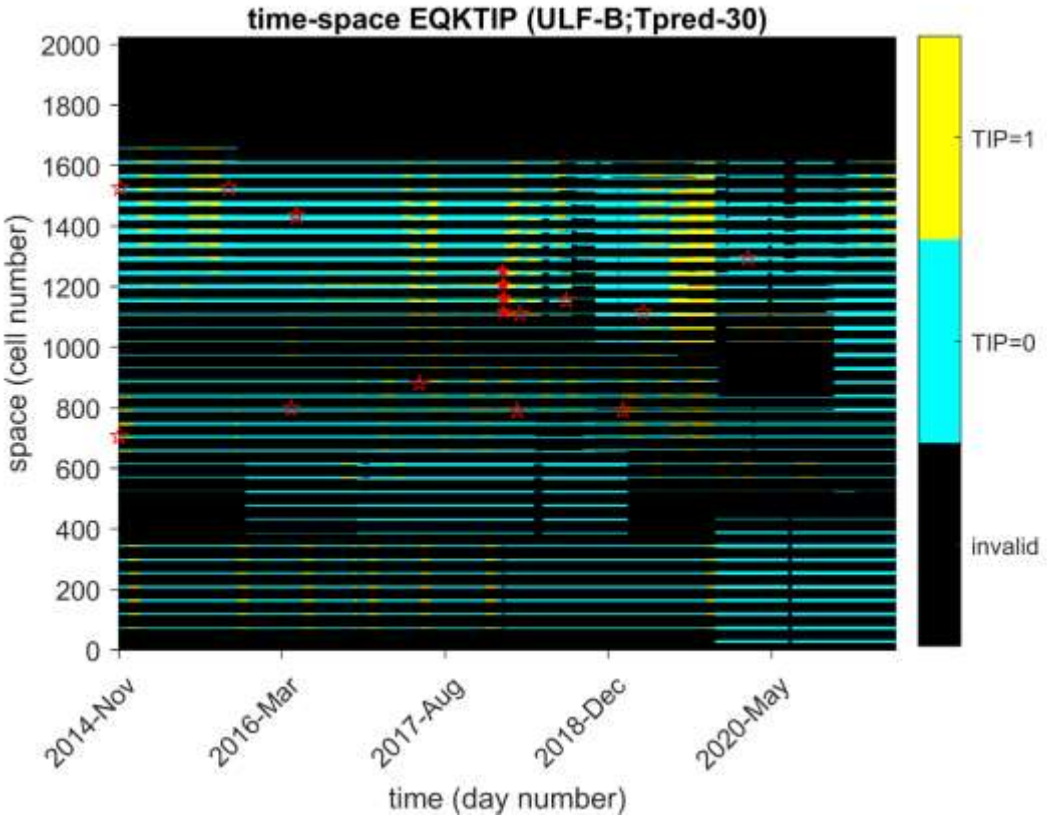

圖 37 承圖 21 及圖 22，預報 TIP 與目標地震一覽。

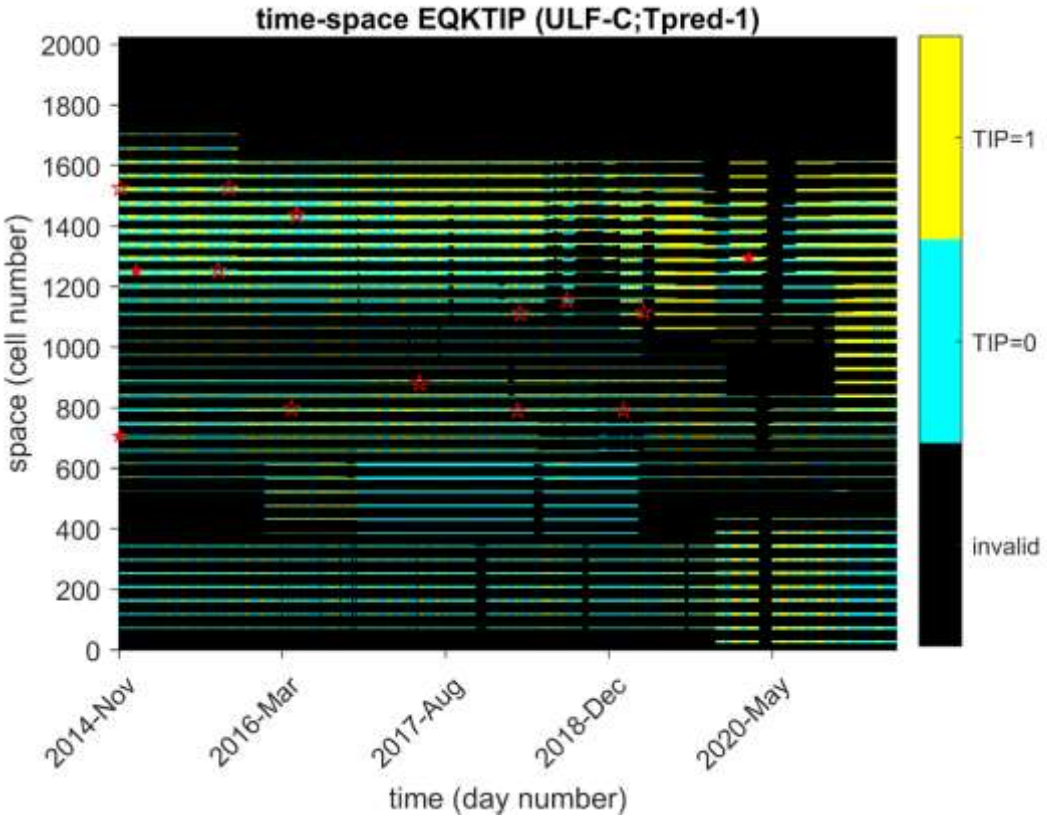

圖 38 承圖 21 及圖 22，預報 TIP 與目標地震一覽。

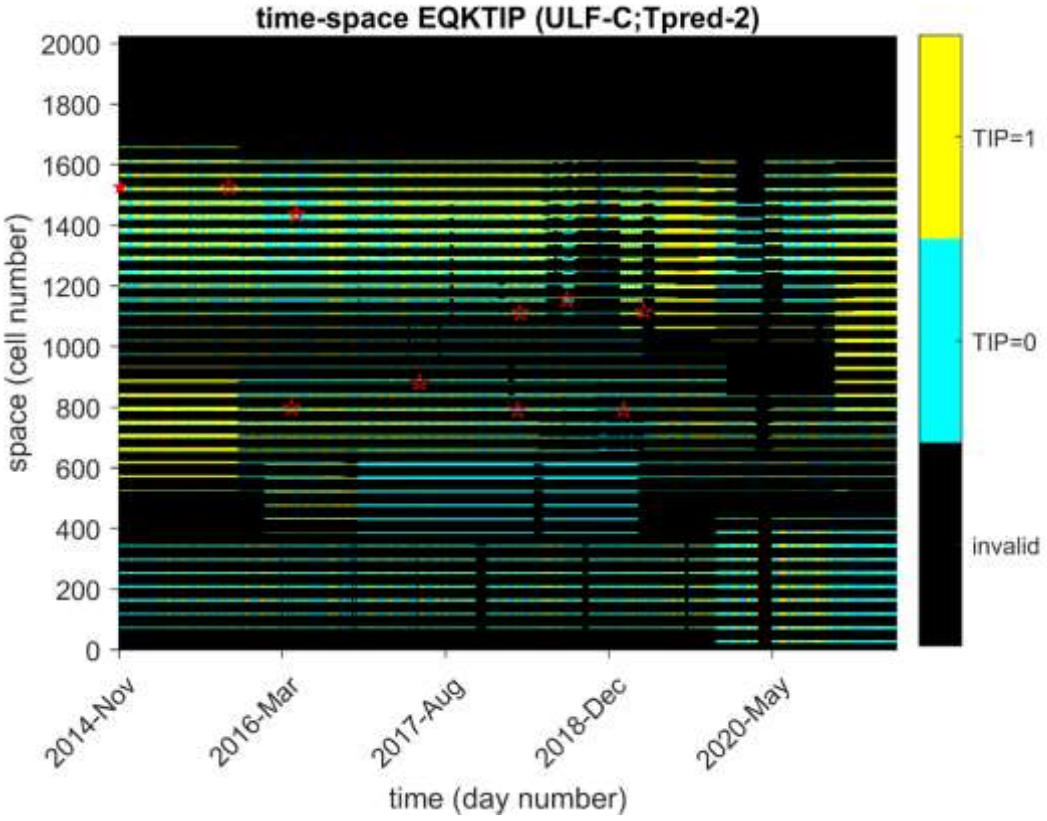

圖 39 承圖 21 及圖 22，預報 TIP 與目標地震一覽。

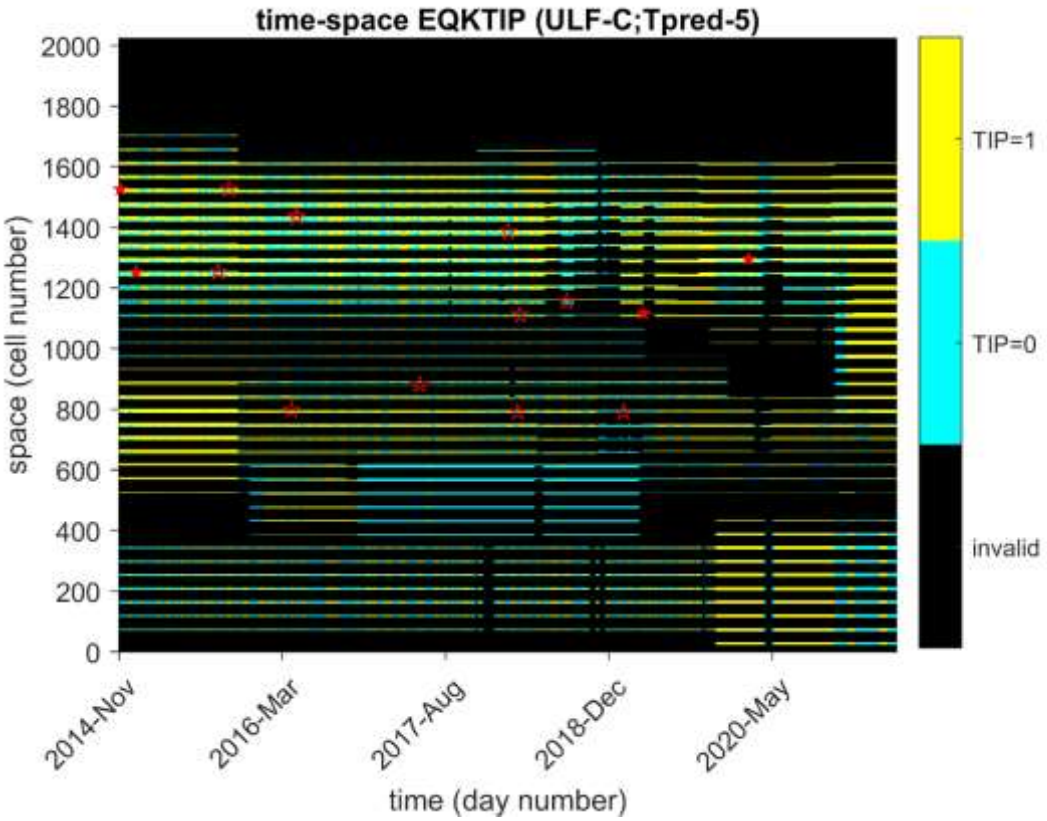

圖 40 承圖 21 及圖 22，預報 TIP 與目標地震一覽。

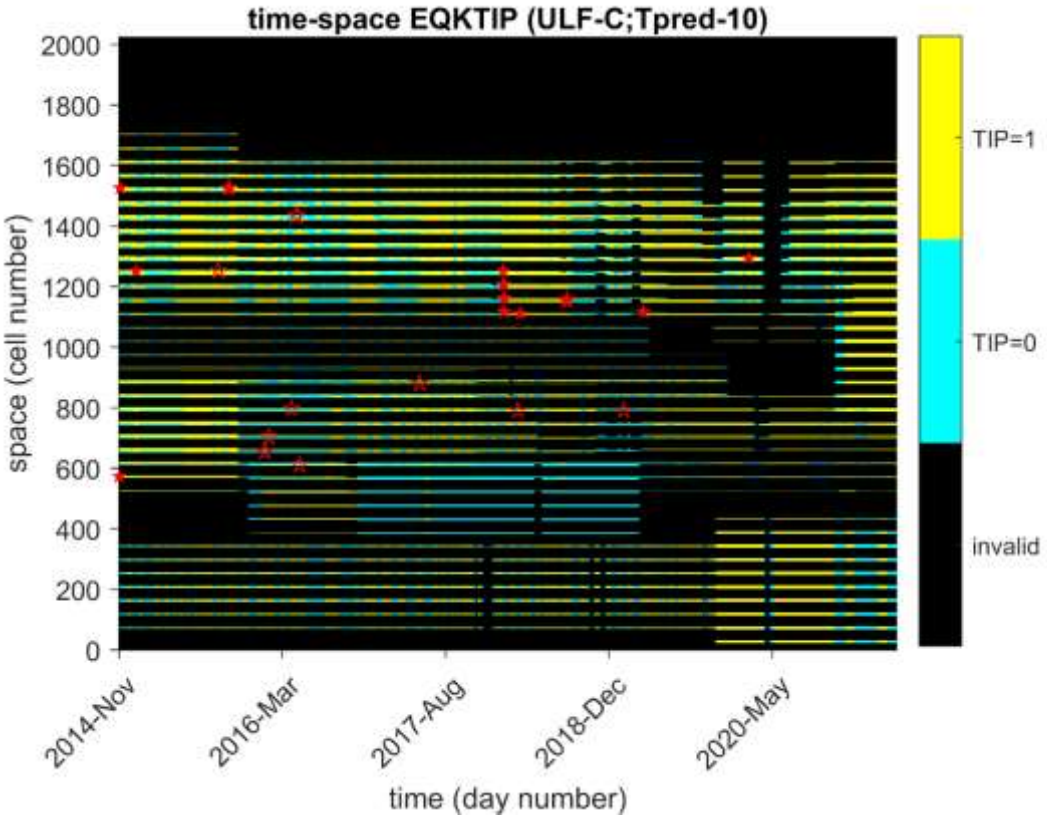

圖 41 承圖 21 及圖 22，預報 TIP 與目標地震一覽。

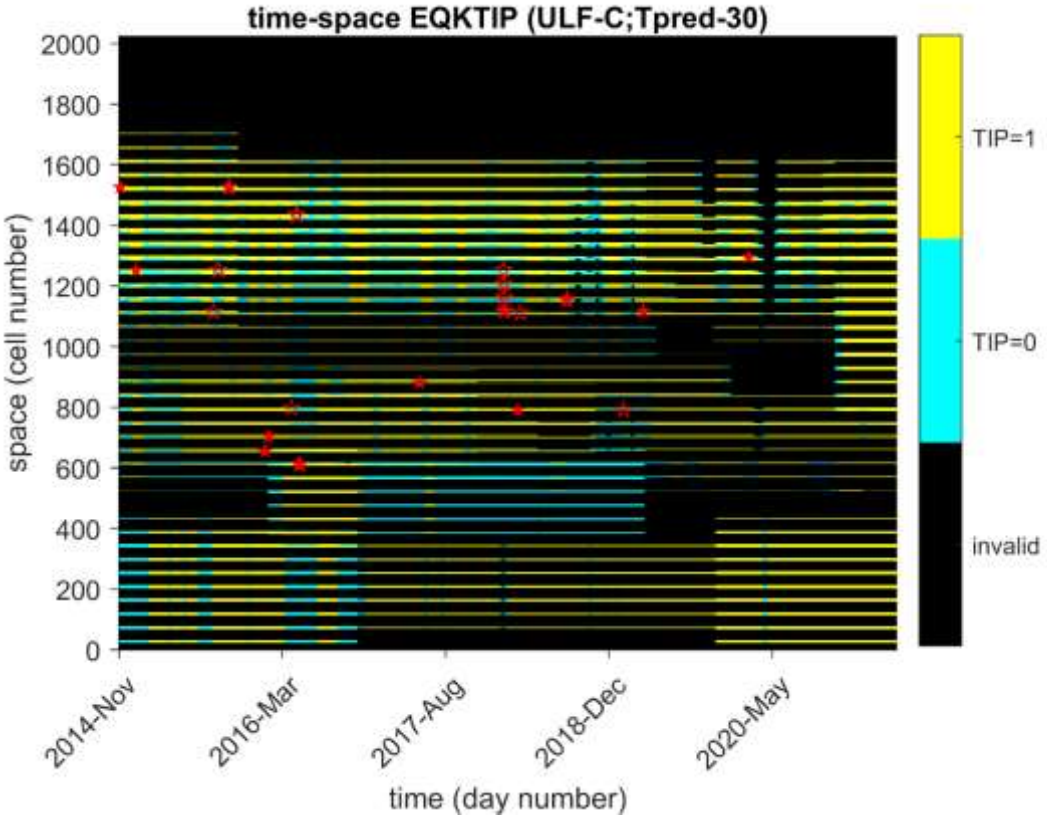

圖 42 承圖 21 及圖 22，預報 TIP 與目標地震一覽。

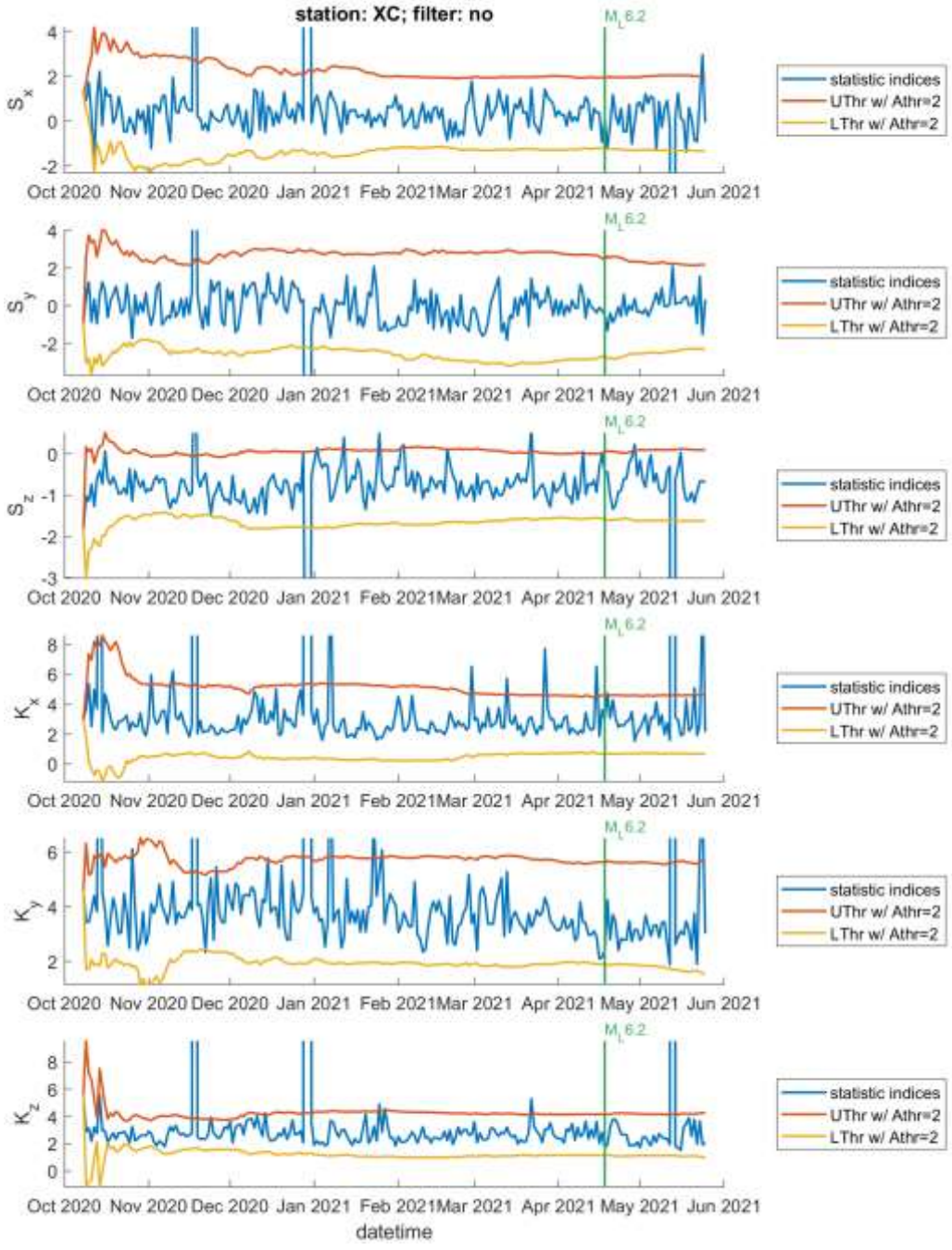

圖 43 新城(XC)站、基於未濾波頻段的三分量地磁資料計算之日統計指標[偏度(S)與峰度(K)]在個案發生前後數月之時間序列。圖中標示了$A_{thr} = 2$ 之參考域值上下界；個案地震以綠色垂直線標示。

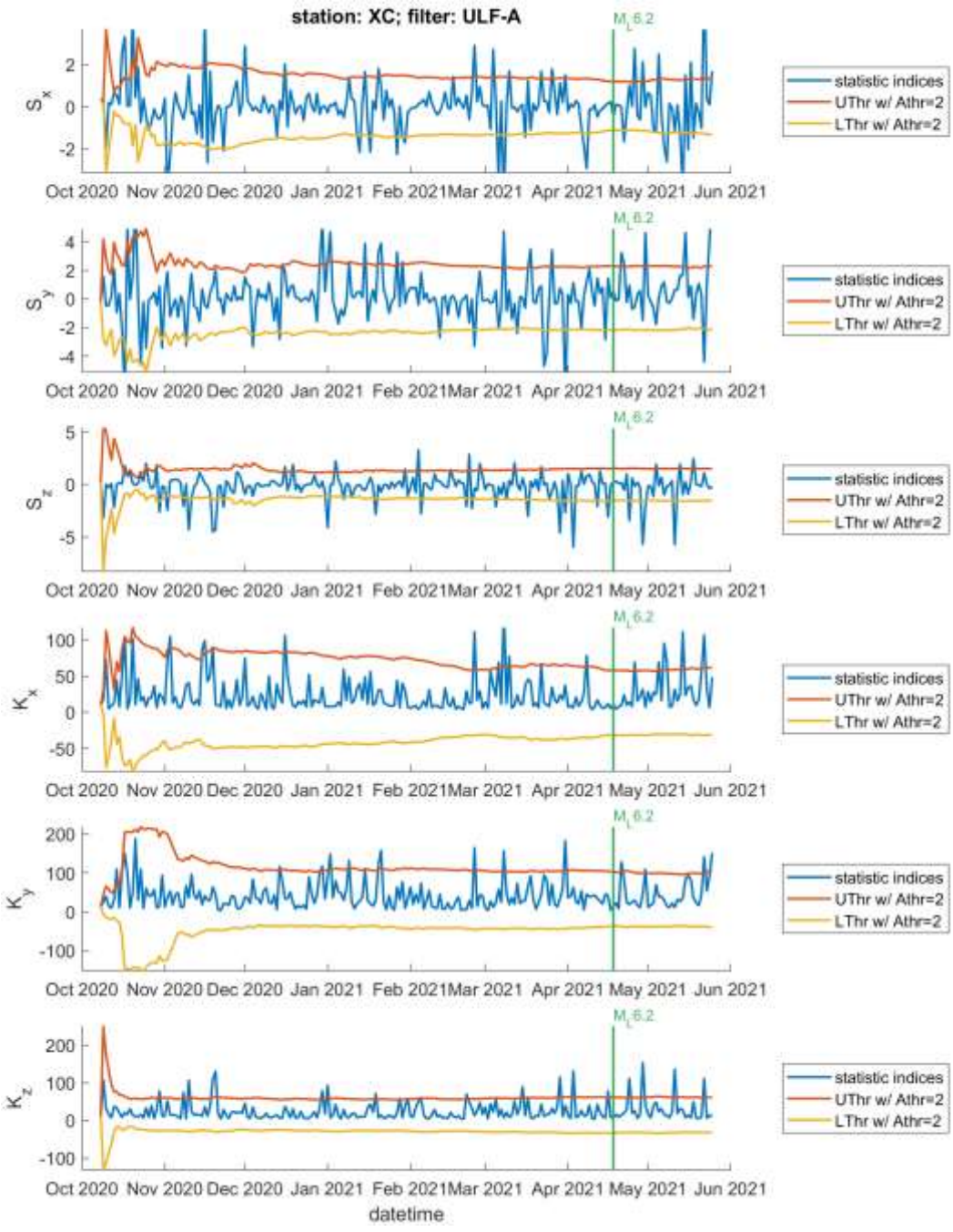

圖 44 新城(XC)站、基於 ULF-A 濾波頻段的三分量地磁資料計算之日統計指標[偏度(S)與峰度(K)]在個案發生前後數月之時間序列。圖中標示了$A_{thr} = 2$ 之參考域值上下界；個案地震以綠色垂直線標示。

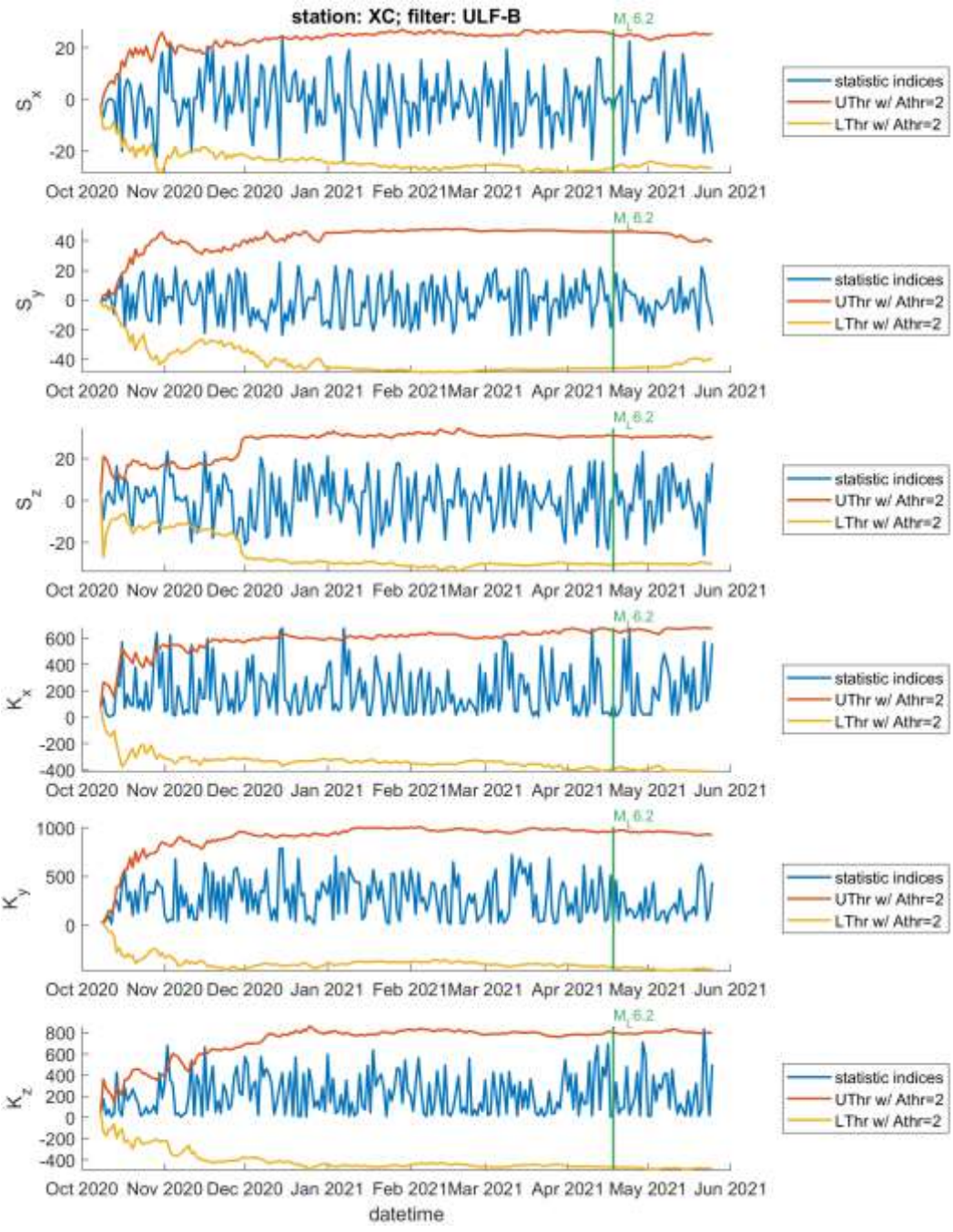

圖 45 新城(XC)站、基於 ULF-B 濾波頻段的三分量地磁資料計算之日統計指標[偏度(S)與峰度(K)]在個案發生前後數月之時間序列。圖中標示了$A_{thr} = 2$ 之參考域值上下界；個案地震以綠色垂直線標示。

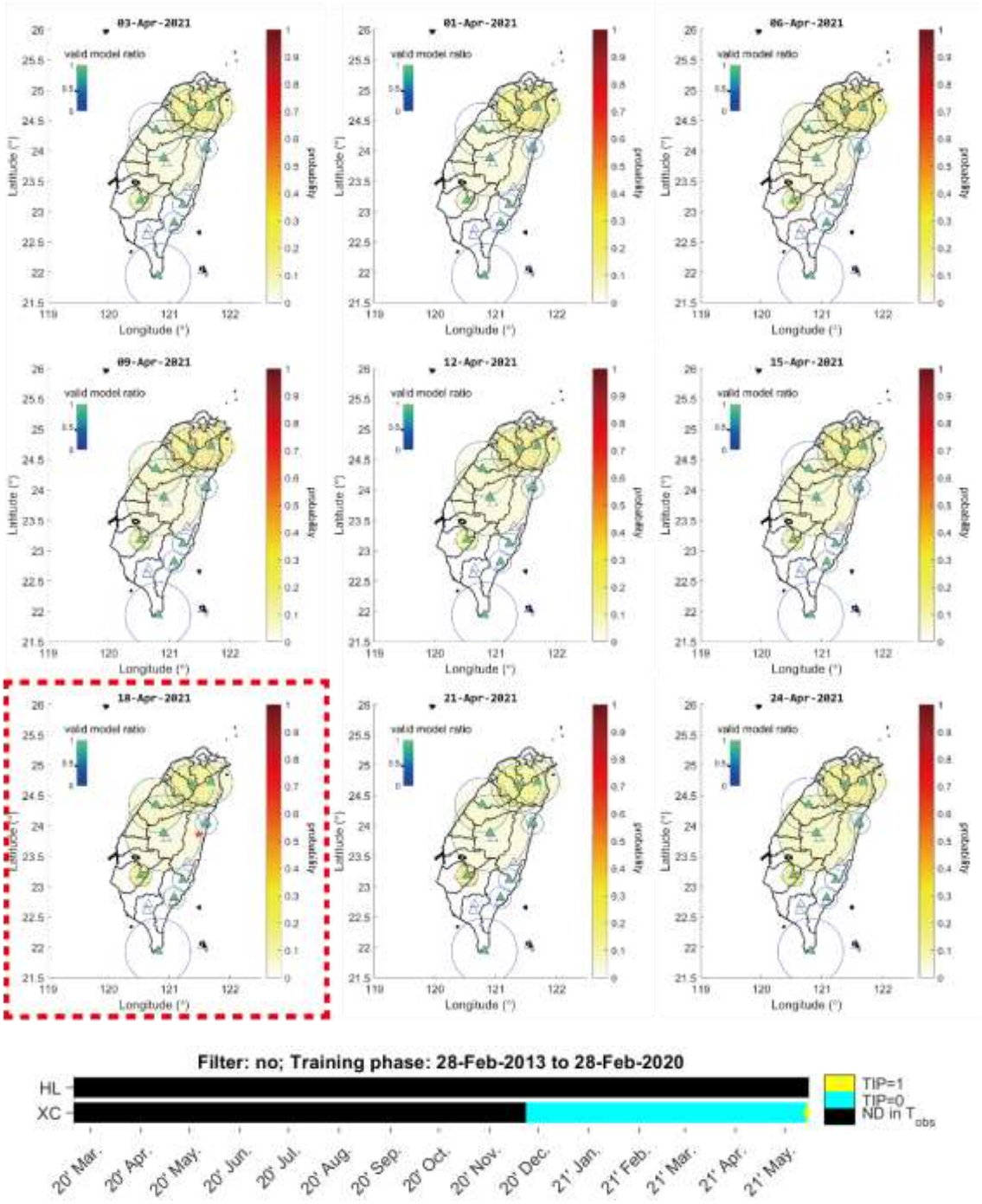

圖 46 (top)個案地震發生該月之 MagTIP 機率預報。機率預報使用 2013 年 2 月 28 日至 2020 年 2 月 28 日的訓練資料進行模型最佳化。 (bottom)最佳模型(rank 1)於訓練期截止後的預報 TIP。

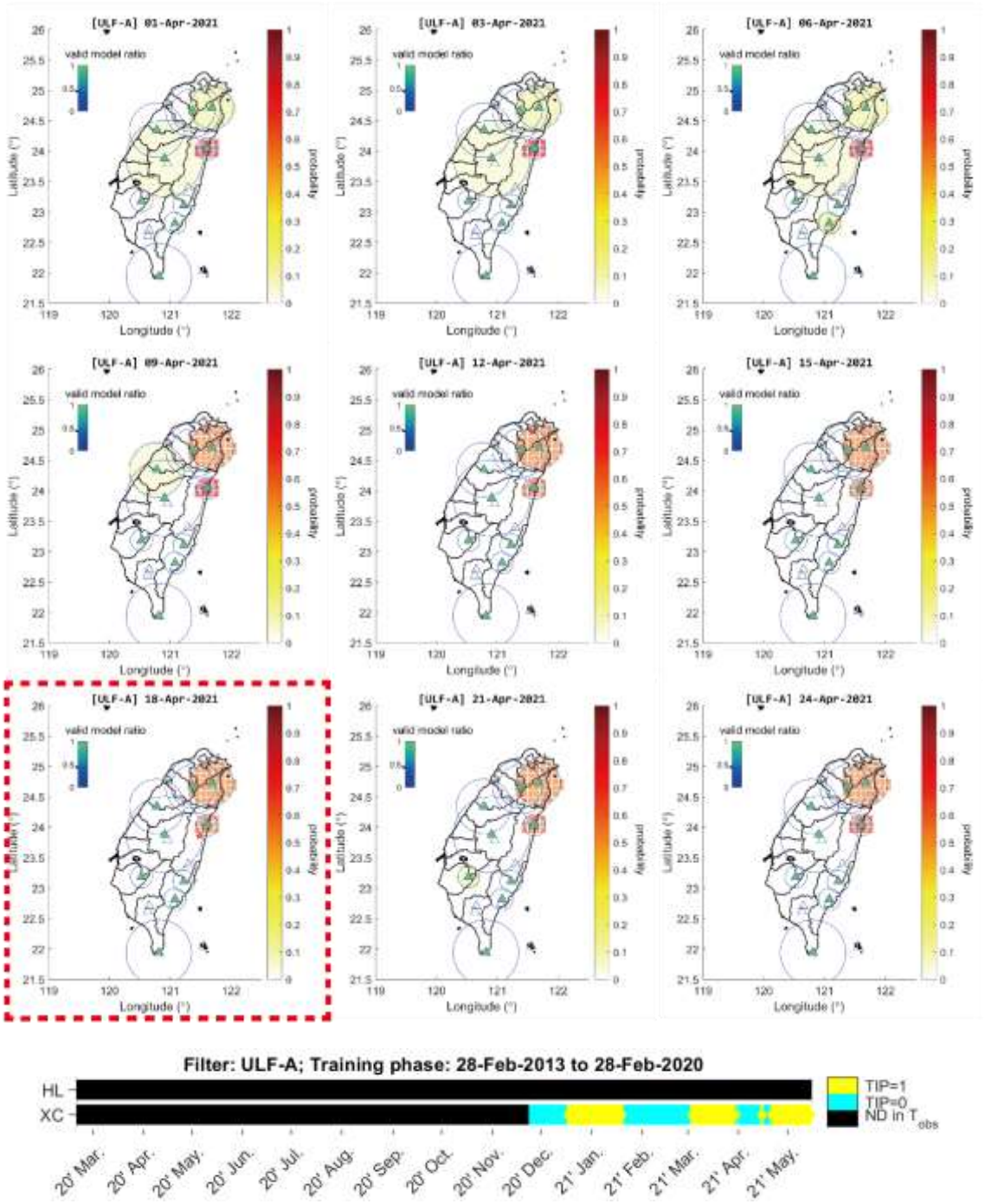

圖 47 (top)個案地震發生該月之 MagTIP 機率預報。機率預報使用 2013 年 2 月 28 日至 2020 年 2 月 28 日的訓練資料進行模型最佳化。 (bottom)最佳模型(rank 1)於訓練期截止後的預報 TIP。

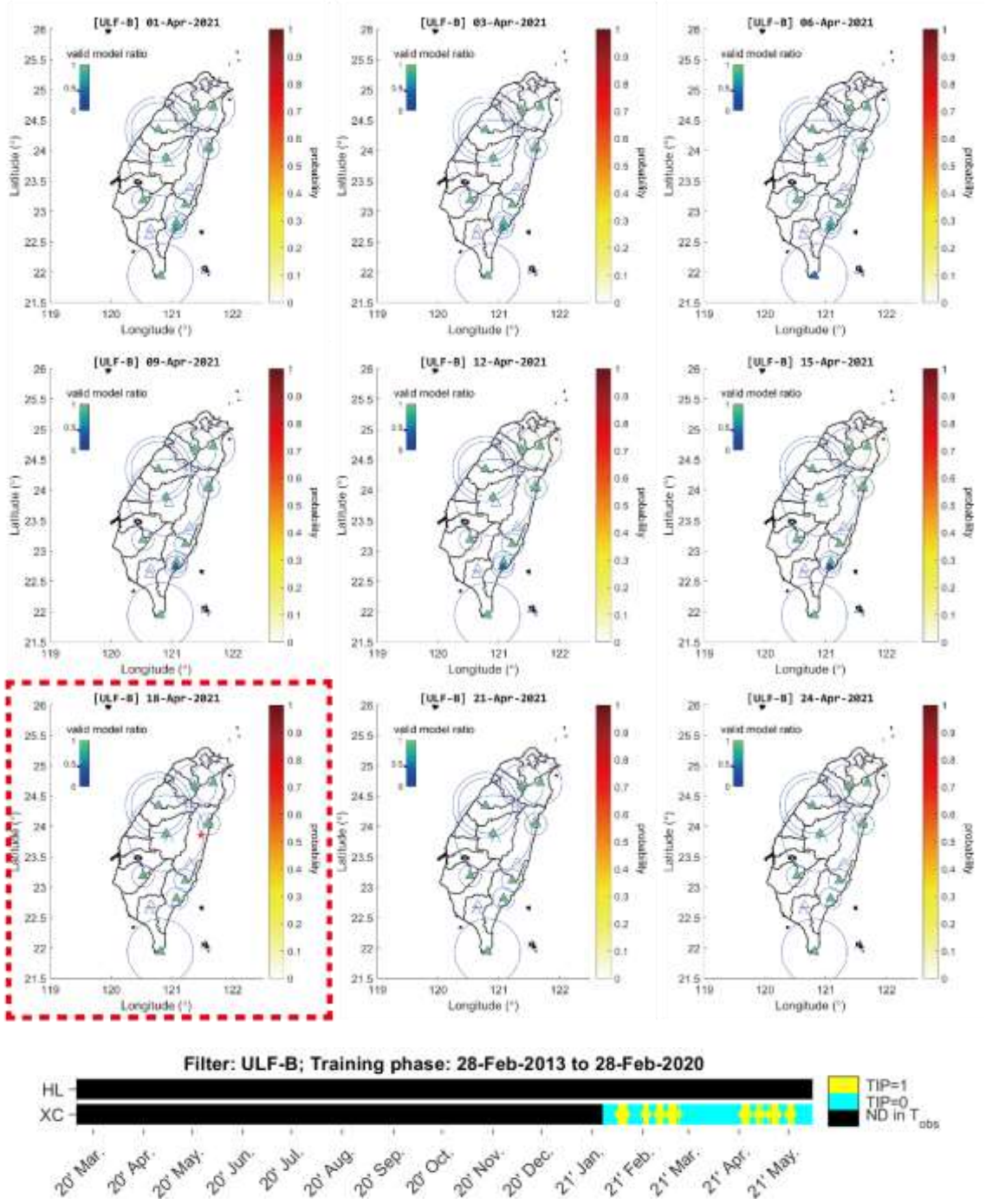

圖 48 (top)個案地震發生該月之 MagTIP 機率預報。機率預報使用 2013 年 2 月 28 日至 2020 年 2 月 28 日的訓練資料進行模型最佳化。 (bottom)最佳模型(rank 1)於訓練期截止後的預報 TIP。

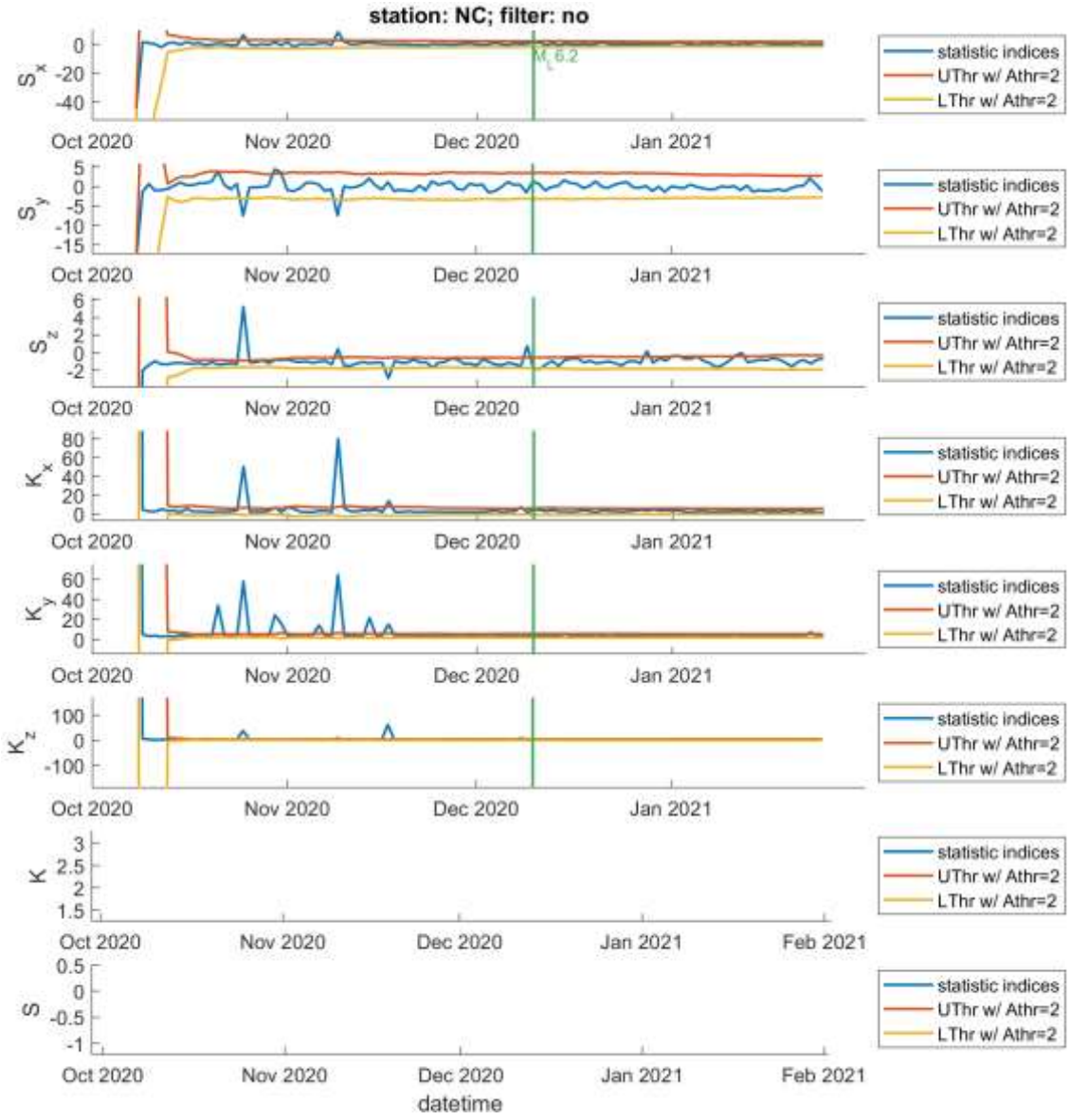

圖 49 內城(NC)站、基於未濾波頻段的三分量地磁資料計算之日統計指標[偏度(S)與峰度(K)]在個案發生前後數月之時間序列。圖中標示了$A_{thr} = 2$ 之參考域值上下界；個案地震以綠色垂直線標示。

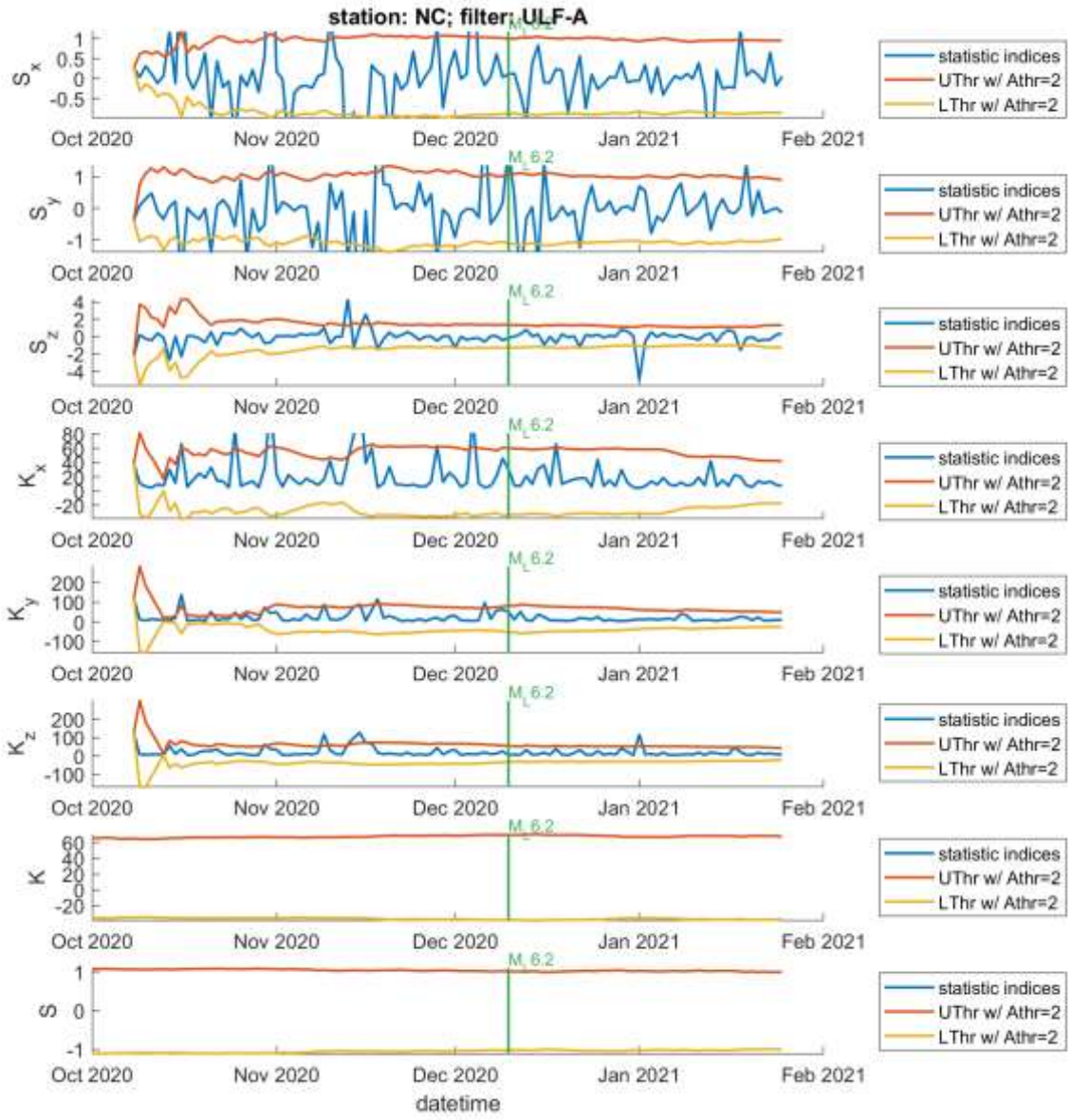

圖 50 內城(NC)站、基於 ULF-A 濾波頻段的三分量地磁資料計算之日統計指標[偏度(S)與峰度(K)]在個案發生前後數月之時間序列。圖中標示了$A_{thr} = 2$ 之參考域值上下界；個案地震以綠色垂直線標示。

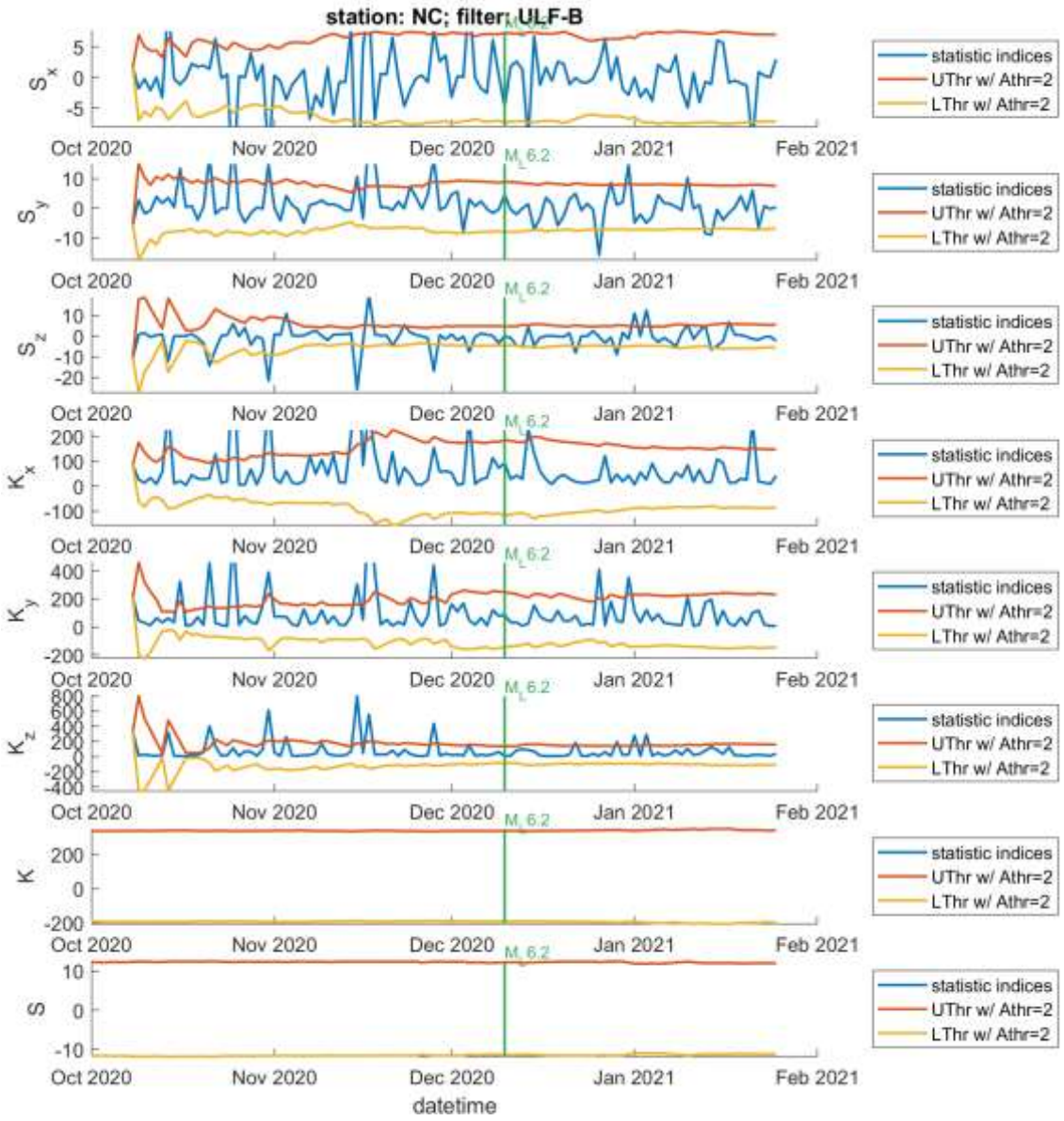

圖 51 內城(NC)站、基於 ULF-B 濾波頻段的三分量地磁資料計算之日統計指標[偏度(S)與峰度(K)]在個案發生前後數月之時間序列。圖中標示了$A_{thr} = 2$ 之參考域值上下界；個案地震以綠色垂直線標示。

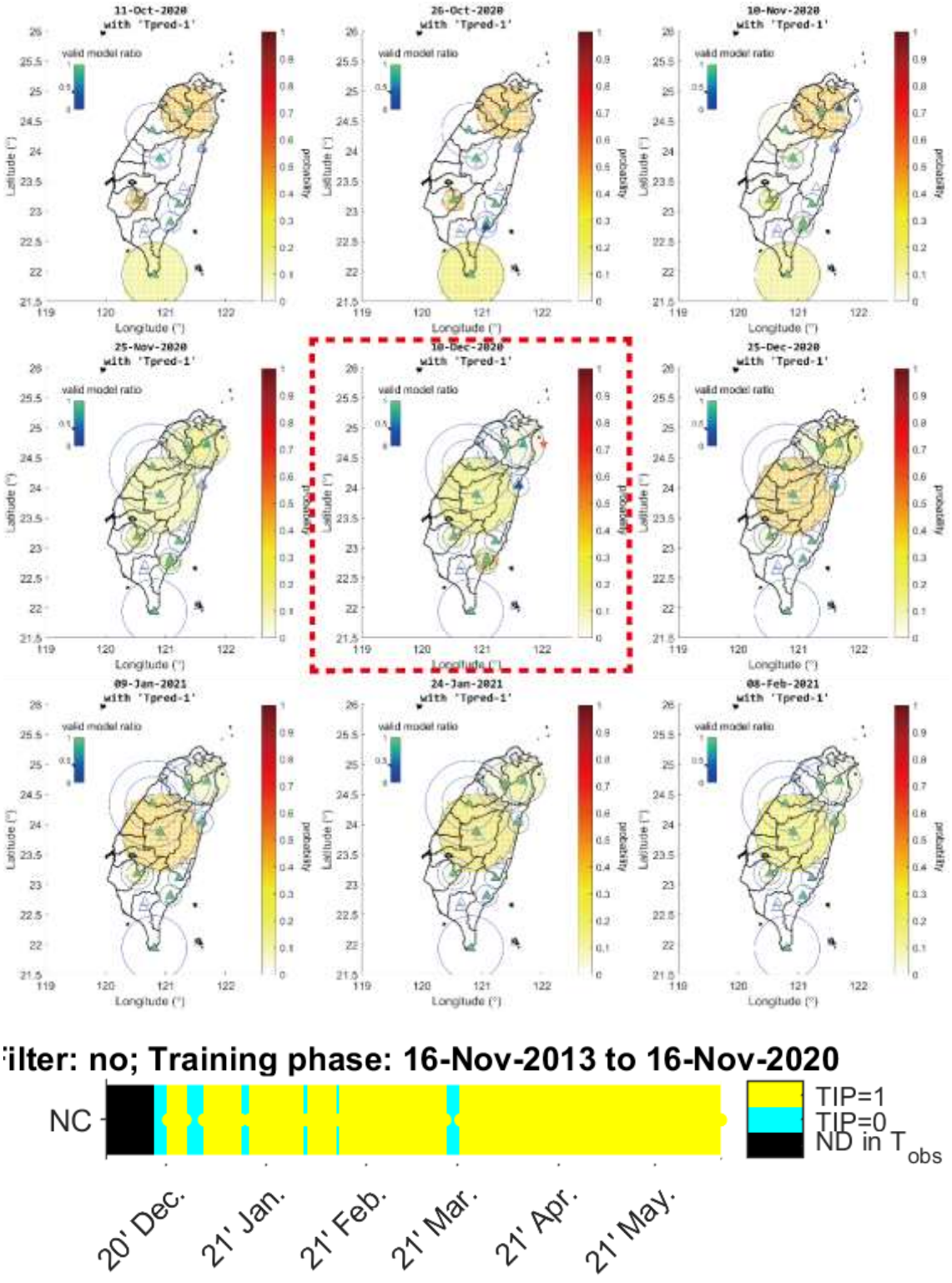

圖 52 (top)個案地震發生前後之 MagTIP 機率預報。機率預報使用 2013 年 11 月 16 日至 2020 年 11 月 16 日的訓練資料進行模型最佳化。(bottom)最佳模型(rank 1)於訓練期截止後的預報 TIP。

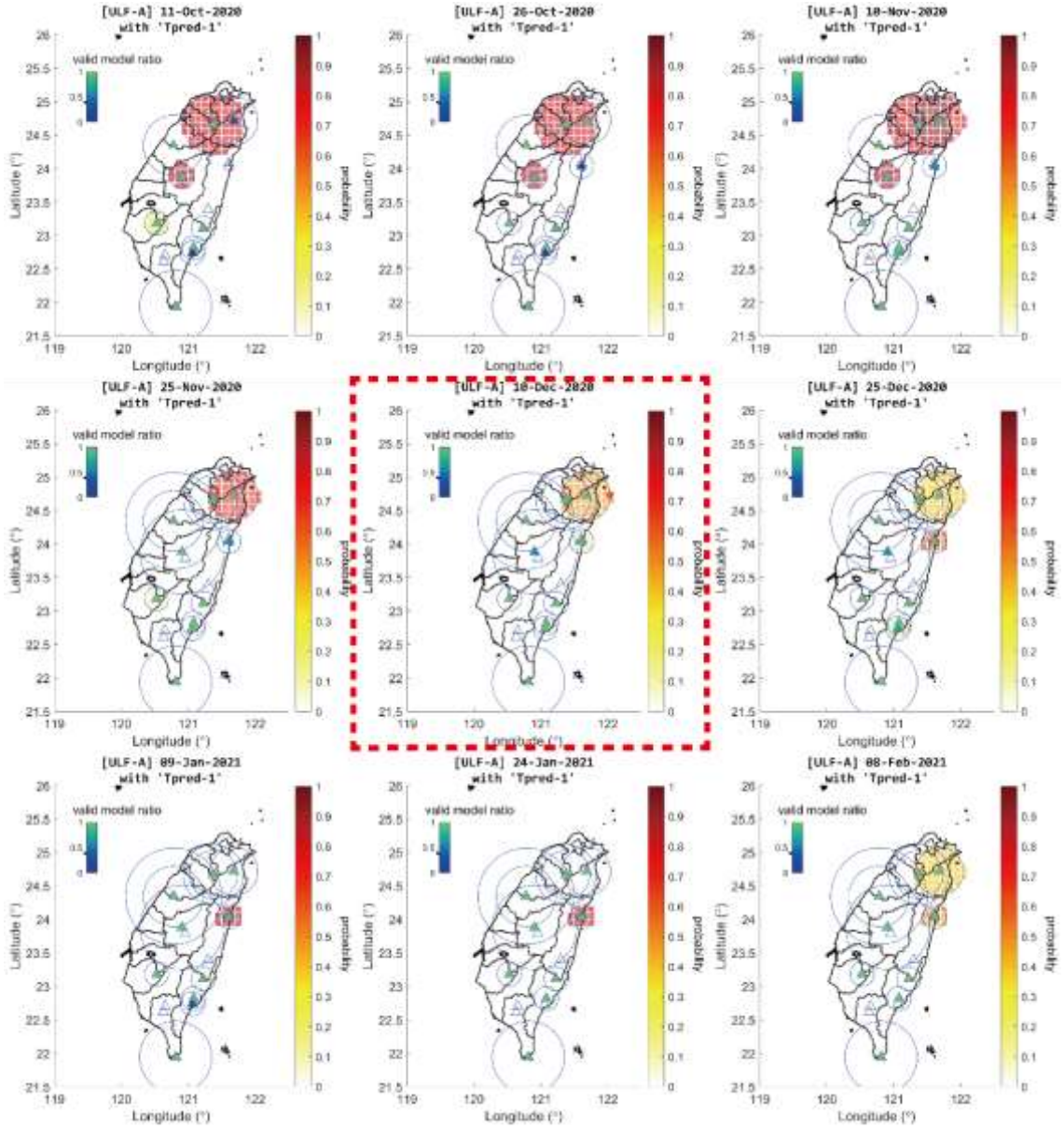

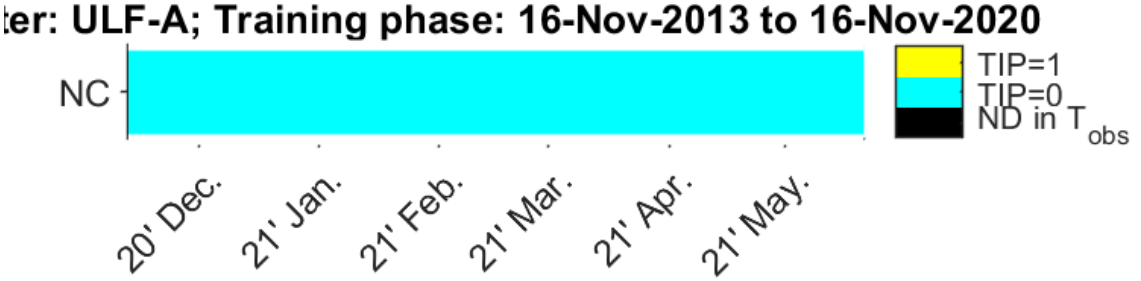

圖 53 (top)個案地震發生前後之 MagTIP 機率預報。機率預報使用 2013 年 11 月 16 日至 2020 年 11 月 16 日的訓練資料進行模型最佳化。(bottom)最佳模型(rank 1)於訓練期截止後的預報 TIP。

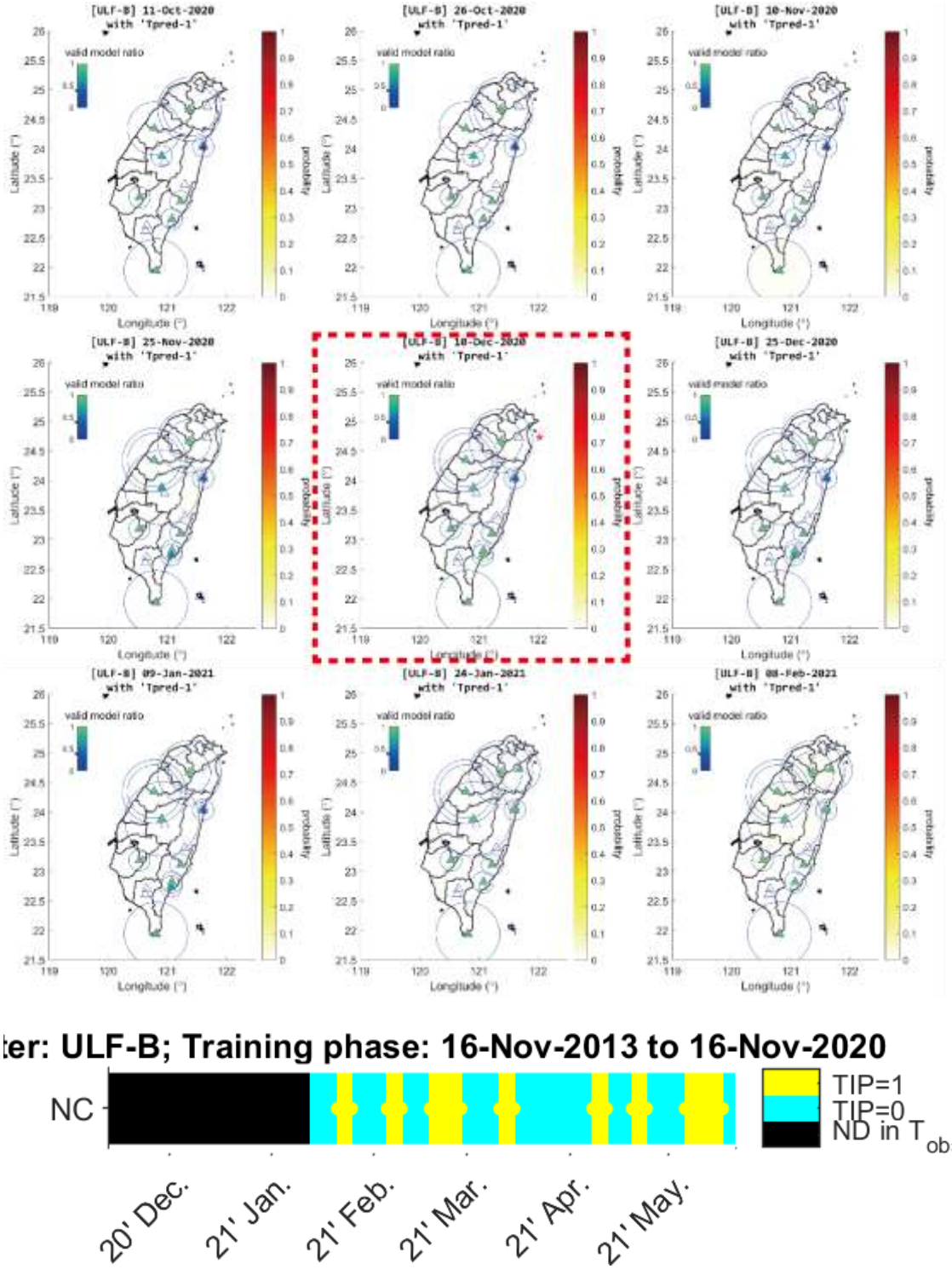

圖 54 (top)個案地震發生前後之 MagTIP 機率預報。機率預報使用 2013 年 11 月 16 日至 2020 年 11 月 16 日的訓練資料進行模型最佳化。(bottom)最佳模型(rank 1)於訓練期截止後的預報 TIP。

附錄: 多變量 MagTIP 演算法說明手冊

多變量 MagTIP 演算法之說明手冊內容包含教程(Introduction and Tutorial)以及函式庫(Library)的詳細說明。此說明手冊將隨程式碼的更新及時更新於以下網址：https://cgrg-lab.github.io/doc-archive/docs/magtip/ (或掃描右方 QR-Code 取得連結)。

說明文件的目錄摘要如下：

Introduction and Tutorial

- Introduction
- Getting Started
    - The Sample Script for Everything
    - Input/Output Directories
- Prepare Your Data
    - Format of Station list and Earthquake Catalog
    - Format of Geomagnetic Data
- The Main Process
- Visualization of the Results
    - Probability Forecast
    - The Matching Diagram

Library

- Main Functions
- Subfunctions
- Tools
    - Plotting
    - Others

臺灣地區 110 年地震前兆監測資料彙整及分析

子計畫三

電離層地震前兆分析研究

陳佳宏　劉正彥　林建宏

國立成功大學地球科學系

摘要

本計畫旨在利用臺灣地區電離層全電子含量(Total Electron Content, TEC)分析電離層地震前兆訊號。過去統計研究發現，在大地震(規模大於等於 5 以上)發生之前一個星期之內，電離層電漿濃度有出現異常減少/增加的情況，因此根據這種特性，我們有機會利用電離層異常出現來作為將來地震發生可能之參考。然而，電離層電漿濃度的變化受到很多因素影響，主要有來自於太陽活動(磁暴、日冕噴發物質)影響電離層高層，以及大氣潮汐作用影響電離層低層。在進行電離層異常天判定時，如果能夠去掉上述主要影響電離層電漿變化的因素，將有很大的機會補捉到來自於地震前地殼作用的影響，以增加電離層地震前兆的判定準確度。本計畫將利用上一期計畫中所建立之臺灣上空長期間(共 25 年)電離層全電子含量資料與電離層異常天之判定結果，並利用太陽活動性指標(Dst index)以及大氣潮汐分解方法去除電離層高層與低層的影響，嘗試尋找電離層地震前兆。

關鍵詞：電離層，全電子含量，地震預警

Abstract

The main purpose of this study is to analyze the seismic precursor signals by employing the ionospheric total electron content (TEC) around the Taiwan area. Previous statistical studies found that before the bigger earthquakes (magnitude larger than 5), the ionospheric anomaly usually occur by the decrease/increase of plasma density. This might be seen as an index of the seismic precursor. However, the variations of ionospheric plasma density will be caused by many effects, such as the solar activity (geomagnetic storm and corona mass ejection) from the upper ionosphere and the atmospheric tidal effect from the lower ionosphere. If these effects can be canceled in the data, it is possible let us to catch the seismic activity before the earthquake and determine the ionospheric anomaly day in more precisely. In this study, the long-term, totally 25-year, ionospheric TEC observations and the results of ionospheric anomalous days developed by the last term project, as well as the solar

activity index (Dst index) data and the atmospheric tidal decomposition method will be employed to find the seismic precursor in the ionosphere.

Key word：Ionosphere，Total Electron Content (TEC)，Earthquake Early Warning

一、前言，研究目的及意義

受到太陽光化游離作用以及地球電流環流系統的影響下，電漿會在南北半球約地磁 10^{o}-20^{o} 之間產生最大濃度的區域，稱為電離層赤道異常區(Equatorial Ionization Anomaly, EIA)。根據電離層物理理論，我們知道 EIA 的最大濃度值、最大濃度位置與最大濃度發生時間，會與背景電場以及磁場作用下產生的電漿漂移(ExB drift)速度有關，同時太陽活動性以及地球大氣潮汐所產生的擾動電場也會改變 EIA 的形態，因此造就 EIA 的日變化(day-to-day variation)。

北半球 EIA 每天通過臺灣正上方，主導著臺灣上空電漿濃度的變化。過去研究發現，在大地震來臨之前，電離層電漿濃度的變化會超過日變化範圍，稱為電離層地震前兆或是地震前電離層異常現象。此異常現象推測是由於大地震前的孕震期間於斷層附近累積的大量電荷，傳導到地表與大氣所造成的電離層電場改變，進而引發電漿濃度的改變。過去利用全球電離圖(Global Ionosphere Map, GIM)研究電離層地震前兆發現，這種電漿濃度改變所影響的區域通常位於 EIA 附近，並且與地震規模有關，說明地震所產生的電場改變似乎會影響 EIA 的形態(濃度值、位置與時間)。Liu et al. [2010]利用 2001 年~2007 年間臺灣地區 150 筆規模大於等於 5 以上之地震進行 EIA 形態與地震之間的關係，發現地震前 EIA 會往磁赤道方向移動造成同緯度地區電漿濃度減少(參考圖一)，並且 EIA 生成時間也會提早，可用於電離層地震前兆之參考。

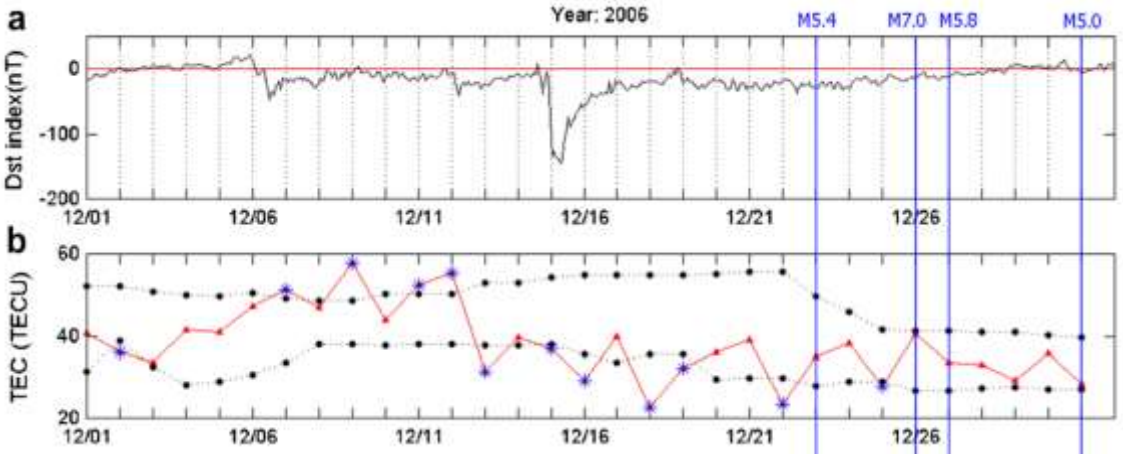

圖一、2016 年 12 月份 Dst index(a)與北半球東經 120^{o}E 赤道異常區(EIA)最大 TEC 濃度(b)變化情形。藍色線標示為臺灣地區地震發生之日期與規模。[Liu et al., 2010]

然而如前所述，EIA 同時也會受到來自於太陽與大氣潮汐的影響。為了了解太陽風暴對於臺灣地區 EIA 的影響，Liu et al. [2013]分析 1994 年到 2003 年間太陽風暴事件，發現太陽風暴會造成電離層電漿濃度增加(正磁暴，positive storm)與減少(負磁暴，negative storm)現象，其中正磁暴反應的速度很快，通常當天或隔天就會

影響電離層，而負磁暴的反應則較慢，但會持續影響電離層濃度改變達 2-4 天。因此，圖一中 12/15 所發生的太陽風暴事件(Dst index 到-150 左右)，造成 12/15、12/16 與 12/18 的 EIA 濃度值降低。雖然都發生在大地震(12/26)之前，但可視為太陽活動所造成的異常現象。

前一期計畫中利用所建立之臺灣地區 1995 年到 2019 年間(共 25 年)長期電離層異常資料庫，嘗試計算地震可能發生之統計參考機率(Statical Reference Probability, SRP)。SPR 值的計算為利用前 5 天的電離層下界異常判定結果(異常值為 1，正常值為 0)乘上電離層下界異常統計機率得到。發現 1999 年 921 地震前 SRP 值有增加的趨勢，並於地震前 1 天達到最大值，地震發生之後則開始下降。然而分析 1999 年一整年地震事件與 SRP 值之間的關係，發現 SRP 值與地磁指數 Dst index 似乎有相關，並且 SRP 值的週期性出現似乎是來自於大氣潮汐的影響，因而影響 SRP 值進行地震可能發生機率之計算結果，這是因為在進行 SRP 值的計算時，並沒有排除來自於太陽與大氣潮汐的影響。為了要得到較正確的 SRP 值，本期研究計畫將著手進行太陽與大氣潮汐的影響，並於 SRP 值計算時排除，並探討 SRP 值反應地震發生之成效。

二、研究方法與進行步驟

1. 首先針對上期計畫審查委員們的建議，進行特定區域電離層地震前兆分析研究。因為無法得知地震發生的位置，因此目前電離層電漿濃度異常的分析位置是鎖定在臺灣的中央位置(緯度 24 度，經度 121 度)。但是因為電離層地震前兆可能會有地域的特性，比如說某些板塊交接帶、斷層附近之地質構造等，造成電荷累積程度以及釋放程度不同，這也是為什麼不是每一筆地震前都看得到電離層電漿濃度異常的原因。為了要更加了解地震前的孕震期間對於電離層電漿濃度的影響，因此本計畫預期將進行特定區域(例如花蓮區域、臺南區域等斷層帶附近)電離層地震前兆分析。這些分析成果也將對於地震空間前兆研究有所幫助。

2. 搜集與上一期計畫所建立之電離層異常資料庫相同期間(1995 年到 2019 年共 25 年間)太陽風暴資料，利用 Liu et al. [2013]分析方法，研究太陽風暴對於臺灣地區電離層電漿濃度、影響時間之特性，並進一步去除太陽風暴期間(1~4 天)的電離層異常天，探討其對於 SRP 值的影響。

3. 上一期計畫中利用全大氣資料同化模式(WACCMX)分析地震前模式電離層電漿的特性，發覺跟真實 GPSTEC 資料完全不同，因此判定 GPSTEC 所得到電離層異常的統計結果有很大的可能性是來自於地震所引發的。此模式資料可以應用於本期計畫中，進行低層電離層(~100 公里)大氣潮汐分析，尋找大氣潮汐影響電離層電漿之特性。將電離層異常天資料進行進行頻譜分析，看是此異常天資料是否含有大氣潮汐成分，若有的話則去除。

4. 在進行去除太陽風暴與大氣潮汐的影響之後，重新計算 SRP 值以及預測成功率。

三、具體成果

電離層地震前兆分區特性分析

研究分析期間從上一期計畫中的 1995 年-2019 年(共 25 年)，擴增為 1994 年-2021 年 4 月(約 27 年)，其間發生 73 筆規模大於等於 6 的地震事件。為了討論臺灣地區特定區域電離層地震前兆特性，將地震區分為以下三個區域：(1) 宜蘭(24.5°N, 121.8°E, 40 筆)；(2) 南投(24°N, 121°E, 18 筆)；(3) 後甲(22.98°N, 120.24°E, 16 筆)。期中報告根據審查委員的建議，重新定義以下三區：(1) 北部(25°N, 121.5°E, 29 筆)；(2) 中部(24°N, 121°E, 27 筆)；(3) 南部(23°N, 120.5°E, 17 筆)，地理位置參考下圖二與表一。北部地區主要是針對歐亞板塊與菲律賓海板塊交界所引發的地震，中部地區則是臺灣正中央地區，而南部地區則是選取與北部和中部地區相等距離，針對南部的地震進行分析。地震的區分為距上述 3 個地點最近距離為準。

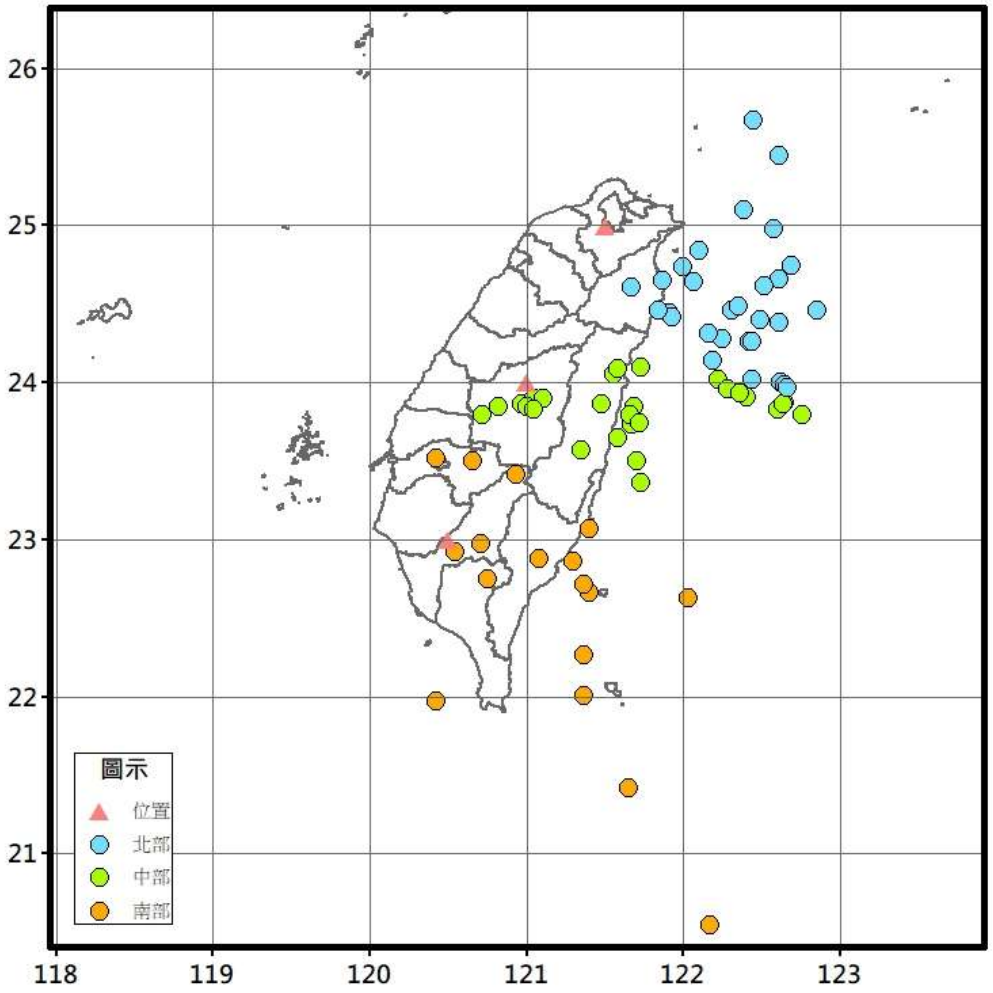

圖二、1994 年到 2021 年 4 月中所發生之 73 筆地震規模大於等於 6 以上之地震分佈位置。圖中藍色點代表北部地區，綠色點代表中部地區，而橘色點則代表南部地區的地震。

表一、臺灣地區三區中心地理位置與地震筆數。

名稱	北部	中部	南部
經度(°E)	121.5	121	120.5
緯度(°N)	25	24	23
地震筆數	29	27	17

分析 1994 年到 2021 年 4 月臺灣地區發生之 73 筆規模大於等於 6 以上地震前電離層異常天，其統計結果如圖三所示。根據統計約 27 年地震前後電離層異常天的整體結果(圖三 a)來看，地震前第 1-5 天為電離層負異常較為明顯，而地震前第 6-13 天(第 8, 9 天除外)則為正異常較為明顯，與上一期研究計畫成果一致。在區分 3 個不同地區之後，可以看到北部地區(圖三 b)地震前第 3-6 天、第 8-9 天以及第 12-15 天為負異常為主，正異常現象則不顯著。中部地區(圖三 c)地震前同樣也是以負異常現象為主，出現於地震前第 2-9 天之間(第 6 天除外)，而正異常則在地震前第 10 天開始出現。南部地區(圖三 d)則與上述 2 個地區有明顯不同的異常趨勢(特別是正異常部分)，此區的地震在地震前第 1-3 天主要為電離層負異常為主，而地震前第 5-15 天則為電離層正異常為主，並且其比例非常高。上述統計結果如表二所示。由上述不同區域的統計結果可以得到以下的結論，整體來說電離層地震前兆負異常天常發生在地震前 1-5 天，而若發生電離層正異常則有可能是南部地區的地震所造成的，並且在發生正異常過後約 5-15 天有可能會發生規模 6 以上的地震。

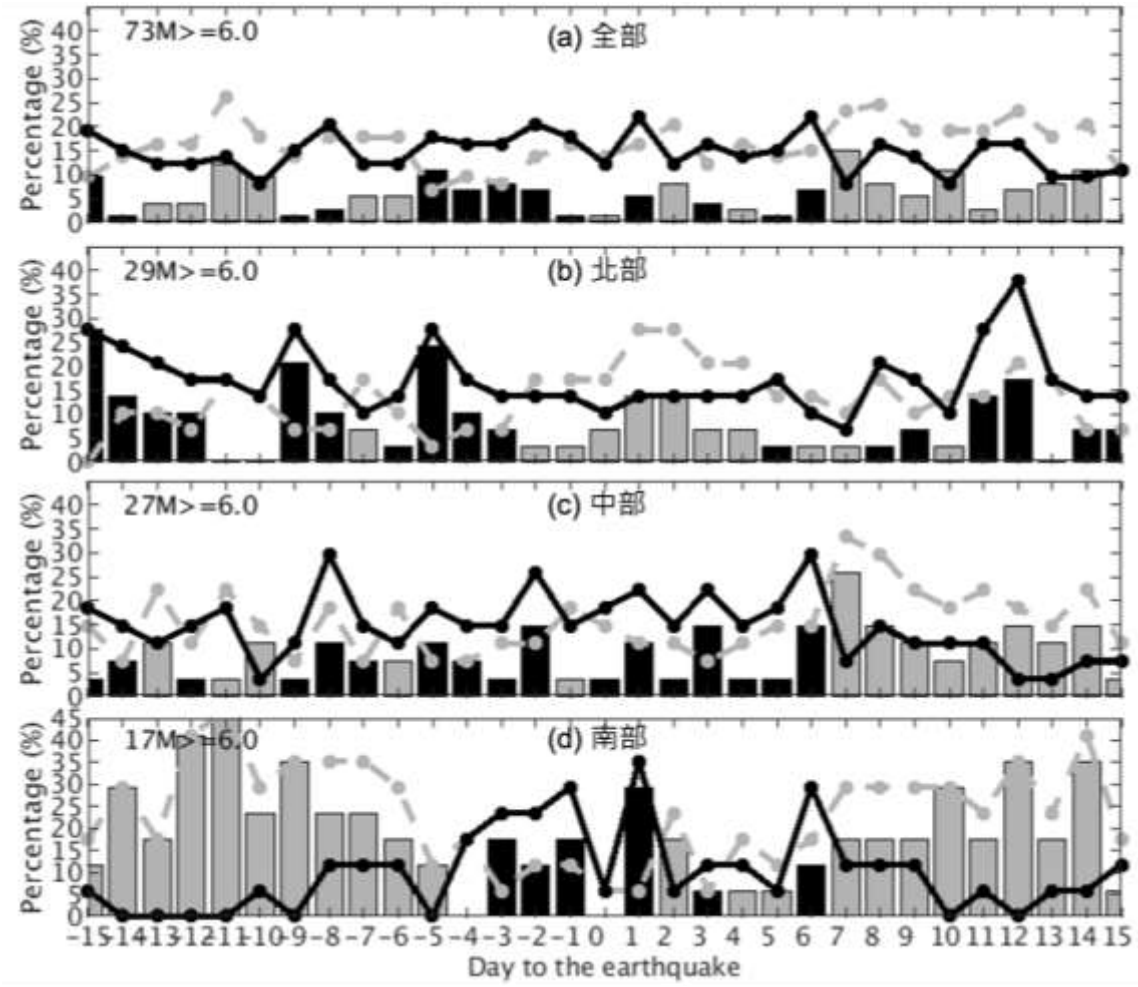

圖三、1994 年到 2021 年 4 月間所發生之 73 筆規模大於等於 6 以上地震前電離層前兆統計結果(a)。第 2 張到第 4 張圖分別為北部(b)、中部(c)與南部(d)地區的統計分析結果。

表二、臺灣地區地震前電離層異常天統計結果。

區域名稱	筆數	負異常天(地震前)	正異常天(地震前)
北部	29	3~6, 8~9, 12~15	1, 2, 7
中部	27	2~5, 7~9	1, 6, 10, 13
南部	17	1~3	5~15
全部	73	1~5, 15	6~7, 10~13

太陽活動影響分析

電離層電漿的擾動來源除了地震前孕震過程中產生的電場之外，還有可能來自於太陽活動(如太陽風暴、日冕物質拋射、太陽閃焰等)影響上層電離層，以及大氣潮汐影響下層電離層。在進行地震前電離層前兆研究時，如何去除掉太陽與大氣潮汐的影響，只留下可能是地震的異常天是一件非常重要的工作。

下圖四是今年(2021 年) 4 月 18 日所發生之規模 6.2 地震資訊，震央位於花蓮縣壽豐鄉。圖五則為地震前後 15 天震央上空電離層電漿濃度的變化情形，結果顯示地震當天(4/18)、地震前第 1 天與第 3 天(4/17, 4/15)為電離層電漿正異常天，而地震前第 9 天與第 15 天(4/9, 4/3)為電離層電漿負異常天。由 Dst 指數的變化得知 4/16 有一小磁暴事件發生，推斷 4/17 與 4/18 的正異常應為磁暴所致。4/15 電漿正異常則為 4/18 地震電離層前兆的可能性很大。4/9 的負異常原因不明，但根據當天 TEC 觀測資料(紅線)來看，因為與下界值很接近時不時出現低於下界值(藍色區塊)而被判定為異常天。

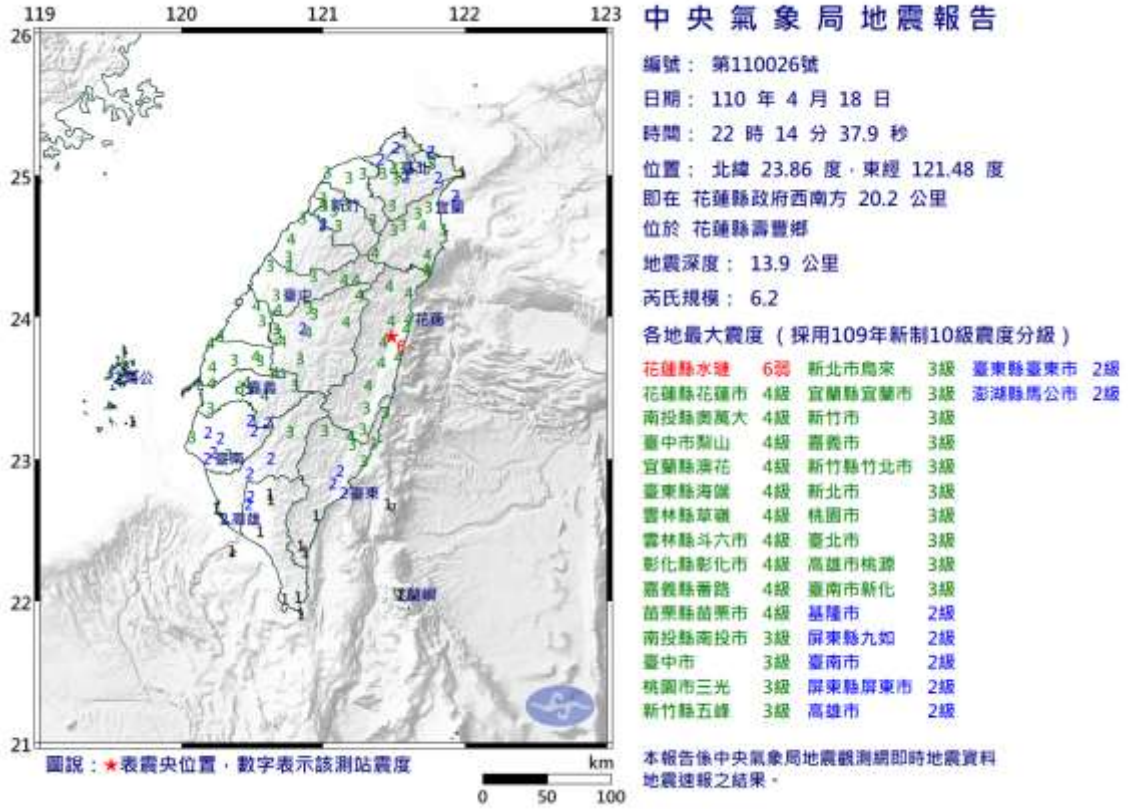

圖四、2021 年 4 月 18 日花蓮地區所發生之規模 6.2 地震資訊。[資料來源：中央氣象局網頁]

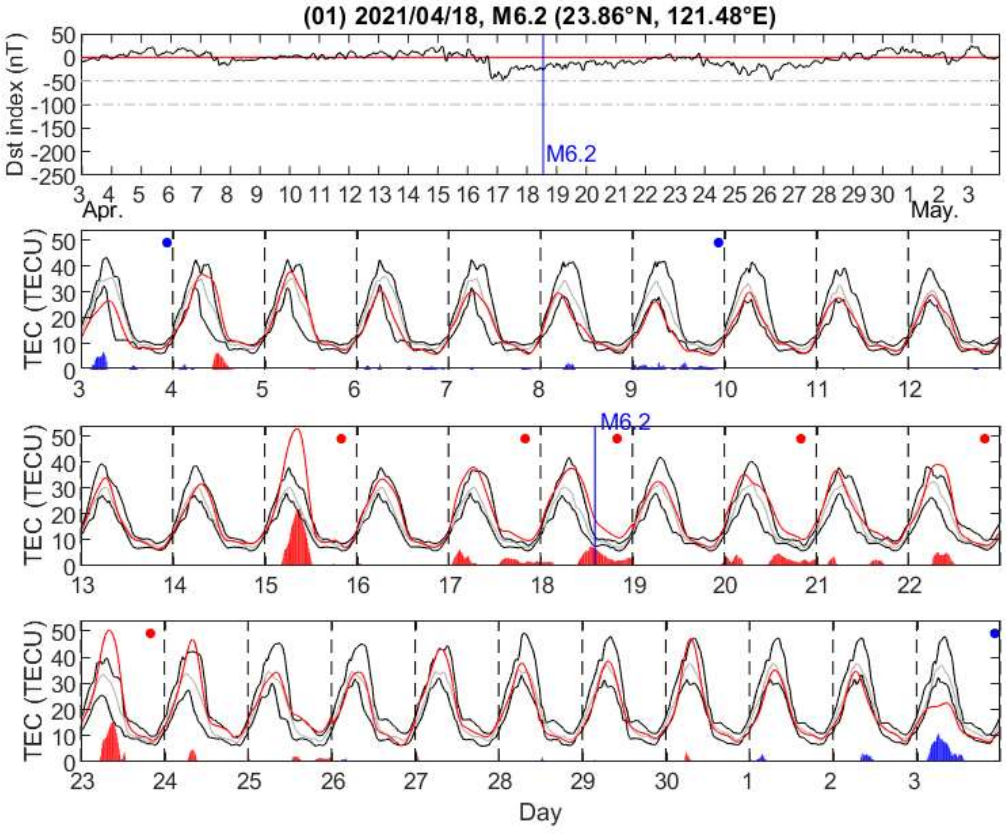

圖五、2021 年 4 月 18 日花蓮 6.2 地震前後 15 天震央上空之電離層電漿濃度變化情形。最上圖為代表太陽活動性指數(Dst index)，第 2-4 圖為當天電漿濃度值(紅色線)、前 15 天平均電漿濃度值(灰色線)，以及電漿濃度上下界值(黑色線)的變化。圖中藍點與紅點分別代表程式根據當天觀測值與上下界值差值(圖中紅藍色區塊)所分析之下界與上界異常天。

圖六為 2021 年 4 月 18 日花蓮 6.2 地震前後 15 天臺灣地區電離層赤道異常現象(EIA)隨時間與緯度的變化，可以看到 4/15(正異常天)EIA 有往高緯度地區移動的情形，並且 EIA 的最大電漿濃度也有增加的情況。根據電離層電動理論，此現象說明震央上空電離層東向電場有增強的趨勢，此增強的東向電場有可能為地震發生前孕震過程中地殼摩擦作用所產生的。

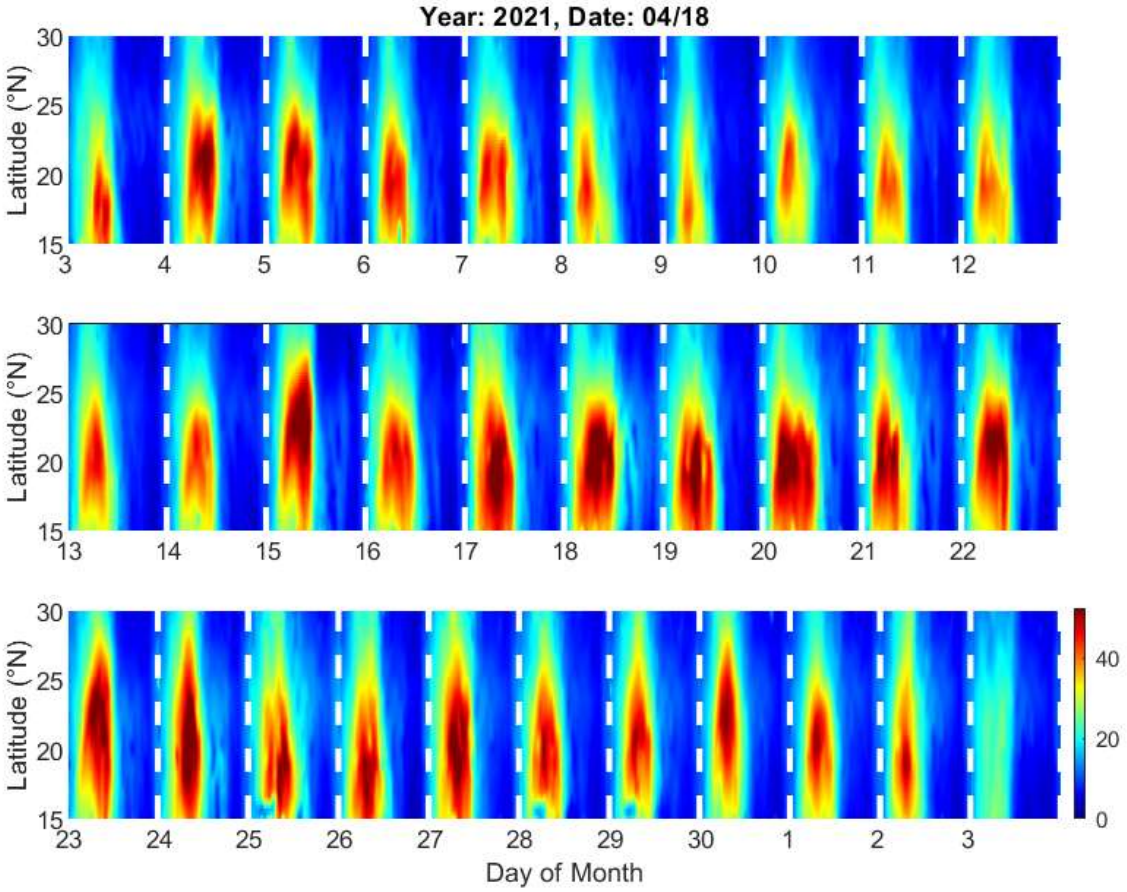

圖六、2021 年 4 月 18 日花蓮 6.2 地震前後 15 天臺灣地區電離層 EIA 變化情形。

為了要去除太陽活動的影響，首先必需要先對太陽活動進行定義。通常會利用地磁擾動指數(Dst index)決定地球電離層受到太陽影響而產生的擾動程度，當 Dst index 小於-50 nT 時定義為小磁暴事件，當 Dst index 小於-100 nT 時定義為中磁暴事件，而當 Dst index 小於-150 nT 時則定義為大磁暴事件。小磁暴事件發生時會影響電離層電漿濃度變化，數小時之後才會回到原來的狀態，而大磁暴事件則可以持續影響電離層電漿濃度變化達數天之久。為了要了解磁暴所造成電離層電漿濃度擾動的影響，將 1994 年到 2021 年 4 月期間所發生的所有磁暴事件，按照磁

暴大小進行統計分析。結果如圖七所示，可以得到一個結論：小磁暴發生後，Dst index 大約 1 天之內就會回復到平常天的水準，中磁暴約為 2 天，而大磁暴則約為 3 天左右。因此，在進行電離層異常天判定時(如圖五)，需要根據 Dst index 值再去掉可能由太陽活動造成的異常天，最後再進行統計分析。圖三 73 筆地震統計結果在去除掉可能由太陽活動所造成的異常之後，得到圖八的統計分析結果。

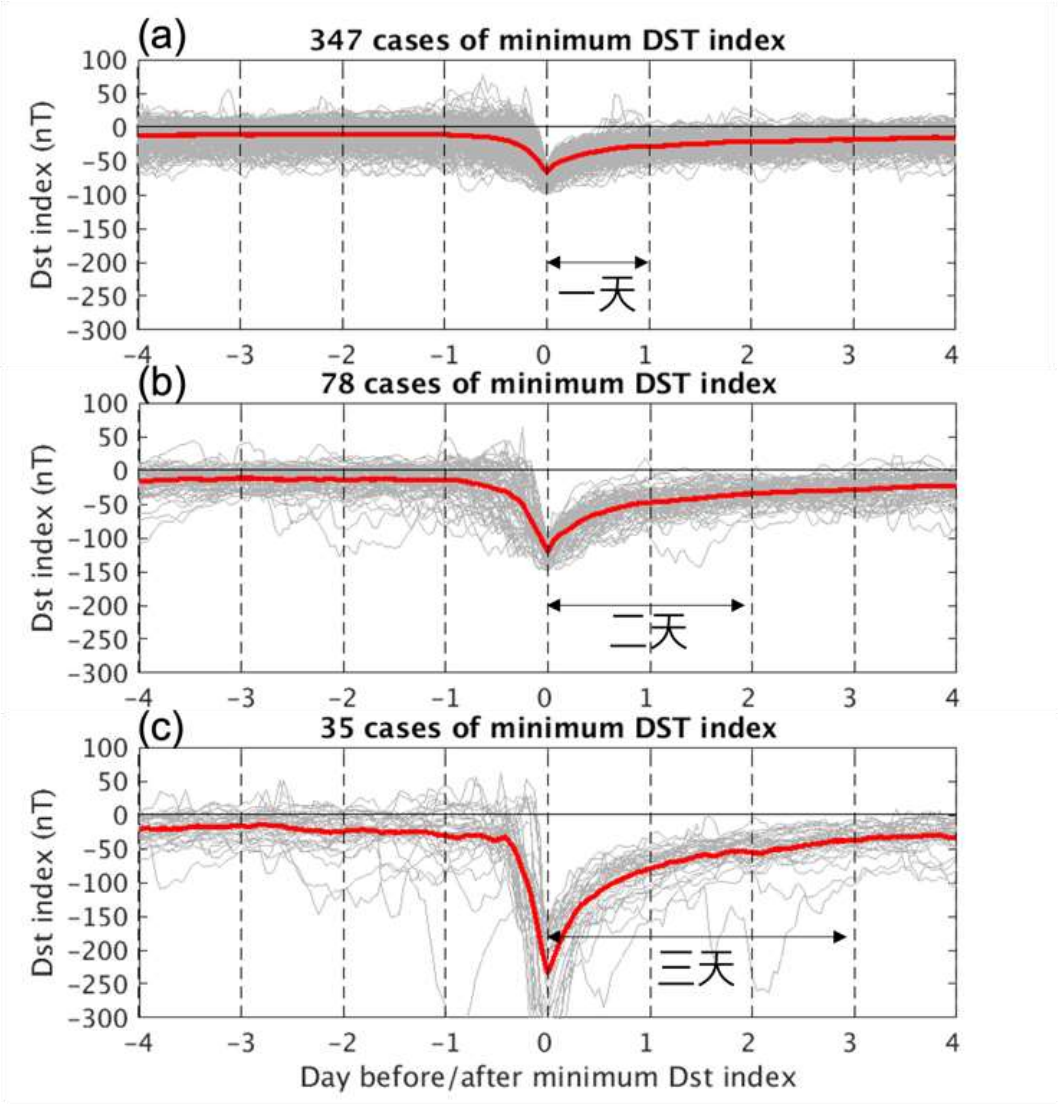

圖七、1994 年到 2021 年 4 月間所發生之 347 筆小磁暴事件(a)、78 筆中磁暴事件(b)與 35 筆大磁暴事件(c) Dst index 前後 4 天的變化情形。圖中灰色線為所有磁暴事件，而紅色線為其平均值。

將圖八統計結果與圖三進行比較，可以看到整體異常天的天數(百分比)有些許下降的情形，說明確實在 73 筆地震事件中，的確有些電離層異常天是受到太陽活動的影響。整體來看，在去掉可能由太陽活動引發的異常天之後，全體在地震前 2-5 天為負異常居多，地震前 10-13 天為正異常居多；北部地區地震前大致上以負異常為主；中部地區的正負異常分布變得較為混亂；南部地區則在地震前 1-3 天為負異常居多，而地震前 4-15 天以正異常居多(除第 6 天之外)。圖八大致上的趨勢仍與圖三相似，統計表格如表三所示。

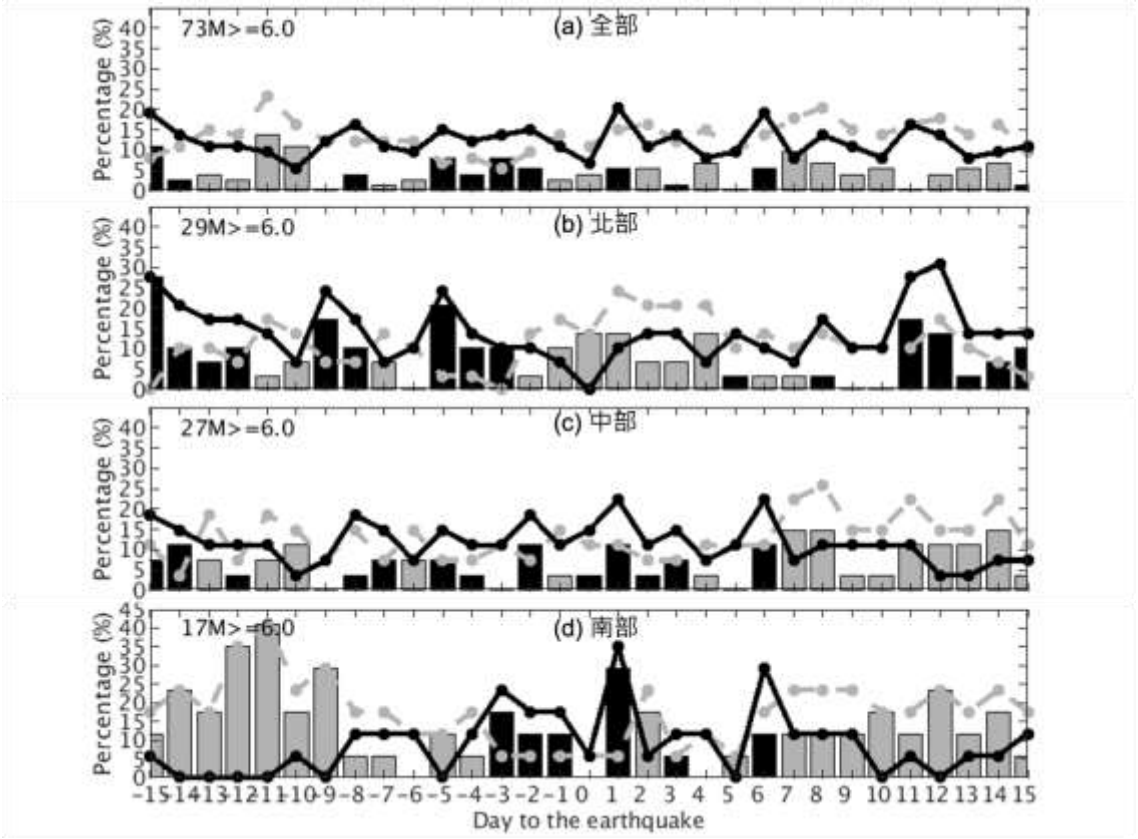

圖八、格式與圖三相同，但是去掉可能的太陽活動所造成的異常天。

表三、臺灣地區地震前電離層異常天統計結果(去除太陽活動影響)。

區域名稱	筆數	負異常天(地震前)	正異常天(地震前)
北部	29	3~5, 8~9, 12~15	1~2, 7, 10~11
中部	27	2, 4~5, 12, 14~15	1, 6, 10~11, 13
南部	17	1~3	4~5, 7~15
全部	73	2~5, 8, 15	6, 10~13

大氣潮汐影響分析

除了來自於電離層上層作用(太陽磁暴)之外，電離層下層的大氣潮汐作用近年也被認為影響電離層電漿濃度擾動變化的原因之一。為了要減少大氣潮汐對電離層電漿造成擾動異常的可能而影響地震前電離層異常天統計分析結果，本研究利用 2000 年到 2014 年(共 15 年)全大氣模式(WACCMX)資料，嘗試尋找地震前電離層正常天與異常天。WACCMX 模式因為只有同化低層大氣觀測資料，不含有地震前大地電場變化所造成的電離層電漿濃度變化，因此 WACCMX 模式所得到的電離層異常情形則有很大的可能是來自於大氣因素(如大氣潮汐效應)。上一期計畫我

們分析了 2000 年到 2014 年間 WACCMX 模式模擬之地震前電離層異常，利用所得到之正負異常天，以及正常天(稱為平靜天)，本研究進一步將平靜天的資料進行潮汐分解，找出不同季節(日期)大氣潮汐的週期與振幅(圖九)，最後再將觀測到的電離層電漿變化(如圖五)減去相對應的平靜天大氣週期，可得到明顯的大氣潮汐作用的電離層異常天。接著將臺灣地區真實電離層觀測資料減去 WACCMX 模式所分析得到之大氣潮汐週期，若原本被判斷為電離層異常天但去掉大氣潮汐之後變成不是異常天的情況，則可視此異常天可能受到大氣潮汐影響的可能性很大，在進行統計分析時可以將其去除。例如圖十的分析範例，電離層原始資料(圖十 a)判定在地震前的 4/3, 4/9 為負異常天而 4/15, 4/17 為正異常天，而減去大氣潮汐結果(圖十 b)則在 4/3 為非異常天，說明 4/3 的異常可能是由大氣潮汐所造成的，因此在進行統計分析時可以將其去除，得到電離層地震前異常天(圖十一)。

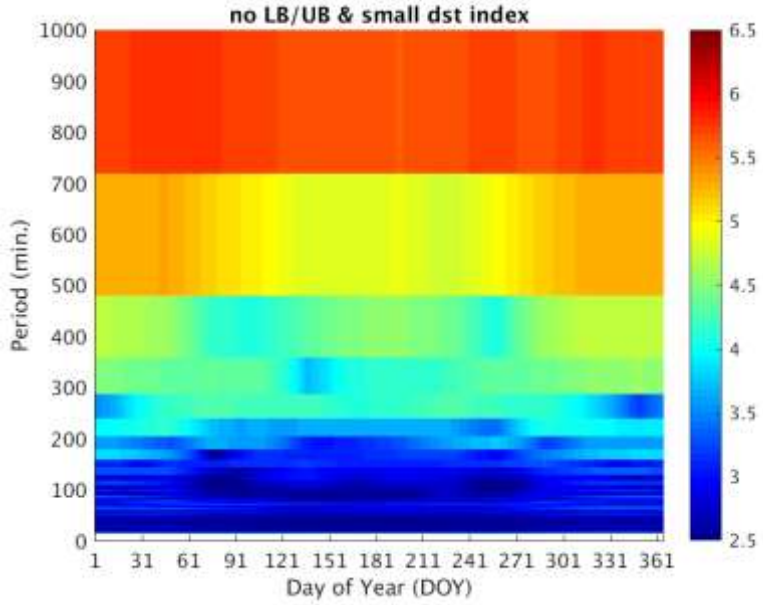

圖九、WACCMX 模式平靜天大氣潮汐週期與振幅一年的變化情形。最主要週期為 700-1000 分鐘，並且冬季大氣潮汐週期較夏季來說有變短的情形。

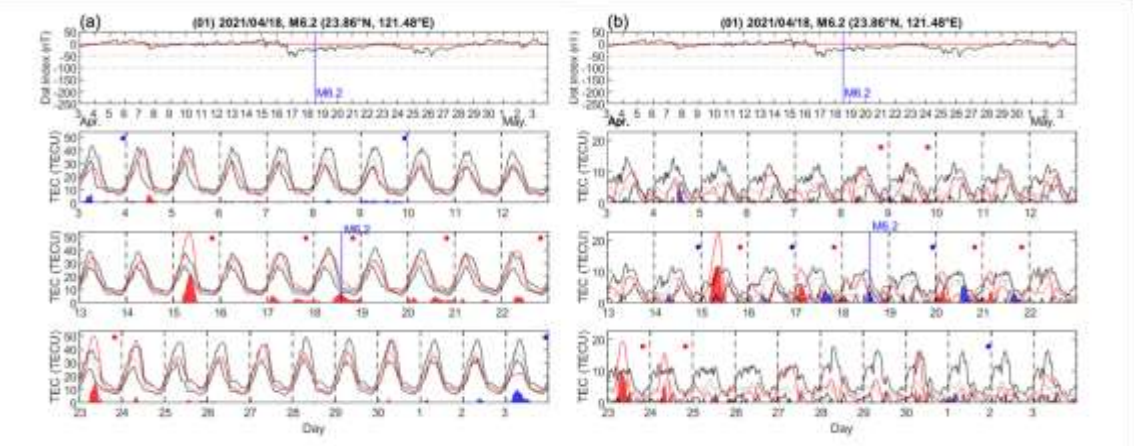

圖十、2021 年 4 月 18 日 M6.2 地震前後 15 天電離層電漿濃度變化情形。(a)為原始電離層電漿資料(同圖五)，(b)為去掉相對應的大氣潮汐效應結果。

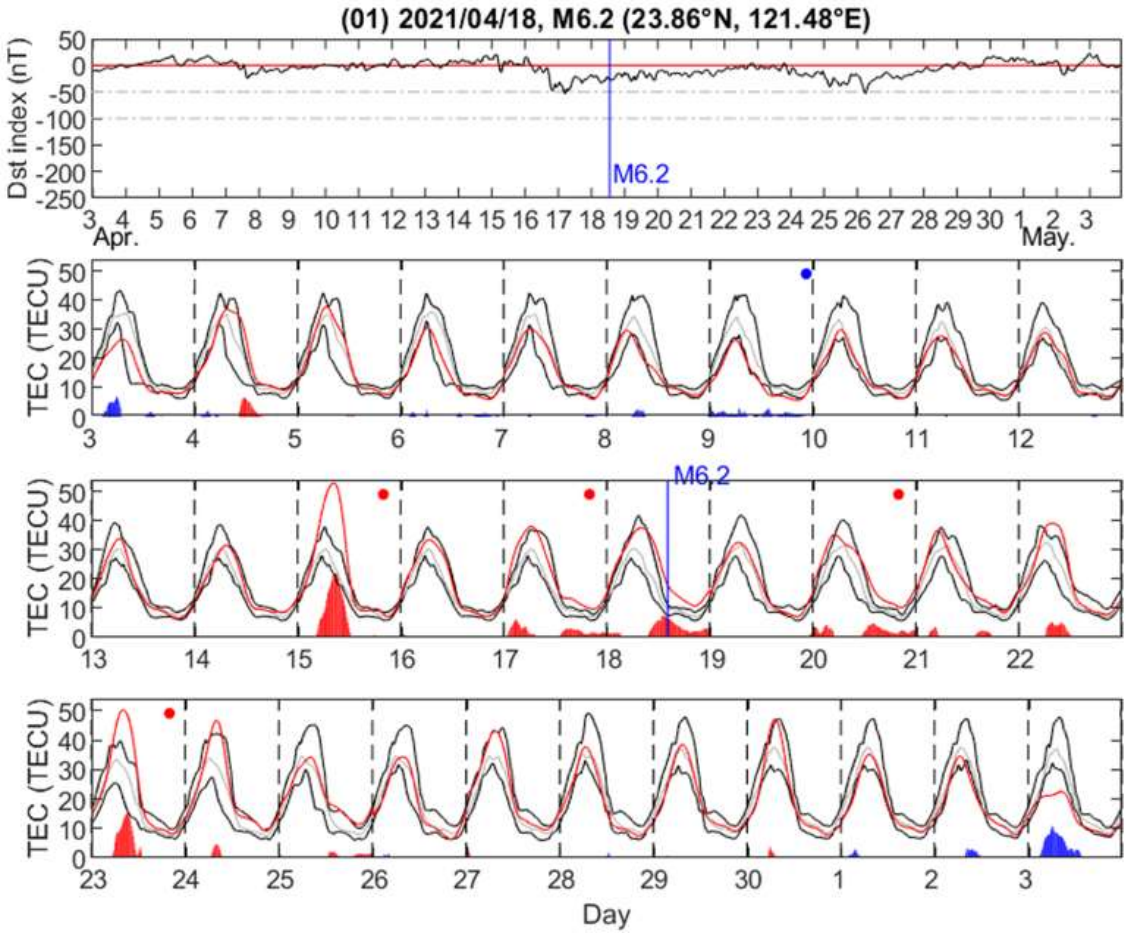

圖十一、格式與圖五相同，但去掉相對應的大氣潮汐影響的電離層異常天。

統計結果如圖十二所示。跟原始統計結果(圖三)比較，明顯可以看到異常天的筆數降低了許多，意味著本研究所採用去除大氣潮汐效應的方法對於電離層異常判定有很大的影響。但以整體正負異常統計分析結果來看，與原始統計結果(圖三)以及去除太陽活動影響(圖八)很相似：臺灣地區全部地震統計結果來看，地震前 2~5 天以負異常，地震前 6~13 天以正異常為主；北部地區地震在地震前 3~9 天(除第 7 天外)、12~15 天為負異常；中部地區則同樣複雜沒有明顯連續異常變化情形；南部地區則在地震前 1、3 天為負異常，地震前 5~15 天為正異常。統計結果整理成表四。

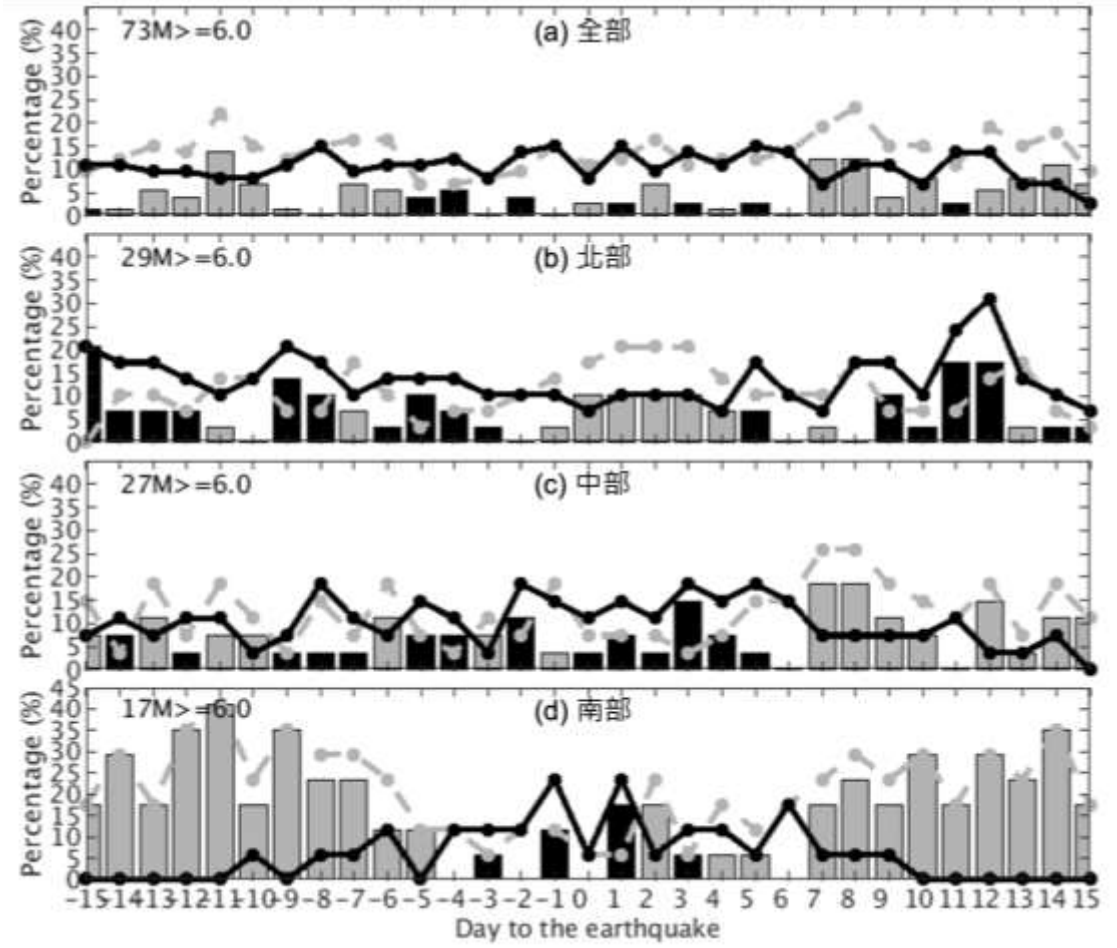

圖十二、格式與圖三相同，但是去掉可能的大氣潮汐效應所造成的異常天。

表四、臺灣地區地震前電離層異常天統計結果(去除大氣潮汐效應)。

區域名稱	筆數	負異常天(地震前)	正異常天(地震前)
北部	29	3~6, 8~9, 12~15	7, 11
中部	27	2, 4~5, 7~9, 12, 14	1, 3, 6, 10~11, 13, 15
南部	17	1, 3	5~15
全部	73	2, 4~5	6~7, 10~13

地震發生統計參考機率

上一期計劃中應用電離層地震前異常天長期統計結果，嘗試計算 5 天內地震發生之統計參考機率(Statistical Reference Probability, SRP)，並利用 1999 年 921 地震進行驗證，發現地震前 SRP 值有逐漸增加的趨勢，並在地震發生之後 SRP 值則逐漸減小為 0。然而，嘗試比較 1999 年一整年 SRP 值地震之間關係，發現 SRP 值

受到太陽活動性影響及大氣潮汐影響很大，因此本研究在去除上述影響因子之後，重新建立較準確的 SRP 預測值。除此之外，為了了解 SRP 值多大以上可視為較高的預測參考機率，因此本研究進行不同 SRP 值對應 1994 年到 2021 年 4 月中 73 筆規模大於等於 6 以上地震進行預測成功率測試，嘗試尋找適合的 SRP 預測門檻值。

首先是 SRP 值的定義與計算。圖十三為地震發生統計參考機率的計算示意圖。配合目前中央氣象局每天計算電離層電漿濃度與異常天的資料，利用前 5 天的電離層下界異常判定結果(異常值為 1，正常值為 0)乘上圖三(a)、圖八(a)或圖十二(a)中電離層下界異常統計機率可以得到地震發生之統計參考機率(SRP 值)。如圖十三所示，如果今天為 1 月 6 日(1/6)，而前 1 天(1/5)的 SRP 值可以做為 1 月 7 日(1/7)之預測值，前 2 天(1/4)的 SRP 值則做為 1 月 8 日(1/8)之預測值，以此類推可以得到 5 天內的 SRP 值變化情形。當今天變為 1 月 7 日(1/7)時，則 1 月 6 日(1/6)計算得到之 SRP 值將做為 1 月 8 日(1/8)的預測值並累計加上前 1 天(1/6)的預測值(來自於 1/4)，以增強地震可能發生的機率。

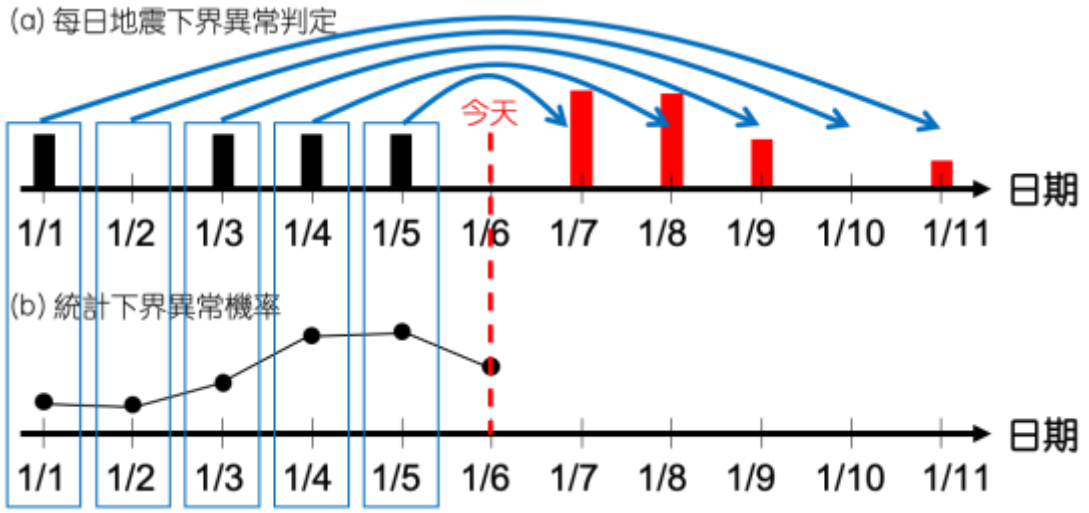

圖十三、地震發生統計參考機率計算示意圖。假設今天日期為 1 月 6 日，(a)為昨天之前所計算之下界異常天(異常值為 1，正常值為 0)。(b)則為圖三(a)、圖八(a)或圖十二(a)地震當天(0)到前 5 天(-5)之過去地震統計發生機率值。

圖十四為 2021 年 4 月 18 日 M6.2 地震 SRP 預測值於不同條件之下的測試結果。圖十四(b)可以看到在地震前第 5 天有最大的 SRP 值，並且在地震發生過後 SRP 值變為 0。由圖十四(a)可以看到，在地震發生前 1 天有一個小型太陽活動事件(Dst 指數到達-50 nT)，當天(4/17)的電離層也被判定為一個正異常，根據圖七的判斷標準在去掉當天(4/17)的異常天之後，重新計算 SRP 值的結果如圖十四(c)所示。整體來說比起圖十四(b)的 SRP 值有些許下降的趨勢。另外一方面，在去除掉大氣潮汐效應重新計算 SRP 值的結果如圖十四(d)所示，在地震前第 9, 11 與 13 天的 SRP 值變為 0，整體 SRP 值有更接近地震發生日期。

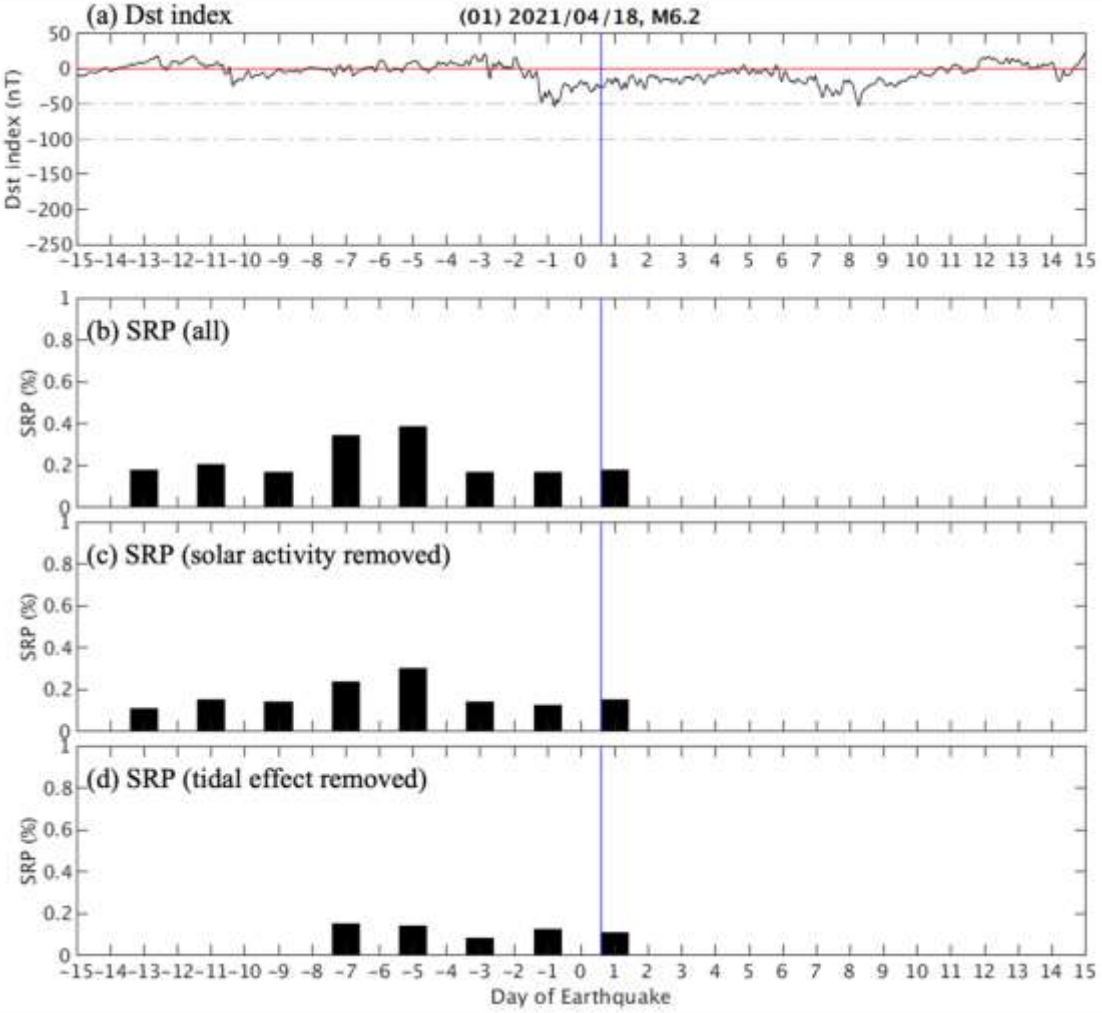

圖十四、2021 年 4 月 18 日 M6.2 地震 SRP 預測值範例。(a)為太陽活動性 Dst 指數；(b)為所有異常天計算結果；(c)去掉太陽活動造成的異常天結果；(d)去掉大氣潮汐效應異常天結果。

接下來則要決定說，出現怎麼樣分布的 SRP 值才算是有成功預測成功，也就是要決定 SRP 的預測門檻值。根據統計的結果發現，在地震前電離層異常天很常成群出現，因此本研究針對 SRP 當天值以及 1~5 天累計值進行預測成功率分析，結果如圖十五所示。可以看到整體的趨勢隨著 SRP 值的增加，成功率有下降的情形。以當天 SRP 值(紅色點線)來看，不管 SRP 值為多少，都沒有超過 50%成功率。而當 SRP 值累計當天與前 1 天(藍色點線)，則可以看到當 SRP 累計值達 0.1 時，預測成功率為 70%，並且隨著 SRP 累計天數的增加，超過 50%成功率的 SRP 值越多，以橘色點線(累計當天到前 5 天的 SRP 值)最為顯著。固定 SRP 累計值=0.3 來看，可以看到當累計天數越多，預測成功率有增加的趨勢，從 25%，41%，49%，60%一路升到 62%，說明累計越多天 SRP 值可以越容易超過 0.3，並且預測成功率也有不斷提升的趨勢。若以 50%成功率以上(紅色虛線)當做是預測目標的話，累計 5 天 SRP 值並且大於 0.5 以上的話，可達 57%的成功率。而 SRP 累計值大於 0.2 以上的話，成功率可達 62%。SRP 累計值大於 0.1 以上的話，成功率更可達 82%。

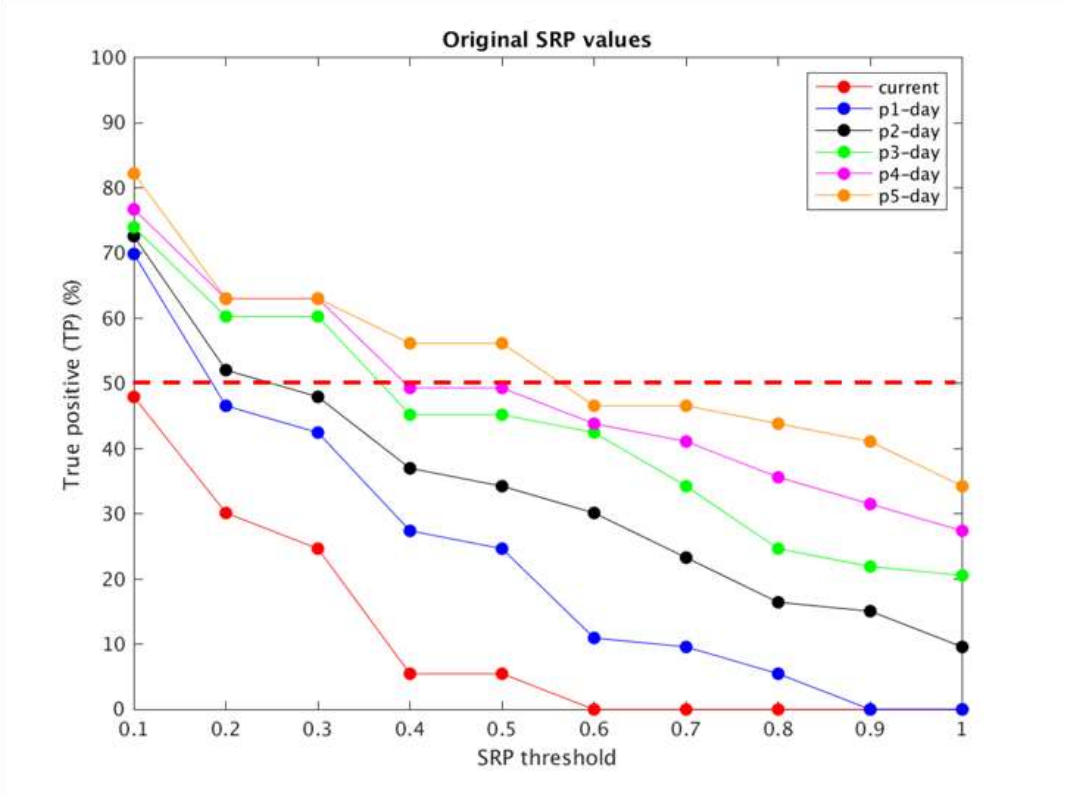

圖十五、預測成功率隨 SRP 值變化曲線。其中紅色點線為當天 SRP 值，藍色到橘色點線分別代表 1~5 天 SRP 累計值。紅色虛線為預測成功率 50%的線。

將太陽活動影響與大氣潮汐效應去掉之後，重新計算 SRP 值與預測成功率的曲線圖如圖十六所示。可以看到整體 SRP 值比起圖十五來說大幅的降低，這是因為圖八與圖十二的異常天比例降低的原因。以圖十六(a)結果來看，超過成功率 50%為 4 天與 5 天 SRP 累計值超過 0.2，以及 1~5 天 SRP 累計值超過 0.1。但可以注意到的是，5 天 SRP 累計值超過 0.2 的門檻設定時有約 59%的預測成功率，比起圖十五同樣設定的成功率(62%)來說，相當接近。根據去掉太陽活動影響的方法(看 Dst 指數決定去掉 1~3 天)，4 天與 5 天的 SRP 累計值受到的影響不大(比起 1~3 天來說)，成功率也可達到約 60%，或許適合用來當做判定 SRP 值的預測門檻值。而圖十六(b)去掉大氣潮汐效應的結果為 2~5 天 SRP 累計值超過 0.1 時，才有 50%的預測成功率，並且最大成功率比起圖十五來說，降低了約 20%。說明此去除大氣潮汐效應的方法似乎不適用於利用 SRP 值來判斷地震預測成功率。

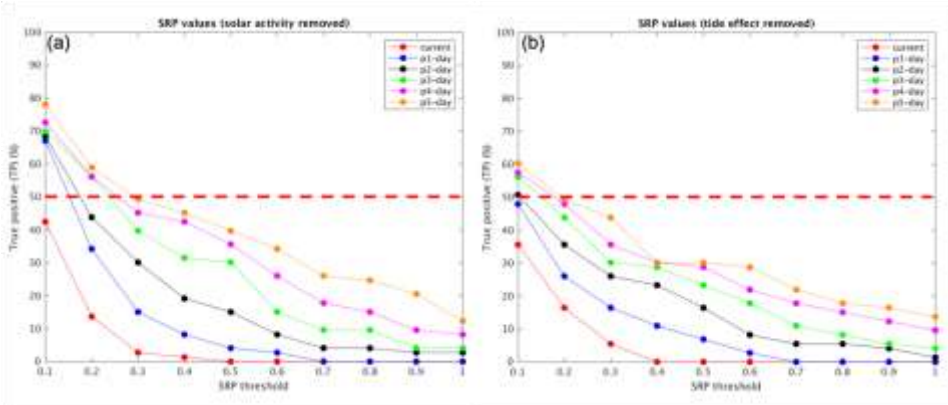

圖十六、與圖十五格式相同。(a)為去掉太陽活動影響的結果。(b)為去掉大氣潮汐影響的結果。

四、結論與建議

本研究將臺灣地區地震區分為北部、中部與南部 3 個地區，分別統計分析 3 區電離層地震前異常天。結果顯示北部與南部的電離層異常形態不太一樣，北部電離層異常大都以負異常為主，南部則為正異常為主並且在接近地震發生日期時轉變為負異常，而中部則是處於北部與南部形態的轉換區間。根據上述分析結果，將來可進一步監測與分析不同區域電離層異常形態，取代目前固定點(24^{o}N, 121^{o}E)的監測方式，或許能夠提供地震發生區域的預測參考。

為了能夠較正確判斷由地震產生的電離層電漿異常，本研究參考 Dst 指數以及利用全大氣模式(WACCMX)去除太陽活動影響以及大氣潮汐效應所產生的電離層電漿擾動。研究發現，在去除上述外來的影響之後，地震前電離層異常天的統計分析結果大致維持與上述相同的北、中、南異常分布形態。3 區整合統計結果來看，地震發生前 10~13 天以正異常較為明顯，而越接近地震於前 1~5 天則轉變為負異常為主。

根據上述統計分析結果，本研究進一步計算 5 一天內地震發生之統計參考機率(SRP 值)，並同時測試 1~5 天的 SRP 累計值與地震發生的次數，嘗試尋找決定地震預測成功機率的 SRP 值門檻值設定。分析結果顯示，5 天 SRP 累計值大於 0.2 的設定門檻對於有無去除太陽活動影響異常天來說，有最好的預測成功率。但對於去除大氣潮汐的結果來看，預測成功率普遍較低，說明本研究所採用去除電離層大氣潮汐效應的方法，似乎不太適合。建議或許可以改成分析 WACCMX 模式的異常天並去除其週期，取代分析平靜天的方法。

本研究採用的 SRP 值為固定點(24^{o}N, 121^{o}E)的計算，並且採取負異常機率以及預測天數設定為 5 天，將來可針對不同區域分別進行計算，以提供較精確區域空間上的地震預測參考機率，並且可進一步嘗試納入正異常計算參考機率，增加 SRP 值的準確性，以及增加預測天數設定。

五、成果的價值與貢獻、落實應用情形

本研究可以提供由電離層異常統計分析的地震發生參考機率資料，以供地震電離層前兆預警的參考。

六、參考文獻

Liu, J. Y., C. H. Chen, Y. I. Chen, W. H. Yang, K. I. Oyama, and K. W. Kuo (2010), A statistical study of ionospheric earthquake precursors monitored by using equatorial ionization anomaly of GPS TEC in Taiwan during 2001-2007. *J. Asian Earth Sci.*, **39**, 76-80, doi: 10.1016/j.jseaes.2010.02.012.

Liu, J. Y., W. H. Yang, C. H. Lin, Y. I. Chen, and I. T. Lee (2013), A statistical study on the characteristics of ionospheric storms in the equatorial ionization anomaly region: GPS-TEC observed over Taiwan, J. Geophys. Res. Space Physics, 118, 3856–3865, doi:10.1002/jgra.50366.

臺灣地區 110 年地震前兆監測資料彙整及分析

子計畫四

臺灣地震前兆的整合性研究

王錦華

中華民國地球物理學會

Abstract

The precursor time, *T*, is the time interval between the occurrence time of a precursor and that of a forthcoming earthquake with local magnitude, M_L. The precursors are classified into four types of earthquake prediction with different time windows: long-term prediction (*T*=3 to 10 years); intermediate-term prediction (*T*=6 months to 3 years); short-term prediction (*T*=8 days to 6 months); and imminent prediction ($T \leq 7$ days). Since the 1999 Chi-Chi earthquake, the precursors for numerous earthquakes in Taiwan have been observed and studied. The values of *T* and M_L are compiled from scientific literature. Two tables to show the values of *T* and M_L for different types of precursors are constructed.

Keywords: Earthquake prediction, Earthquake precursors, Precursor time, Earthquake magnitude

Notation

b: the b value of the frequency-magnitude law

d: the focal depth

DR=T_{ds}/T_{ns}: T_{ds} and T_{ns} are the total duration times of seismograms of an event recorded at a distant station and a nearby one, respectively

DRR: diurnal range ratio

EA: E_{index} anomaly

E_{index}: the OLR anomaly divided by a standard deviation

ELF: extremely low frequency (3−30 Hz)

EM: electromagnetic

EP: European Plate

ETAS: the Epidemic-Type Aftershock-Sequences

f_oF_2: the highest (or critical) frequency on an O-mode ionogram

GEMS: Geoelectric Monitoring System

GEMSTIP model: GEMS Earthquake-alarm Model

GPS: the global position system
LV: Longitudinal Valley
M_L: the local magnitude of an earthquake
M_{Lm}: the local magnitude of a mainshock
M_{Lf}: the local magnitude of the largest foreshock of a mainshock
M_H: Hsu's magnitude
M_D: duration magnitude
M_s: surface-wave magnitude
M_w: moment magnitude
N_mF_2: the greatest electron density in the ionosphere
n T (nano Tesla): a unit of geomagnetic induction (1 T=1 Weber/meter^2)
OLR: outgoing long-wave radiation
pCi/L: picocuries per liter of air (level of radon gas)
PI: pattern informatics
POEA: preseismic OLR E_{Index} anomaly
PSP: Philippine Sea Plate
Q_p: P-wave attenuation factor
Rn: radon
RTL: region-time-length
T: the precursor time
T_p: the time of a decrease in *b*-value from its peak
T_{Rn}: the precursor time of radon
T_{gr}: the precursor time of gamma ray emission
t_0: the appearance time of a precursor
t_r: the occurrence time of an earthquake
TEC: total electron content of the ionosphere
TGI: total geomagnetic intensity
TIRL thermal infrared radiation
ULF: ultra low frequency (300−3000 Hz)
v_p: P-wave velocity
Z/G: the ratio of vertical magnetic field, *Z*, to the horizontal one, *G*
ZIZ: the zero isoporic zone
Δ: the epicentral distance
δt_p: P-wave travel-time residue
γ-ray: gamma ray

1. Introduction

Wu and Feng (1975) made the first study of precursor for Taiwan's earthquake. They reported that the gas well pressure fluctuations occurred about 9 days before the January 18, 1964 M_L6.3 Tainan-Chiayi (Paiho) earthquake. The May 10, 1983 M_L6.4 (M_D5.7) Taipingshan earthquake is the first event for which several different types of

precursors were reported: *b*-value anomalies and foreshocks by Chen and Wang (1984) and Chen et al. (1990), changes of duration ratios of seismograms by Wang (1988), and radon (^{222}Rn) concentration changes by Liu et al. (1984). The radon (^{222}Rn) is simply denoted by Rn hereafter.

An abnormal increase in seismicity during 1977−1978 in Taiwan encouraged earthquake scientists of Taiwan and USA to promote a joint research program of earthquake precursors under the sponsors by National Science Council (NSC), ROC and U.S. Geological Surveys, USA. Tsai et al. (1983) reviewed the preliminary studies of precursors done by the colleagues of Institute of Earth Sciences, Academia Sinica and University of Southern California before 1983. However, they only described the installation of instruments and the studies of observations of five geophysical and geochemical phenomena (including spatial and temporal variations in micro-earthquakes, horizontal crustal deformations in eastern Taiwan, temporal variations in microgravity, temporal variations in geomagnetic total intensities, and changes of Rn concentrations in geothermal waters). Although the authors tried to correlate the changes of gravity and Rn concentrations with some earthquakes, they did not obtain positive correlations.

The 1999 Chi-Chi earthquake ruptured the Chelungpu fault in central Taiwan (e.g., Ma et al, 1999; Shin and Teng, 2001; Wang et al., 2005). Its epicenter is displayed with a solid star in Fig. 1. Unfortunately, this event was not predicted or forecasted by Taiwan's earthquake scientists because the Chelungpu fault was classified to be the Type-II active fault by the Central Geological Survey before 1999. After the earthquake, numerous earthquake scientists examined the recorded data and tried to search for the possible precursors before the event. Wang (2021) reviewed the observed precursors before the earthquak, compiled their precursor times from scientific literature, and discussed their reliability. Under sponsor by both Ministry of Education and NSC, a research program, entitled 'the Integrated Search for Taiwan Earthquake Precursors (iSTEP), was conducted by the earthquake scientists of National Central University (NCU) from April 2002 to July 2005 (Tsai et al., 2004). This program includes mainly five major components, i.e., identification of potential seismological, geomagnetic, geodetic and ionospheric precursors and statistical testing of any identified precursors. Tsai et al. (2004, 2006) reviewed the studies of numerous precursors, especially for the Chi-Chi earthquake, under the iSTEP program. In addition to the studies shown in the Tsai et al. (2004, 2006), Tsai et al. (2018) reviewed some chemical precursors done by geochemists of National Taiwan University. In addition, Liu et al. (2000) reported the anomalies of ionospheric f_oF_2 for $M_L \geq 5$ earthquakes. Liu et al. (2004a) reported the anomalies of ionospheric TEC for $M_L \geq 6$ earthquakes. Liu et al. (2006) reported the seismo-geomagnetic anomalies for $M_L \geq 5$ earthquakes. Liu et al. (2015) reported the anomalous lightning activities for $M_L \geq 5$ earthquakes. Chen et al. (2009) reported the preseismic geomagnetic anomalies. Chen et al. (2013b) reported the groundwater level changes for $M_L \geq 6$ earthquakes. Fu and Lee (2018) reviewed geochemical precursors.

The time interval between the occurrence of a certain precursor and that of the forthcoming earthquake is called the precursor time, T (Wang et al., 2016). The precursor time may be dependent upon the magnitude of a forthcoming earthquake and varies in different seismogenic-zone structures which may be distinct in different tectonic provinces. Wang (2021) define five types of earthquake prediction with different time windows for earthquakes in Taiwan: very-long-term prediction (T>10 years or longer); long-term prediction (T=3 to 10 years); intermediate-term prediction (T=6 months to 3 years); short-term prediction (T=8 days to 6 months); and imminent

prediction (T≤7 days).

In this study, we will compile the precursor times of long-term, intermediate-term, short-term, and imminent precursors of Taiwan's earthquakes from given scientific literature. The earthquakes of Taiwan were quantified with different magnitude scales (Shin, 1992; Wang and Miyamura, 1990; Wang, 1992, 1998), i.e., Hsu's magnitude M_H, duration magnitude M_D, surface-wave magnitude M_s, moment magnitude M_w, and local magnitude M_L, in different time periods. In the followings, the earthquake magnitude is unified to be the local magnitude, M_L, determined by the Central Weather Bureau (CWB) (Shin, 1992). The focal depth of an earthquake is denoted by d (in km) and the epicentral distance from an event to an observation station is shown by Δ (in km). Almost all authors took the earthquake data (including occurrences times, locations, and magnitudes) from the CWB.

2. Long-term Prediction

2.1 Mechanical Precursors

2.1.1 Stress Orientation Changes

Wu et al. (2010) determined the stress axes from the fault plane solutions of 4761 events of Taiwan during 1991−2007. They denoted the orientation of the maximum horizontal compressive stress axes to be SH. They recognized a counterclockwise rotation of SH in the entire ruptured area between 1991 and 1999 before the 1999 Chi-Chi earthquake. From the same data set, Hsu et al. (2010) also inferred changes of the distribution of the coefficients of friction and that of the pore pressures during 1991 to 1999. From the two studies, the precursor time is ~9 years (listed in Table 1).

2.1.2 Temporal Variation in Seismicity Pattern

The description about the studies of seismicity patterns can see Wang (2021). By applying the pattern informatics (PI) algorithm (Rundle et al., 2003; and cited references herein) to analyze M_L≥3.4 earthquakes with d≤20 km, Chen et al. (2005) found anomalous changes of seismicity and seismic quiescence over a time period of ~6 years before the 1999 Chi-Chi earthquake. Wu and Chen (2007) computed the standard normal deviate Z-values (cf. Meyer, 1975) for the temporal variation of monthly numbers of M_L≥2 events occurring from 1994 to 2006. They found that the areas with relatively high seismicity in eastern Taiwan from 1994 to 1998 became abnormally quiet before the mainshock; while the area with relatively low seismicity from 1994 to the occurrence of the mainshock in central Taiwan showed unusually active after the mainshock. The precursor time is ~6 years (listed in Table 1).

From the calculated PI values of seismicity before the December 26, 2006 Pingtung offshore doublet earthquakes with M_L=6.7 and 6.4, Wu et al. (2008, 2012) found that seismicity changed in March 2004 about 2.7 years before the mainshock. The precursor time is 2.7 years (listed in Table 1). Wen and Chen (2017) applied the region-time-length (RTL) algorithm to investigate the seismicity rate changes prior to the February 5, 2016 M_L6.6 Meinong earthquake in southern Taiwan. Seismic quiescence occurred soon after the February 26, 2012 M_L6.4 Wutai earthquake and then lasted until the occurrence of the 2016 Meinong earthquake, and the latter happened near a patch that was recognized as the seismic quiescence by Wen and Chen (2017). The precursor time is 4 years (listed in Table 1).

2.1.2 *b*-value Anomaly

The *b*-value anomalies before earthquakes have also been studied by numerous

researchers (see Wang et al., 2015, 2016; and cited references therein). As displayed in Fig. 2, the abnormal *b*-value started at t_0 and lasted until the occurrence of the mainshock. Thus, the total time period of abnormal *b*-values may be several years. Usually, there are two precursor times of abnormal *b*-values in literature (e.g., Wang et al., 2016): the first one is measured from the beginning of an increase in *b*-value to the occurrence time of an earthquake and the second one (denoted by T_p) done from the time of a decrease in *b*-value from its peak. Wang et al. (2016) compiled the values of T and T_p from the temporal variations in *b*-values of 45 earthquakes with $3 \leq M \leq 9$ occurred in various tectonic provinces. Their results show that both T and T_p increase with M. It is fine to take either T or T_p as the precursor time. From Fig. 2, the precursor time T includes both the increase and decrease in *b*-values, while the precursor time T_p includes only the decrease in *b*-values. Based on the model proposed by Wang (2016), T may represent the whole process of variation in *b*-value. Hence, T is better than T_p as the precursor time of the *b*-value anomalies.

Before the May 20, 1983 M_L6.4 (M_D5.7) Taipingshan earthquake, Chen and Wang (1984) and Chen et al. (1990) estimated the average *b*-value in every one year for seismicity from 1973 to 1982. Results show that in the source area the *b*-values gradually increased from 1978 and reached its peak in 1981, and then decreased. However, in the surrounding region of the source area the *b*-values increased markedly about 4.4 years before the mainshock and then decreased before it. The precursor time is ~4.4 years (listed in Table 1).

Based on the time series of *b*-values for $M_L \geq 2.0$ events with $d \leq 40$ km from January 1, 1994 to August 31, 1999 in three regions surrounding the source area of the Chi-Chi earthquake, Tsai et al. (2006) assumed that the *b*-value anomalies in northern and middle regions are a possible precursor of the mainshock. The precursor time is ~6 years (listed in Table 1).

Wu and Chiao (2006) calculated the *b*-values from a data set of 66069 $M_L \geq 2.0$ events with $d \leq 40$ km from January 1994 to the 1999 Chi-Chi earthquake. The time series of *b*-values reveal a decrease of *b*-value and an increase of seismicity in the area surrounding the source about 9 months before the earthquake. Their results give T_p=9 months. Chan et al. (2012) also measured the average value of T (≈3 years) for 23 Taiwan's earthquakes with $M_L \geq 6$, including the Chi-Chi earthquake, yet they did not provide the value of T for each event.

Wu et al. (2008) measured the *b*-values for the December 26, 2006 Pingtung offshore doublet earthquakes with M_L=6.7 and 6.4. Results show that the *b*-value changed about three years before the Pingtung doublets. Hence, the precursor time is 3 years (listed in Table 1).

2.1.3 Changes in the *P*-wave Travel-time Residuals

The general pattern of temporal variation in *P*-wave travel-time residuals (denoted as δt_p) before a forthcoming earthquake is simplified by a dashed line in Fig. 2. Lee and Tsai (2004) measured the mean values of δt_p at 11 seismic stations around the source area in three time periods: (1) the first period from January 1, 1991 to December 31, 1993; (2) the second period from January 1, 1994 to September 21, 1999; and (3) the third period from September 22, 1999 to December 31, 2002. The first and second periods were before the mainshock and the third one after the mainshock. The ranges of differences between the mean values of δt_p in the first period and those in the second one are: from +0.009±0.068 sec to +0.273±0.144 sec at 8 stations immediately west of the Chelungpu fault; from -0.053±0.083 sec to -0.117±0.087 sec at two stations

southeast of the fault; and from -0.149±0.151 at a station far west of the fault. Results show that δt_p increased at the stations immediately west of the Chelungpu fault about six years before the earthquake. It implies that *P*-wave velocity, v_p, began to decrease (like the left segment in Fig. 2) in 1994, about 6 years before the mainshock. The precursor time is ~6 years (listed in Table 1).

3. Intermediate-term Prediction

3.1 Mechanical Precursors

3.1.1 Crustal and Surface Deformations

From the ERS-2 radar images, Tsai et al. (2006) found that surface deformation began at least 3 years before the earthquake in an area immediately to the west of the northern segment of the fault. Hence, the precursor time is ~3 years (listed in Table 1).

3.1.2 Seismicity Pattern, Seismic Quiescence, and Foreshocks

Foreshocks are usually considered as one of the most significant premonitory phenomenon of a forthcoming earthquake, because they may accurately pinpoint the time and location of the mainshock. Before the May 20, 1983 M_L6.4 (M_D5.7) Taipingshan earthquake, Chen and Wang (1984) and Chen et al. (1990) observed two groups of foreshocks. The first one (called the forerunners here) occurred southeast of the source area from September 1, 1982 to April 30, 1983 about 8 months before the mainshock. The second one (i.e., the common foreshocks) took place within the source area on May 16 about four days before the mainshock. The precursor times are 8 months and 4 days, respectively, for the forerunners and foreshocks (listed in Table 1).

Wu and Chiao (2006) calculated the standard normal deviate *Z*-value (cf. Meyer, 1975) for seismicity before and after the 1999 Chi-Chi earthquake. Results exhibit that a decrease of seismicity rate started in January 1999 and lasted about 9 months, until the occurrence of the mainshock. They also claimed that the appearance of seismic quiescence was attributed essentially to a remarkable decrease in smaller-sized events with M_L<4. Wu and Chen (2007) also observed that the monthly number of events remarkably decreased in the source area from January 1999 to the occurrence of the mainshock. Their observation is similar to that established in Wu and Chiao (2006). From the studies of the two groups of researchers, the precursor time is ~9 months (listed in Table 1). The decrease of *b*-values observed by Wu and Chiao (2006) is consistent with the seismic quiescence found by Wu and Chen (2006).

Kawamura and Chen (2013) applied the Epidemic-Type Aftershock-Sequences (ETAS) model to study M_L≥2.4 events before the Chi-Chi earthquake. They found that seismic quiescence appeared within several areas near the mainshock epicenter from January 1, 1998 to September 20, 1999. The first seismic quiescence appeared about 21 months before the mainshock. Hence, the precursor time for seismic quiescence is 21 months (listed in Table 1). Kawamura et al. (2014) applied three approaches, e.g., the ETAS model, the PI method, and the ZMAP method that is similar to the Z-value method, to study seismicity pattern change in a broad area before two Nantou earthquakes. The first event with M_L=6.2 occurred on March 27, 2013 and the second one with M_L=6.3 happened on June 2, 2013. They found that before the first event, seismic quiescence appeared in three areas surrounding the epicenter. The first seismic quiescence appeared about ~1.5 years before the event and the second and third ones happened later. The precursor time is ~1.5 years or 18 months (listed in Table 1). Wen and Chen (2017) found the precursor time of seismic quiescence before the 2016 M_L6.4

Meinong earthquake is 4 years (listed in Table 1).

3.1.3 Groundwater Level Changes

According to the anomalous frequency characteristics of groundwater level from the corrected data at 54 wells, Chen et al. (2013b, 2015) observed abnormally changed groundwater levels at 78% (=42/54) of wells, which are located to the west of the mainshock epicenter, before the Chi-Chi earthquake. For example, at the Huatang (HT) station (shown with an open triangle in Fig. 1) the temporal variation in groundwater level from August 1, 1997 to September 19, 1999 is schematically displayed by thick line segments in Fig. 3 that is simplified from a figure in Chen et al. (2015) and the dashed line denotes the regular decrease in groundwater level. Clearly, the groundwater level decreased about 250 days (from January 17), reached the bottom (~-1.5 m) then immediately increased about 130 days (from May 18), and returned to a local maximum about 13 days (from September 7) before the mainshock. For all stations in consideration, they observed that groundwater level changes ranged from 2 m to 4 m. The precursor time is ~250 days (listed in Table 1).

Chen et al. (2013b) examined variations of amplitude of water-level changes at a particular frequency band between 0.02 day^{-1} and 0.04 day^{-1} for M_L>6 earthquakes in Taiwan from August 1, 1997 to December 31, 2009. They found that the enhanced amplitudes in the frequency band were consistently observed prior to the July 27, 1998 M_L6.2 Reili and November 5, 2009 M_L6.2 Mingjian earthquakes during the 12.5-year study period. However, they did not provide the precursor time.

3.2 Electromagnetic Precursors: Geomagnetic Annual Changing Rate

Since 1988, a geomagnetic network (abbreviated as the IESGN) consisting of 22 stations has been installed in Taiwan by the IES (Yeh et al., 1981). Among them, 8 stations are also equipped with continuous recording systems. Among the eight stations, the Lunping (LP) station (shown by a solid square in Fig. 1) is located at a low-seismicity area and thus commonly taken as a reference station, while others (shown by open squares in Fig. 1) are all located at the seismically active areas. Other seven stations are Liyutan (LY), Tsengwen (TW), Neicheng (NC), Hualien (HL), Yuli (YL), Taitung (TT), and Hengchun (HC).

Chen et al. (2004a) took the LP station as a reference one for others and examined the temporal variations in the total geomagnetic field recorded at the eight stations from 1999 to 2001. Their results exhibit that a zero isoporic zone (ZIZ), which is defined as the annual change rate of geomagnetic parameters≤±5 nT/yr, appeared near the source area about 2 years before the 1999 Chi-Chi earthquake. Up to date, this precursor is the only one intermediate-term EM precursor that has been observed in Taiwan. The precursor time is ~2 years (listed in Table 1).

3.3 Chemical Anomalies: Changes of Geochemical Compositions

Song et al. (2003) analyzed the anions, e.g., SO_4^{-2}, and NO_3^{-1}, of the bottled water (named as Chingjing water), which was pumped from wells at Puli (displayed by a larger-size open circle in Fig. 1), Nanton County in central Taiwan, from December 1, 1998 until after the event. Results show steady increases in concentrations of both sulfate (SO_4^{-2}) and nitrate (NO_3^{-1}) from the average constant levels, which were measured from December 1, 1998 to March 31, 1999, after April 1, 1999. The concentrations reached the peak with an excess of 129.9 and 94.7% in April 1999, then remarkably dropped from July 1999, and finally decreased until the mainshock. The precursor time is ~7 months (listed in Table 1). Wang et al. (2005) reported isotopic and hydrological changes prior to the Chi-Chi earthquake. But, they did not provide the

times of changes.

4. Short-term Prediction

4.1 Mechanical Precursors

4.1.1 Subsurface Deformations

Kuo et al. (2010) estimated the aseismic crustal strain at the Antung hot spring prior to three events, i.e., the December 10, 2003 M_L6.4 (M_w6.8) Chengkung earthquake with d=17.7 km and Δ=20 km, the April 1, 2006 M_L6.0 (M_w6.1) Taitung earthquake with d=17.9 km and Δ=55 km, and the February 17, 2008 M_L5.4 (M_w5.0) Antung earthquake with d=28.3 km and Δ=11 km. The strain increased about 3, 2.5, and 2.5 months, before the 2003, 2006, and 2008 events, respectively. Hence, the precursor time is 2.5−3 months (listed in Table 1).

Chen et al. (2011a,b) used the GPS index method to study crustal deformations for 32 $M_L \geq 5$ earthquakes during 2006−2009. Results show that the crustal deformations were re-oriented into a parallel direction a few days before 63% (=20/32) events. Such a parallelism of GPS index becomes random in order when the stress is close to the threshold of faulting. They found that the time period from the presence of random orientation of crustal deformations to earthquake occurrence is positively related to earthquake magnitude. The precursor time is a few days (listed in Table 1). Chen et al. (2013a) calculated the GPS index before the March 4, 2010 M_L6.4 Jiashian earthquake. They found that an average of ~60^o and GPS index=~0.017 gradually appeared in an area around (22.5^{o}N, 120.7^{o}E), which is to the south of the mainshock epicenter (22.97^{o}N, 120.71^{o}E), about 8 days before the mainshock. This phenomenon suggests that the stresses related to the mainshock was gradually disturbed on the crust and thus induced subsurface movements toward the NE direction. The precursor time is 8 days (listed in Table 1).

From the GPS data, Fu et al. (2017b) observed a decrease in extension rate about 4 months before the October 31, 2013 M_L6.4 Rueisuei earthquake. The precursor time is 4 months (listed in Table 1).

4.1.2 Variation in *b*-values

Lin (2010) estimated the *b*-values of background seismicity and foreshocks before the March 4, 2008 M_L5.2 Taoyuan earthquake in southern Taiwan. He found that the *b*-value of foreshocks occurred about one month before the mainshock was higher than that of background seismicity because a remarkable decrease in M_L>2.2 events. The precursor time is one month (listed in Table 1).

4.1.3 Q_p Changes

Wen et al. (2015) measured the temporal variation in Q_p of *P*-waves from January 2009 to January 2010. Results show that the Q_p began to decrease at all stations about 2-months before the November 5, 2009 M_L6.2 Ming-Jen earthquake. The precursor time is 2 months (listed in Table 1)

4.1.4 Groundwater Level Changes

Yu and Mitchell (1988) observed clear groundwater level change at a well, which has a depth of 500 m and is located at the Chingshui River in Ilan, northeastern Taiwan. This abnormal phenomenon appeared about 10 days before the January 16, 1986 M_L6.2 offshore Ilan earthquake. The precursor time is 10 days (listed in Table 1).

4.1.5 Gas Well Pressure Fluctuation

Wu (1975) and Wu and Feng (1975) reported that the gas well pressure fluctuations occurred about 9 days before the January 18, 1964 M_L6.3 Tainan-Chiayi (Paiho) earthquake. The precursor time is 9 days (listed in Table 1).

4.2 Electromagnetic Precursors

4.2.1 Geoelectric Field Anomalies

Chen and Chen (2016) installed a network (named as the GEMS network) including 22 stations (illustrated by crosses in Fig. 1) in Taiwan to monitor the geoelectric field. They also developed an earthquake-alarm model (called the GEMSTIP model) based on the skewness and kurtosis anomalies of geoelectric field. Using the model, they studied the anomalies of geoelectric field for $M_L \geq 5$ earthquakes. Results reveal that the precursor times are 5−80 days (with a median value of 60 days) at different stations. A time lag that exists between clusters of anomalies and earthquakes depends on local geological structures and the durations of anomalies. Chen et al. (2017) observed the appearance of anomalies at four stations, i.e., LIOQ, WANL, KAOH, and CHCH, near the epicenter before the February 6, 2016 M_L6.6 Meinong earthquake. The precursor times are 20 days at the CHCH station and 50 days at the KAOH station. The precursor time is 5−80 days (listed in Table 1).

4.2.2 Seismo-geomagnetic Anomalies

From the analyses of the data recorded by the IESGN, Yen et al. (2004) observed significant fluctuations, with the largest amplitude up to 200 nTs, in the differences of total geomagnetic intensity (TGI) between the LY station and the LP station during mid-August (about 1.1 months before the 1999 Chi-Chi earthquake) to November 1999. The precursor time is ~1.1 months (listed in Table 1).

From the data recorded by the IESGN during 1988–2001, Liu et al. (2006) studied the temporal variations in TGI before $M_L \geq 5$ earthquakes. First, they computed the diurnal range ratio, DRR, of TGI at a station over that at the LY station. Secondly, they calculated the ratio of monitored number of each DRR to the total monitored number in five different time intervals before and after an earthquake and the average ratio of monitored number of each DRR in the whole 13 years. They took the average ratio as the reference. Finally, they plotted the distributions of the ratio in five different time intervals. Their results show that the distribution of the ratio in the month before the mainshock and that in the month during and after the mainshock clearly departed from the reference one. They assumed that changes of underground conductivities/currents underneath the epicentral area and focal mechanism of a forthcoming mainshock are the main factors in affecting the preseismic TGI. Compared with the results by Yen et al. (2004), the precursor time for TGI anomalies observed by Liu et al. (2006) is ~1 month (listed in Table 1).

Chen et al. (2009) studied the possible geomagnetic anomalies before 181 $M_L \geq 4$ earthquakes during 2002−2005 by applying the singular value decomposition (SVD) technique to analyze the 3-component records through a window of 900 s for every 5-day period in four years. Results reveal that anomalous geomagnetic fields appeared about 10 days before the earthquakes. Hence, the precursor time is 10 days (listed in Table 1).

4.2.3 Thermal Infrared Radiation

From a large dataset of night-time measurements of thermal infrared radiation (TIR) from Geostationary Meteorological Satellite/Visible and Infrared Spin-Scan Radiometer (GMS-5/VISSR), Genzano et al. (2015) identified three significant sequences of TIR

anomalies before the 1999 Chi-Chi earthquake and one of them appeared about 14 days before and very close to the epicenter. The precursor time is 14 days (listed in Table 1). Pulinets and Dunajeck (2007) analyzed the transient long-wave radiation (OLR) observed by NASA Aqua/AIRS prior to an M_L5.6 (or M_s5.9) earthquake (with d=15.3 km) that occurred offshore southeast Taiwan on Feb. 19, 2009. They obtained the normalized residual on 4 days in the day-time and 1, 6, and 9 days in the night-time before the earthquake. Hence, the precursor time is 9 days (listed in Table 1). Pulinets and Ouzounov (2011) analyzed the transient OLR observed by NASA Aqua/AIRS prior to an M_L6.0 (or M_s6.2) earthquake (with d=27.1 km) that occurred offshore southeast Taiwan on May 19, 2004. They measured the static 5-year standard deviation in the time period during May 2003 to December 2007 and the static mean of 18th–20th of five years from 3 day moving mean samples. Finally, they obtained the normalized residual in the time interval of May 18–20, 2004. This led to the appearance of E_{index} anomaly in this time interval. This suggests that the POEA appeared one day before the earthquake. Hence, the precursor time for this earthquake is 1 day (listed in Table 1).

Fu et al. (2020) proposed a method to detect the variation in OLR from the satellite data. They defined the standardized anomaly E_{Index} to be the OLR anomaly divided by a standard deviation and considered an anomaly, *EA*, of E_{Index} as the preseismic signal. By applying this method to analyze the satellite data for 35 M_L≥6 earthquakes during 2009−2019, they found that typhoons and focal depths are two significant factors in influencing the variation in E_{Index}. From the plot of the number of precursory *EAs* versus M_L, they found that the number only slightly increases with M_L because the data points are scattered. They observed consecutive appearances of *EAs* of LWR about 2–15 days before 77% of earthquakes and thus they considered this phenomenon as a preseismic OLR E_{Index} anomaly (POEA). From the figures in Fu et al. (2020), we can see that the spatial distribution of POEA is quite random and the POEA appeared only on several days in either day time or night time before the forthcoming earthquakes. This is similar to the observation by Ouzounov et al. (2018). Meanwhile, the OLR anomalies vary very much for different earthquakes. In this study, we take the largest value of days before a forthcoming event to be the precursor time. From the four studies, the precursor times are 1–25 days (listed in Table 1).

4.2.4 ULF Emissions

For the 1999 Chi-Chi earthquake, Akinaga et al. (2001) measured the polarization that is the ratio, *Z/G*, of vertical magnetic field, *Z*, to the horizontal one, *G*, from the records of ultra low frequency (ULF, 3003−000 Hz) emissions recorded at the LP station. Results exhibit a significant increase in *Z/G* about two months before the mainshock. Hence, the precursor time is ~2 months (listed in Table 1).

4.2.5 Atmospheric Electric Field Anomalies and Lightning

Liu et al. (2015) examined lightning activities 30 days before and after 78 inland and 230 offshore M_L≥5 earthquakes during 1993–2004. They studied the correlations between lightning activities and the location, depth, and magnitude of earthquakes. Results show that lightning activities appear mainly in the area around the forthcoming earthquake and were significantly enhanced in 1−30 days, with the largest values from 17 to 19 days, before the M_L≥6 inland events with d≤20 km. This suggests that preseismic slip of an earthquake with d>20 km are unable to generate lightning. Moreover, they mentioned that the area around a mainshock epicenter specified with enhanced lightning activity is proportional to M_L. The precursor time is 1−30 days (listed in Table 1).

4.3 Chemical Anomalies

4.3.1 Changes of Geochemical Compositions

Yang et al. (2006) constructed an automatic gas station (denoted by CL and illustrated by an open triangle in Fig. 1) near the Chuko fault and the Chiayi fault in southwestern Taiwan to continuously monitor the contents of CO_2, CH_4, N_2 and H_2O. They observed significant anomalies in the CO_2/CH_4 ratio about 0.1−28.1 days before several $M_L \geq 4.0$ earthquakes. The precursor time is 0.1−28.1 days (listed in Table 1).

4.3.2 Changes of Radon Concentrations

Liu et al. (1983) first observed the Rn concentrations in soils. Liu et al. (1984) measured Rn concentration in geothermal waters and CO_2-rich cold spring waters at four stations in northern Taiwan from July 1980 to December 1983. Spike-like Rn anomalies were recorded at three stations for 7 $M_L \geq 4.6$ offshore Ilan earthquakes. Except one, anomalies appeared about 4−51 days before the events with $d<10$ km and $\Delta=14-45$ km. The precursor time is 4−51 days (listed in Table 1).

Rn concentration anomalies were observed at the CL station. Anomalies appeared about 0.49−7.40 days prior to 15 $M_L \geq 3.7$ earthquakes with $d=2.1-25$ km and $\Delta=4.8-93$ km (Chyi et al., 2001) and about 0.49−6.82 days prior to 35 $M_L \geq 3.7$ events with $d=2.1-32.2$ km and $\Delta=1.5-257.5$ km (Chyi et al., 2005). But, there were two particular events. Anomalies appeared 8.36 days before an event with $d=3.0$ km and $\Delta=39.3$ km and 13.0 days before the other with $d=6.7$ km and $\Delta=3.0$ km. Yang et al. (2005) observed some spike-like anomalously high radon and thoron concentrations in soil gases. They also obtained a similar soil Rn spectrum from another station, which was 100 m away from the CL station. Anomalies occurred 1.3−14.2 days before 30 $M_L \geq 4.5$ events with $d=2.5-88.8$ km and $\Delta=4.9-152.4$ km. Fu et al. (2017c) observed a significant increase in soil Rn concentrations at CL, HH, PT, and CS stations (all illustrated by open triangles in Fig. 1) about 14 days before the February 6, 2016 M_L6.6 Meinong earthquake in southern Taiwan. From the four studies, the precursor time is 0.49−14.2 days (listed in Table 1).

Fu et al. (2009) observed Rn concentrations in soil gases across the Chihshang Fault on the LV in eastern Taiwan. They found some high Rn concentration anomalies a few days before local earthquakes. However, they did not provide the magnitude range of events. The precursor time is few days (listed in Table 1). At the DHUG station (illustrated by an open triangle in Fig. 1) on the National Dong-Hua University in eastern Taiwan, Rn concentrations significantly increased about 60 days before the October 31, 2013 M_L6.4 Rueisuei earthquake and 21 days before the May 21, 2014 M_L5.9 Fanglin earthquake (Fu et al., 2017b). The two events occurred in the LV area. The precursor times are 21 days and 60 days (listed in Table 1).

Fu et al. (2017a) studied the spatial distribution and temporal variation of anomalies of He, Rn, N_2, CO_2, and CH_4 in soil gases before 25 events with $M_L = 3.2-7.0$, $d=7.9-132.1$ km, and $\Delta=7.0-320.1$ km in northern Taiwan. They assumed that spatial anomalies are related to tectonic faults because they found the appearance of high helium and nitrogen concentrations in samples obtained from some specific sites which are associated with the structural setting of the area. They constructed an automatic soil-gas station at Tapingti (denoted by TPT and showed by an open triangle in Fig. 1). They found that for 25 earthquakes, anomalously high Rn concentrations recorded at the station appeared about 0.2−17.4 days before 13 events, yet not before other 12 events. Among the 12 events, 11 events had $\Delta>58$ km and a small one of $M_L=3.5$ had $\Delta=7.8$ km.

This might indicate that Rn concentration anomalies cannot be induced by either distant events or small ones. The precursor time is 0.2−17.4 days (listed in Table 1).

At the TPT station, Fu et al. (2019) observed anomalous Rn concentrations before 20 of 37 M_L=2.3−6.7 events that happened during July 1, 2014 to June 1, 2015. The magnitudes of the 15 events are M_L=2.7−6.7. The authors divided 37 events in study into two groups: 27 $M_L \geq 5.0$ events for the first group and 10 $M_L \leq 4.0$ events for the second one. For the first group, expect for one with M_L=5.1 and Δ=37.0 km, anomalies were not observed for the events with Δ>55.0 km. This seems to suggest that for the study area, Δ=55.0 km may be an upper bound for the generation of anomalies due to preseimic slip. For the second group, anomalies appeared only before 3 events: 1 day before an event with M_L=3.5, d=10.0 km, and Δ=64.0 km; 3 days before an event with M_L=2.3, d=6.2 km, and Δ=71.0 km, and 4 days before an event with M_L=2.9, d=6.0 km, and Δ=70.0 km. Consequently, the precursor times are 1−23 days (listed in Table 1).

Kuo et al. (2006a,b, 2010) measured the Rn concentrations at the D1 station (illustrated by an open triangle in Fig. 1) at Antung before three events as mentioned in Sub-section 4.4.1. They found that Rn concentrations decreased from background levels of 791±46, 762±57, and 735±48 pCi/L to the minima of 326±9, 371±9, and 480±43 pCi/L about 3, 2.5, and 2.5 months, before the 2003, 2006, and 2008 events, respectively. Kuo et al. (2017, 2018, 2019) measured the Rn concentrations recorded at the P1 station (illustrated by an open triangle in Fig. 1) at Peiho before five earthquakes, i.e., the March 4, 2010 M_L6.4 (M_w6.3) Jiasian earthquake with d=22.6 km and Δ=46 km, July 12, 2011 M_L5.3 (M_w5.0) Chimei earthquake with d=31.2 km and Δ=47 km, March 27, 2013 M_L6.2 (M_w6.0) Jenan earthquake with d=19.4 km and Δ=87 km, June 2, 2013 M_L6.5 (M_w6.3) Yuchi earthquake with d=31.5 km and Δ=78 km, and February 5, 2016 M_L6.4 (M_w6.4) Meinong earthquake with d=16.7 km and Δ=45 km. They found that Rn concentrations decreased from background levels of 144±7, 752±24, 134±5, 137±8, and 137±8 pCi/L to minima of 104±8, 447±18, 85±4, 97±9, and 97±9 pCi/L about 80, 54, 104, 171, and 54 days before the 2010 Jiasian, 2011 Chimei, 2013 Jenai, 2013 Yuchi, and 2016 Meinong earthquakes, respectively. Hence, the precursor times obtained by Kuo and his co-authors are 54−171 days (listed in Table 1). They also found that the Rn concentration decreased and the aseismic crustal strain increased before the seven thrust-faulting events.

4.3.3 Changes of γ-ray Emissions

The gamma-ray (written as γ-ray hereafter) emission is mainly produced from the radioactive decay of Rn or from thunderstorms (e.g., Minnehan, 2015). Since fluctuations of γ-ray records are inversely correlated with atmospheric temperature, this effect must be removed from the recorded data. Four automatically monitoring γ-ray stations (as illustrated with open diamond symbols in Fig. 1) have been installed in Taiwan (Fu et al., 2015). The four stations are: the YMSG station at the Taiwan Volcano Observatory (TVO) in Mt. Yangming, northern Taiwan the DHUG station at National Dong-Hwa University in Hualien, eastern Taiwan, the CCUG station at National Chung-Cheng University in Chiyi, western Taiwan, and the KTPG station at Kenting National Park in Pingtung, southern Taiwan.

Fu et al. (2015) observed anomalous γ-ray emission rate at DHUG station a few days before some earthquakes in eastern Taiwan. In 2014, the γ-ray emission rate remarkably increased about 7 days before two earthquake swarms: from March 20 to 26 before a swarm (with a maximum magnitude of 4.4) of March 26−27 and from April 22

to May 1 before the other (with a maximum magnitude of 5.3) of May 3−5. Furthermore, an anomaly in γ-ray emission continuously increased (~8%) about 14 days before the May 21, 2014 M_L5.9 Fanglin earthquake. The precursor time is few to 14 days (listed in Table 1).

At the YMSG station, Fu et al. (2019) observed anomalous γ-ray emissions before 20 of 37 M_L=2.3−6.7 events that happened during July 1, 2014 to June 1, 2015. The magnitudes of the 20 events are M_L=2.8−6.7. The authors divided 37 events in study into two groups: 27 M_L≥5.0 events for the first group and 10 M_L≤4.0 events for the second one. For the first group, anomalies appeared about 3−20 before13 events; while for the second group, anomalies appeared about 2−7 before 7 events. Consequently, the precursor time is T=2−20 days (listed in Table 1).

5. Imminent Prediction

5.1 Mechanical Precursor

5.1.1 Foreshocks

Chen and Wang (1984) and Chen et al. (1990) observed foreshocks that occurred within a small area about 4 days before the May 20, 1983 M_L6.4 Taipingshan earthquake. The M_L value of the largest foreshock was 5.5. The mainshock occurred in the southern part of the foreshock area. The precursor time is ~4 days (listed in Table 1).

Lin (2009) studied foreshock activities of 10 M_L≥5 earthquake sequences with M_L≥4.0 felt foreshocks during 1990−2004. He stressed that when the largest foreshock and the mainshock have the similar focal mechanism, the former commonly occurred 5 days before and at a distance of 15 km from the latter. He also addressed that such a kind of felt foreshock often happens at the strongly heterogeneous crust, particularly along the convergent zone between the EP and PSP. The precursor time is 5 days (listed in Table 1)

Lin (2010) studied the foreshock activities of the March 4, 2008 M_L5.2 Taoyuan earthquake in southern Taiwan. He found that the earthquake was preceded by two groups (A and B) of foreshocks that clustered along the major fault plane and dipped to southeast. Group A, consisting of 29 micro-events with 0.6≤M_L≤2.2, occurred several hours before the mainshock. Group B, including 35 events with the largest one having M_L=4.0, started about 20 minutes before the mainshock. The precursor times are from 0.3 to several hours (listed in Table 1).

Before the M_L6.2 (M_w6.3) Hualien earthquake of February 6, 2018, there were foreshocks with the largest one of M_L=5.8 or M_w=6.1 (e.g., Chan et al., 2019). The precursor time is 2 days (listed in Table 1).

5.1.2 Slow-slip Events

Based on the surface crustal deformations integrated from broadband velocity seismograms of the CWB, Lin (2012) found significant deviations of the vertical displacement from a normal Earth tidal pattern during 15−19 September before the 1999 Chi-Chi earthquake. He assumed that this phenomenon was caused by a series of slow-slip events on the nearly horizontal plane (i.e., the decollement) of the Chelungpu fault at depths of 10−12 km. The precursor time is ~5 days (listed in Table 1).

5.1.3 Infrasound

From the records of an infrasound recording system installed by the Institute of Acoustics, Chinese Academy of Science at Beijing, PRC, Xia et al. (2011) observed

anomalous infrasound signals with a peak amplitude of 1100 mV at 16:00–16:40pm on September 18 that was about 3 days before the 1999 Chi-Chi earthquake. The precursor time is ~3 days (listed in Table 1).

5.1.4 Duration ratio

Wang (1988) estimated the change of coda waves before and after an earthquake from a comparison between the code-wave attenuation between an earthquake and a distant station and that between the event and a nearby station. He defined the duration ratio to be $DR=T_{ds}/T_{ns}$ where T_{ds} and T_{ns} are the total duration times of seismograms of an event recorded at a distant station and a nearby one, respectively. The way to determine the duration of a seismogram is based on the waveform amplitude. Before the May 10, 1983 M_L6.4 Taipingshan earthquake, four distant stations and one nearby station of the Taiwan Telemetered Seismographic Network operated by the IES (Wang, 1989) had the same gain with 72 dB. From the seismograms recorded at the five stations, Wang (1988) measured the daily *DR* values in ten days before the earthquake. Results show that the *DR* values show increased about 4 days before the earthquake. Hence, the precursor time is 4 days (listed in Table 1).

5.2 EM Precursors

5.2.1 TEC and f_oF_2 Anomalies

Liu et al. (2001) first used two methods to study the seismo-ionospheric signatures prior to an earthquake. First, they measured the TEC recorded by a network of the GPS receivers in Taiwan. Secondly, they analyzed the time series of TEC recorded by an ionosonde that is a sweep frequency pulsed radar device located at (25.0°N, 121.l°E) in Chungli (illustrated with a larger-sized open circle in Fig. 1). The time series obtained from the two methods reveal a similar tendency of temporal variation. Liu et al. (2001, 2004a,b) applied the two methods to study the temporal variation in TEC prior to the 1999 Chi-Chi earthquake. The temporal variation in TEC is schematically displayed in Fig. 4 where the solid line and dotted lines represent the observations and references (previous 15-day median), respectively. Note that this figure is simplified because the fluctuations are not included. From a comparison between the disturbed data and reference ones, they suggested that TEC decreased significantly in the afternoons about 4, 3, and 1 days before the mainshock.

Chuo et al. (2002) analyzed the temporal variation in f_oF_2 recorded at the ChungLi ionosonde station before and after the 1999 Chi-Chi earthquake. Their results are similar to Fig. 14. Results show that the perturbation appeared few days before the event. From Liu et al. (2001, 2004a,b) and Chuo et al. (2002), the precursor times are 3−4 days (listed in Table 1).

Liu et al. (2004b) examined preseismic TEC anomalies for 20 $M_L\geq6$ earthquakes in Taiwan from September 1999 to December 2002. Results show that the anomalies appeared about 5 days prior to 16 events (about 80% of events in study). Liu et al. (2000, 2004a, 2018) examined anomalies of f_oF_2 and TEC for 144 $M_L\geq5$ earthquakes during 1997−1999. Results show that remarkable decreases in f_oF_2 and TEC about 4 days before the events. Liu et al. (2008) measured the TEC and N_mF_2, which is the greatest electron density in the ionosphere, before the December 26, 2006 M_L7.0 offshore Pingtung earthquake doublet. Results show abnormal decreases in TEC and N_mF_2 about 4 days before the earthquake doublets. The precursor time is 3−5 days (listed in Table 1). Liu et al. (2008) also reported the appearance of quasi 3-minute fluctuations of pronounced vertical motion in the ionosphere also appeared during the last two days prior to the earthquake doublets.

5.2.2 Atmospheric Electric Field Anomalies and Lightning

From the records of cloud-to-ground lightning occurred 15 days before and after the 1999 Chi-Chi earthquake, Tsai et al. (2006) and Liu et al. (2015) reported that the frequency of lightning significantly increased on September 17, 1999 about 4 days before the mainshock, and the lightning occurred mainly on the southern end of the Chelungpu fault near the epicenter. The precursor time is ~4 days (listed in Table 1).

Based on the corona current measurements, Kamogawa et al. (2004) observed that the atmospheric electric field (AEF) anomalies appeared about 2 and 4 hours before the March 31, 2002 M_L6.8 Jiashian earthquake. The precursor time is about 2−4 hours (listed in Table 1).

5.2.3 Sub-ionospheric ELF/ULF Emissions

From the sub-ionospheric ELF/ULF emissions recorded at Nakatsugawa observatory (35.4^{o}N, 137.5^{o}E) in Gifu Prefecture, Japan, during January 1 to September 21 in 1999, Ohta et al. (2001) observed a remarkable change in ELF emissions in 1.5 hours during 20:30–22:00pm (Taiwan Local Time) on September 20. The phase difference of the ELF emissions indicates that the signals had propagated in the sub-ionospheric waveguide over a long distance and the main direction of the ELF/ULF emissions pointed toward Taiwan. This suggests that the ELF/ULF emissions were produced from the preseismic slip of the 1999 Chi-Chi earthquake. The precursor time is ~4 hours (listed in Table 1).

Magnetic storms may strongly influence geomagnetic fields. In order to remove the effect by magnetic storms, Wen et al. (2012) isolated amplitude enhancements from the computation of the cross correlations between amplitudes in the earthquake- related frequency band of 0.1–0.01 Hz and those in the comparable low frequency band of 0.01–0.001 Hz. They took the computed value as an index of identifying the seismo-geomagnetic anomalies. Results reveal that the index suddenly decreased near the mainshock epicenter a few days before 6 of 9 $M_L \geq 5$ earthquakes that occurred between September 2010 and March 2011. The precursor time is few days (listed in Table 1).

5.2.4 Sky and Earthquake Lights

Chen et al. (2000) reported preseismic sky light (with different colors) and coseismic seismic (green) light before and after the 1999 Chi-Chi earthquake. The ‘sky light’ might be the earthquake light because it was associated with the earthquake (e.g., Lockner et al., 1983; Lockner and Byerlee, 1985; Derr, 1973, 1986; and cited references therein). Preseismic sky lights were seen by local people several times from north to south along the Chelungpu fault. The precursor time is few hours (listed in Table 1).

5.3 Chemical Anomalies

5.3.1 Changes of Geochemical Compositions

Song et al. (2006) measured cation and anion concentrations from water samples at Kuantzeling (denoted by KTL and displayed with a larger-sized open circle in Fig. 1), Chiayi in west-central Taiwan from July 15, 1999 to the end of August 2001. Results reveal that the concentrations of chloride and sulfate ion abruptly increased on September 19 about two days prior to the 1999 Chi-Chi earthquake. The precursor time is ~2 days (listed in Table 1).

Walia et al. (2009) measured soil-gas compositions at stations near the Hsincheng fault, Hsinchu from January 1, 2006 to July 14, 2008 and at those near the Hsinhua fault, Tainan from October 30, 2006 to July 14, 2008. Near the Hsinhua fault, they observed

28 anomalies and 22 of them were associated with 22 of 28 events that occurred in the south or southeastern part of Taiwan. Near the Hsincheng fault, they observed 29 anomalies and 18 of them were related to 18 of 38 events that occurred along Okinawa Trough and Ryukyu Trough. The success ratio is higher for the stations near the Hsinhua fault (79%) than for those close to the Hsincheng fault (62%). For some cases, the precursor time is 1–5 days. Since Walia et al. (2009) did not provide the values of T, M_L, d, and Δ for all events in use, their results are given only in Table 1, yet not in Fig. 6. Based on the technique developed by Walia et al. (2009), Walia et al. (2013) observed the appearance of anomalies 3 days before the October 4, 2009 M_L6.1 earthquake with d=29.6 km in eastern Taiwan and 5 days before the March 4, 2010 M_L6.4 earthquake with d=22.6 km in southern Taiwan. The precursor time is 3–5 days (listed in Table 1).

5.4 Biological precursors: Anomalous Animal Activities

Chen et al. (2000) collected the data of anomalous activities for 12 kinds of animals at 28 locations before the 1999 Chi-Chi earthquake. Except for the 28th location at Jiou-Fen-Erl-Shan with an epicentral distance >10 km, other 27 locations are very close the Chelungpu fault. Jiou-Fen-Erl-Shan is almost in between the Chelungpu fault and Puli. The aberrant behavior of ants occurred as early as 8−10 weeks at a location and 3 days at four other places before the mainshock. The aberrant behavior of cicadas occurred 4−6 weeks at a locality before the mainshock. The aberrant behavior of earthwarms, diplopods, and fishes occurred about 1−2 weeks at some locations before the mainshock. The aberrant behavior of birds occurred ≤7 days at three locations before the event. The roachs abnormally appeared 3 days at a location before the mainshock. The cats abruptly disappeared and turtles abruptly appeared at the same local area ~1 day before the mainshock. The aberrant behavior of dogs occurred at several locations <1 day before the mainshock. The snakes abruptly appeared at a location ~2 hours before the mainshock. The precursor times for all animals in study are listed in Table 2 where there are three time windows: week, days, and hours.

6. Summary

Earthquake prediction has been a long-term debatable problem in earthquake science. In order to resolve the problem, one of the ways is to study the possible precursors of a single earthquake. Since the occurrence of the 1999 Chi-Chi earthquake of 20 September, 1999, numerous precursors have been widely observed and studied for many earthquakes in Taiwan. This makes us a chance to explore the debatable problem. In this study, except for the very long-term prediction specified with earthquake recurrence all precursors collected from scientific literature are classified into four categories: (1) mechanical precursors, including seismicity pattern changes, seismic quiescence, crustal deformations, b-value anomalies, changes of seismic-wave velocities, hydrological changes, slow-slip events, infrasound, etc.; (2) electromagnetic (EM) precursors, including earthquake lights, thermal infrared radiations or long-wave radiation, geomagnetic fluctuations, sub-ionospheric EM ELF/VHF emissions, cloud-to-ground lightning, anomalies TEC and f_oF_2, etc.; (3) chemical precursors, including changes of geochemical compositions and radon, gamma (γ) ray emissions, etc.; and (4) biological precursors, including anomalous behavior of animals.

Based on the time window (or the precursor time, T), earthquake prediction is defined as follows: long-term prediction (ten years>T>three years); intermediate-term prediction (T=six months to three years); short-term prediction (T=eight days to six months); and imminent prediction (T≤seven days). The precursor times and ranges of

local magnitudes of related events have been compiled and listed in two tables for different time windows.

For the long-term prediction, only mechanical precursors were observed for the 1999 Chi-Chi earthquake and a few larger-sized events. The substantial results are: the change of stress field before the 1999 Chi-Chi earthquake; the change of seismicity pattern before several earthquakes; the appearance of b-value anomalies and changes of *P*-wave travel-time residuals before the Chi-Chi earthquake.

For the intermediate-term prediction, four mechanical precursors, an EM precursor, and a geochemical precursor were observed for the 1999 Chi-Chi earthquake and a few larger-sized events. The substantial results are: the appearance of seismic quiescence before the Chi-Chi earthquake and a positive correlation between the ground water level changes and geochemical composition changes before the 1999 Chi-Chi earthquake. The changes of groundwater levels and geochemical compositions may be interpreted by the temporal variation of stresses in the topmost layer above the source area.

For the short-term and imminent prediction, there are abundant observations of four categories of precursors for the 1999 Chi-Chi earthquake and a few larger-sized events. Hence, the observations and studies of precursors of the two types of prediction are particular important on and directly related to the prediction of earthquakes. I expect that more observations and studies of short-term and imminent precursors should be conducted in the future.

In addition, during the 1999 Chi-Chi earthquake the biological precursors (Chen et al., 2000) occurred near the fault in both short-term and imminent time windows. The observations are very interesting even though the number of data is small and the reliability of data is still debated. The report by Chen et al. (2000) is the first formal scientific literature of biological precursors in Taiwan.

Acknowledgments

I would like to thank Prof. Chien-Chih Chen (NCU) for providing the localities of geoelectric stations. This study was financially supported by the Central Weather Bureau (Grand No.: MOTC-CWB-110-E-01) and Institute of Earth Sciences, Academia Sinica, TAIWAN.

References

Akinaga, Y., M. Hayakawa, J.Y. Liu, K. Yumoto, and K. Hattori, 2001: A precursory ULF signature for the Chi-Chi earthquake in Taiwan. *Nat. Hazards Earth Syst. Sci.*, **1**, 33-36.

Chan, C.H., K.F. Ma, Y.T. Lee, and Y.J. Wang, 2019: Rethinking seismic source model of probabilistic hazard assessment in Taiwan after the 2018 Hualien, Taiwan, earthquake sequence. *Seism. Res. Letts.*, **90**(1), pp1-pp2.

Chan, C.H., Y.M. Wu, T.L. Tseng, T.L. Lin, and C.C. Chen, 2012: Spatial and temporal evolution of *b*-values before large earthquakes in Taiwan. *Tectonophys.*, **532**, 215-222.

Chen, A.T., T. Ouchi, A. Lin, and T. Maruyama, 2000: Phenomena associated with the 1999 Chi-Chi earthquake in Taiwan, possible precursors and after effects. *Terr. Atmos. Ocean. Sci.*, **11**(3), 689-700.

Chen, C.C., J.B. Rundle, J.R. Holliday, K.Z. Nanjo, D.L. Turcotte, S.C. Li, and K.F.

Tiampo, 2005: The 1999 Chi-Chi, Taiwan, earthquake as a typical example of seismic activation and quiescence. *Geophys. Res. Lett.*, **32**, L22315.

Chen, C.H., J.Y. Liu, H.Y. Yen, X. Zeng, and Y.H. Yeh, 2004a: Changes of geomagnetic total field and occurrences of earthquakes in Taiwan. *Terr. Atmos. Ocean. Sci.*, **15**, 361-370.

Chen, C.H., C.H. Wang, S. Wen, T.K. Yeh, J.Y. Liu, and H.Y. Yen, 2011a: Seismo-crust displacements associated with earthquakes (M≥5) during 2006–2009. Taiwan. *J. Natl. Taiwan Mus.*, **6**4, 71-82 (in Chinese with English abstract).

Chen, C.H., J.Y. Liu, W.H. Yang, H.Y. Yen, K. Hattori, C.R. Lin, and Y.H. Yeh, 2009: SMART analysis of geomagnetic data observed in Taiwan. *Phys. Chem. Earth*, **34**, 350-359. http://dx.doi.org/10.1016/j.pce.2008.09.002.

Chen, C.H., T.K. Yeh, J.Y. Liu, C.H. Wang, S. Wen, H.Y. Yen, and S.H. Chang, 2011b: Surface deformation and seismic rebound: implications and applications. *Surv. Geophys.*, **32**, 291-313, http://dx.doi.org/10.1007/s10712-011-9117-3.

Chen, C.H., S. Wen, T.K. Yeh, C.H. Wang, H.Y. Yen, J.Y. Liu, Y. Hobara, and P. Han, 2013a: Observation of surface displacements from GPS analyses before and after the Jiashian earthquake (*M*=6.4) in Taiwan. *J. Asian Earth Sci.*, **62**, 662-671. http://dx.doi.org/10.1016/j.jseaes.2012.11.016.

Chen, C.H., C.H. Wang, S. Wen, T.K. Yeh, C.H. Lin, J.Y. Liu, H.Y. Yen, C. Lin, R.J. Rau, and T.W. Lin, 2013b: Anomalous frequency characteristics of groundwater level before major earthquakes in Taiwan. *Hydrol. Earth Syst. Sci.*, **17**, 1693-1703, doi:10.5194/hess-17-1693-2013.

Chen, C.H., C.C. Tang, K.C. Cheng, C.H. Wang, S. Wen, C.H. Lin, Y.Y. Wen, H. Meng, T.K. Yeh, J.C. Jan, H.Y. Yen, and J.Y. Liu, 2015: Groundwater-strain coupling before the 1999 M_w7.6 Taiwan Chi-Chi earthquake. *J. Hydrol.*, **524**, 378-384.

Chen, H.J., and C.C. Chen, 2016: Testing the correlations between anomalies of statistical indexes of the geoelectric system and earthquakes. *Nat. Hazards*, **84**, 877-895, doi:10.1007/s11069-016-2460-4.

Chen, H.J., C.C. Chen, G. Ouillon, and D. Sornette, 2017: Using geoelectric field skewness and kurtosis to forecast the 2016/2/6 M_L6.6 Meinong, Taiwan, earthquake. *Terr. Atmos. Ocean. Sci.*, **28**, 745-761, doi:10.3319/TAO.2016.11.01.01.

Chen, K.C., and J.H. Wang, 1984: On the study of 10 May, 1983 Taipingshan, Taiwan, earthquake sequence. *Bull. Inst. Earth Sci., Acad. Sin., ROC*, **4**, 1-28.

Chen, K.C., J.H. Wang, and Y.L. Yeh, 1990: Premonitory phenomena of a moderate Taiwan earthquake. *Terr. Atmos. Ocean. Sci.*, **1**, 1-21.

Chuo, Y.J., J.Y. Liu, S.A. Pulinets, and Y.I. Chen, 2002: Ionospheric perturbations prior to Chi-Chi and Chia-Yi earthquakes. *J. Geodyn.***, 33**, 509-517.

Chyi, L.L., C.Y. Chou, F.T. Yang, and C.H. Chen, 2001: Continuous radon measurements in faults and earthquake precursor pattern recognition. *Western Pacific Earth Sci.*, **1**(2), 43-72.

Chyi, L.L., T.J. Quick, F.T. Yang, and C.H. Chen, 2005: Soil gas radon spectra and earthquakes. *Terr. Atmos. Ocean Sci.*, **16**, 763-774.

Fu, C.C., and L.C. Lee**,** 2018: Continuous monitoring of fluid and gas geochemistry for seismic study in Taiwan. In: Ouzounov, D., S. Pulinets, K. Hattori, and P.

Taylor, (Eds.), Pre-Earthquake Processes: A Multidisciplinary Approach to Earthquake Prediction Studies. *AGU Geophys. Monog. Series, **234**,* 199-218.

Fu, C.C., L.C. Lee, D. Ouzounov, and J.C. Jan, 2020: Earth's Outgoing longwave radiation variability prior to $M \geq 6.0$ earthquakes in the Taiwan area during 2009–2019. *Front. Earth Sci.*, **8**:364. doi:10.3389/feart.2020.00364

Fu, C.C., T.F. Yang, V. Walia, T.K. Liu, S.J. Lin, C.H. Chen, and C.S. Hou, 2009: Variations of soil-gas composition around the active Chihshang Fault in a plate suture zone, eastern Taiwan. *Radiat. Meas.*, **44**, 940-944.

Fu, C.C., P.K. Wang, L.C. Lee, C.H. Lin, W.Y. Chang, G. Giuliani, and D. Ouzounov, 2015: Temporal variation of gamma rays as a possible precursor of earthquake in the Longitudinal Valley of eastern Taiwan. *J. Asian Earth Sci.*, **114**(2), 362-372.

Fu, C.C. T.F. Yang, C.H. Chen, L.C. Lee, Y.M. Wu, T.K. Liu, and V. Walia, A. Kumar, and T.H. Lai, 2017a: Spatial and temporal anomalies of soil gas in northern Taiwan and its tectonic andseismic implications. *J. Asian Earth Sci.*, **149**, 64-77.

Fu, C.C., T.F. Yang, M.C. Tsai, L.C. Lee, T.K. Liu, V. Walia, C.H. Chen, W.Y. Chang, A. Kumar, and T.H. Lai, 2017b: Exploring the relationship between soil degassing and seismic activity by continuous radon monitoring in the Longitudinal Valley of eastern Taiwan. *Chem. Geol.*, **469**, 163-175.

Fu, C.C., V. Walia, T.F. Yang, L.C. Lee, T.K. Liu, C.H. Chen, A. Kumar, T.H. Lai, and K.L. Wen, 2017c: Preseismic anomalies in soil-gas radon associated with 2016 M6.6 Meinong earthquake, Southern Taiwan. *Terr. Atmos. Ocean. Sci.*, **28**(5), 787-798.

Fu, C.C., L.C. Lee, T.F. Yang, C.H. Lin, C.H. Chen, V. Walia, T.K. Liu, D. Ouzounov, G. Giuliani, T.H. Lai, and P.K. Wang, 2019: Gamma ray and radon anomalies in Northern Taiwan as a possible pre-earthquake indicator around the plate boundary. *Geofluids*, **2019**, Article ID 4734513, 14 pages, doi:10.1155/ 2019/4734513.

Hsu, Y.J., L. Rivera, Y.M. Wu, C.H. Chang, and H. Kanamori, 2010: Spatial heterogeneity of tectonic stress and friction in the crust: new evidence from earthquake focal mechanisms in Taiwan. *Geophys. J. Int.*, **182**, 329-342.

Kamogawa, M., J.Y. Liu, H. Fujiwara, Y.J. Chuo, Y.B. Tsai, K. Hattori, T. Nagao, S. Uyeda, and Y.H. Ohtsuki, 2004: Atmospheric field variations before the March 31, 2002 *M*6.8 earthquake in Taiwan. *Terr. Atmos. Ocean. Sci.*, **15**(3), 397-412.

Kawamura, M., and C.C. Chen, 2013: Precursory change in seismicity revealed by the Epidemic-Type Aftershock-Sequences model: a case study of the 1999 Chi-Chi, Taiwan, earthquake. *Tectonophys.*, **592**, 141-149.

Kawamura M., C.C. Chen, and Y.M. Wu, 2014: Seismicity change revealed by ETAS, PI, and Z-value methods: a case study of the 2013 Nantou, Taiwan, earthquake. *Tectonophys.*, **634**, 139-155.

Kuo, T., W. Chen, and C. Ho, 2018: Anomalous decrease in groundwater radon before 2016 M_w6.4 Meinong earthquake and its application in Taiwan. *Appl. Radiat. Isot.*, **136,** 68-72.

Kuo, T., K. Fan, H. Kuochen, and W. Chen, 2006a: A mechanism for anomalous decline in radon precursory to an earthquake. *Ground Water*, **44**, 642-647, doi:10. 1111/j.1745-6584.2006.00219.x.

Kuo, T., H. Kuochen, C. Ho, and W. Chen, 2017: A stress condition in aquifer rock for detecting anomalous radon decline precursory to an earthquake. *Pure Appl. Geophys.,* **174,** 1291-1301.

Kuo, T., W. Chen, C. Ho, H. Kuochen, and C. Chiang, 2019: In-situ radon volatilization in an undrained fractured aquifer. *Proc., 44th Workshop Geothermal Reservoir Engineer.,* Stanford Univ., Stanford, California, Feb. 11- 13.

Kuo, T., H. Kuochen, C. Ho, and W. Chen, 2017: A stress condition in aquifer rock for detecting anomalous radon decline precursory to an earthquake. *Pure Appl. Geophys.*, **174**, 1291-1301.

Kuo, T., W. Chen, C. Ho, H. Kuochen, and C. Chiang, 2019: In-situ radon volatilization in an undrained fractured aquifer. *Proc., 44th Workshop Geothermal Reservoir Engineer.,* Stanford Univ., Stanford, California, Feb. 11- 13.

Kuo, T., K. Fan, H. Kuochen, Y. Han, H. Chu, and Y. Lee, 2006b: Anomalous decreases in groundwater radon before the Taiwan *M*6.8 Chengkung earthquake. *J. Environ. Radio.*, **88**, 101-106.

Kuo, T., C. Lin, G. Chang, K. Fan, W. Cheng, and C. Lewis, 2010: Estimation of aseismic crustal strain using radon precursors of the 2003 M6.8, 2006 M6.1, and 2008 *M*5.0 earthquakes in eastern Taiwan. *Nat. Hazards*, **53**, 219-228.

Lee, C.P., and Y.B. Tsai, 2004: Variations of *P*-wave travel-time residuals before and after the 1999 Chi-Chi, Taiwan, earthquake. *Bull. Seism. Soc. Am.*, **94**(6), 2348-2365.

Lin, C.H., 2009: Foreshock characteristics in Taiwan: Potential earthquake warning. *J. Asian Earth Sci.*, **34**, 655-662. doi:10.1016/j.jseaes.2008.09.006.

Lin, C.H., 2010: Temporal *b*-value variations throughout a seismic faulting process: the 2008 Taoyuan earthquake in Taiwan. *Terr. Atmos. Ocean. Sci.*, **21**(2), 229-234. doi:10.3319/TAO.2009.02.09.01(T).

Lin, C.H., 2012: The possible observation of slow slip events priori the occurrence of the 1999 Chi-Chi earthquake. *Terr. Atmos. Ocean. Sci.*, **23**(2), 145-159. dx:doi. org/10.3319/TAO.2011.09.23.01(T).

Liu, J.Y., K. Hattori, and Y.J. Chen, 2018: Application of total electron content derived from the global navigation satellite system for detecting earthquake precursors. In: Ouzounov, D., S. Pulinets, K. Hattori, and P. Taylor, (Eds.), *Pre-Earthquake Processes: A Multidisciplinary Approach to Earthquake Prediction Studies, Geophys. Monog. Series*, **234**, 305-317.

Liu, J.Y., H.F. Tsai, and T.K. Jung, 1996: Total electron content obtained by using the global positioning system. *Terr. Atmos. Ocean. Sci.*, **7**, 107-117.

Liu, J.Y., Y.I. Chen, Y.J. Chuo, and H.F. Tsai, 2001: Variations of ionospheric total electron content during the Chi-Chi earthquake. *Geophys. Res. Lett.*, **28**, 1381-1386.

Liu, J.Y., Y.I. Chen, H.K. Jhuang, and Y.H. Lin, 2004a: Ionospheric foF2 and TEC anomalous days associated with *M*≥5.0 earthquakes in Taiwan during 1997– 1999. *Terr. Atmos. Ocean. Sci.,* **15**, 371-383.

Liu, J.Y., Y.I. Chen, S.A. Pulinets, Y.B. Tsai, and Y.J. Chuo, 2000: Seismo-ionospheric signatures prior to *M*≥6 Taiwan earthquakes. *Geophys. Res. Lett.*, **27**, 3113-3116.

Liu, J.Y., Y.I. Chen, C.H. Huang, Y.Y. Ho, and C.H. Chen, 2015: A statistical study of lightning activities and *M*≥5.0 earthquakes in Taiwan during 1993–2004. *Surv. Geophys.*, **36**, 851-859. doi:10.1007/s10712-015-9342-2.

Liu, J.Y., C.H. Chen, Y.I. Chen, H.Y. Yen, K. Hattori, and K. Yumoto, 2006:

Seismo-geomagnetic anomalies and $M \geq 5.0$ earthquakes observed in Taiwan during 1988−2001. *Phys. Chem. Earth*, **31**, 215-222.

Liu, J.Y., Y.J. Chuo, S.J. Shan, Y.B. Tsai, Y.I. Chen, S.A. Pulinets, and S.B. Yu, 2004b: Pre-earthquake ionospheric anomalies registered by continuous GPS TEC measurements. *Ann. Geophys*., **22**, 1585-1593.

Liu, J.Y., S.W. Chen, Y.C. Chen, H.Y. Yen, C.P. Chang, W.Y. Chang, L.C. Tsai, C.H. Chen, and W.H. Yang, 2008: Seismo-ionospheric precursors of the 26 December 2006 M7.0 Pingtung earthquake doublet. *Terr. Atmos. Ocean. Sci.*, **19**, 751-759, doi:10.3319/TAO.2008.19.6.751(PT).

Liu, K.K., Y.B. Tsai, Y.H. Yeh, T.F. Yui, and T.L. Teng, 1984: Variations of radon content in ground waters and possible correlation with seismic activities in northern Taiwan. *Pure Appl. Geophys.*, **122**, 231-244.

Liu, S.H., K.H. Sun, S.H. Huang, and P.S. Wen, 1983: A sensitive method for radon measurement. *Nucl. Sci.*, **20**(4), 189-196. (in Chinese)

Ma, K.F., C.T., Lee, Y.B., Tsai, T.C. Shin, and J. Mori, 1999: The Chi-Chi, Taiwan, earthquake: Large surface displacements on an inland thrust fault. *Eos, Transaction, AGU*, **80**, 605-611.

Meyer, S.L., 1975: *Data Analysis for Scientists and Engineers*. John Wiley & Dons, New York, pp. 280-281.

Minnehan, C., 2015: Newly discovered properties of elusive gamma ray flashes, *Eos*, **96**, doi:10.1029/2015EO032431..

Ohta, K., K. Umeda, N. Watanabe, and M. Hayakawa, 2001: ULF/ELF emission observed in Japan, possible associated with the Chi-Chi earthquake in Taiwan. *Nat. Hazards Earth Syst. Sci.*, **1**, 37-42.

Ouzounov, D., S. Pulinets, M. Kafatos, and P. Taylor, 2018: Thermal radiation anomalies associated with major earthquakes. In: Ouzounov, D., S. Pulinets, K. Hattori, and P. Taylor, (Eds.), *Pre-Earthquake Processes: A Multidisciplinary Approach to Earthquake Prediction Studies,* Geophy. Monog. Series**, 234**, 259-274, doi:10.1002/9781119156949.ch15.

Pulinets, S.A., and M.A. Dunajeck, 2007: Specific variations of air temperature and relative humidity around the time of Michoacan earthquake M8.1 September 19, 1985 as a possible indicator of interaction between tectonic plates. *Tectonophys*., **431**, 221-230. doi:10.1016/j.tecto.2006.05.044

Pulinets, S.A., and D. Ouzounov, 2011: Lithosphere-Atmosphere-Ionosphere Coupling (LAIC) model−An unified concept for earthquake precursors validation. *J. Asian Earth Sci.*, **41**, 371-382. doi:10.1016/j.jseaes.2010.03.00.

Shin, T.C., 1992: The calculation of local magnitude from the simulated Wood-Anderson seismograms of the short-period seismograms in the Taiwan area. *Terr. Atmos. Ocean. Sci.*, **4**(2), 155-170.

Shin, T.C., and T.L. Teng, 2001: An overview of the 1999 Chi-Chi, Taiwan, earthquake. *Bull. Seism. Soc. Am.*, **91**, 895-913.

Shrivastava, A., 2014: Are pre-seismic ULF electromagnetic emissions considered as a reliable diagnostics for earthquake prediction?. *Current Sci.*, **107**(4), 596-600.

Song, S.R., W.Y. Ku, Y.L. Chen, Y.C. Lin, C.M. Liu, L.W. Kuo, T.F. Yang, and H.J. Lo, 2003: Groundwater chemical anomaly before and after the Chi-Chi earthquake in Taiwan. *Terr. Atmos. Ocean. Sci.*, **14**, 311-320.

Song, S.R., Y.L. Chen, C.M. Liu, W.Y. Ku, H.F. Chen, Y.J. Liu, L.W. Kuo, T.F. Yang, C.H. Chen, T.K. Liu, and M. Lee, 2005: Hydrochemical changes in spring waters in Taiwan: Implications for evaluating sites for earthquake precursory monitoring. *Terr. Atmos. Ocean. Sci.*, **16**, 745-762.

Song, S.R., W.Y. Ku, Y.L. Chen, C.M. Liu, H.F. Chen, P.S. Chan, Y.G. Chen, T.F. Yang, C.H. Chen, T.K. Liu, and M. Lee, 2006: Hydrogeochemical anomalies in the springs of the Chiayi area in West-central Taiwan as possible precursors to earthquakes. *Pure Appl. Geophys.*, **163**, 675-691, DOI:10.1007/s00024-006-0046-x.

Tsai, Y.B., J.Y. Liu, T.C. Shin, H.Y. Yen, and C.H. Chen, 2018: Multidisciplinary earthquake prediction studies in Taiwan: A review and future prospects. In: Ouzounov, D., S. Pulinets, K. Hattori, and P. Taylor, (Eds.), *Pre-Earthquake Processes: A Multidisciplinary Approach to Earthquake Prediction Studies*, Geophy. Monog. Series**, 234**, 41-66.

Tsai, Y.B., T.L. Teng, Y.H. Yeh, S.B. Yu, K.K. Liu, and J.H. Wang, 1983: Status of earthquake prediction research in Taiwan, ROC. *Bull. Inst. Earth Sci., Acad. Sin., ROC*, **3**, 1-26.

Tsai, Y.B., J.Y. Liu, K.F. Ma, H.Y. Yen, K.S. Chen, Y.I. Chen, and C.P. Lee, 2004: Preliminary results of the iSTEP Program on integrated search for Taiwan earthquake precursors. *Terr. Atoms. Ocean Sci.*, **15**(3), 345-562.

Tsai, Y.B., J.Y. Liu, K.F. Ma, H.Y. Yen, K.S. Chen, Y.I. Chen, and C.P. Lee, 2006: Precursory phenomena associated with the 1999 Chi-Chi earthquake in Taiwan as identified under the iSTEP program. *Phys. Chem. Earth*, **31**, 365-377.

Walia, V., S.J. Lin, W.L. Hong, C.C. Fu, T.F. Yang, K.L. Wen, and C.H. Chen, 2009: Continuous temporal soil-gas composition variation for earthquake precursory studies along Hsincheng and Hsinhua faults in Taiwan. *Radiat. Meas.*, **44**, 934-939.

Walia, V., T.F. Yang, S.J. Lin, A. Kumar, C.C. Fu, J.M. Chiu, H.H. Chang, K.L. Wen, and C.H. Chen, 2013: Temporal variation of soil gas compositions for earthquake surveillance in Taiwan. *Radiat. Meas.*, **50**, 154-159.

Wang, C.H., C.Y. Wang, C.H. Kuo, and W.F. Chen, 2005: Some isotopic and hydrological changes associated with the 1999 Chi-Chi earthquake, Taiwan. *The Island Arc*, **14**, 37-54.

Wang, J.H., 1988: Temporal change of duration ratios for foreshocks and aftershocks of a moderate Taiwan earthquake. *Proc. Geol. Soc. China*, **31**, 99-110.

Wang, J.H., 1989: The Taiwan Telemetered Seismographic Network. *Phys. Earth Planet. Inter.*, **58**, 9-18.

Wang, J.H., 1992: Magnitude scales and their relations for Taiwan earthquakes: A review. *Terr. Atmos. Ocean. Sci.*, **3**, 449-468.

Wang, J. H., 1998: Studies of earthquake seismology in Taiwan during the 1897−1996 period. *J. Geol. Soc. China*, **41**, 291-336.

Wang, J.H., 2016: A mechanism causing b-value anomalies prior to a mainshock. *Bull. Seism. Soc. Am.*, **106**(1), 1663-1671, doi:10.1785/0120150335.

Wang, J.H., 2021: A review on precursors of the 1999 M_w7.6 Chi-Chi, Taiwan, earthquake. *Terr. Atmos. Ocean. Sci.*, **32**(3), 275-304, doi:10.3319/TAO.2021.03.24.0.

Wang, J.H., and S. Miyamura, 1990: Comparison of several instrumentally determined magnitude scales for Taiwan earthquakes (1900−1978). *Proc. Geol. Soc. China*, **33**, 89-109.

Wang, J.H., K.C. Chen, P.L. Leu, and C.H. Chang, 2015: *b*-value observations in Taiwan: A review. *Terr. Atmos. Ocean. Sci.*, **26**(5), 475-492, doi:10.3319/TAO. 2015.04. 28.01(T).

Wang, J.H., K.C. Chen, P.L. Leu, and C.H. Chang, 2016: Precursor times of abnormal *b*-values prior to earthquakes. *J. Seismol.*, **20**(3), 905-919, DOI:10.1007/s10950-016-9567-7.

Wang, J.H., C.Y. Wang, Q.C. Song, T.C. Shin, S.B. Yu, C.F. Shieh, K.L. Wen, S.L. Chung, M. Lee, K.M. Kuo, K.C. Chang, and S.L. Chung (Eds.), 2005: *The 921 Chi-Chi Major Earthquake*, Office of Inter-Ministry Science & Technology Program for Earthquake and Active-fault Research, National Science Council, 582pp. (in Chinese)

Wen, S., C.H. Chen, Y.J. Ji, Y.Z. Chang, and C.H. Chen, 2015: The seismogenic deformation and Q_p temporal variation before the M6.2 Mingjen earthquake, Taiwan. *J. Asian Earth Sci.*, **114**, 403-413, http://dx.doi.org/10.1016/j.jseaes. 2015.06.011.

Wen, S., C.H. Chen, H.Y. Yen, T.K. Yeh, J.Y. Liu, K. Katsumi, P. Han, C.H. Wang, and T.C. Shin, 2012: Magnetic storm free ULF analysis in relation with earthquakes in Taiwan. *Nat. Hazards Earth Syst. Sci.*, **12**, 1747-1754. http://dx.doi.org/10.5194/ nhess-12-1747-2012.

Wen, Y.Y., and C.C. Chen, 2017: Seismicity variations prior to the 2016 M_L6.6 Meinong, Taiwan earthquake. *Terr. Atmos. Ocean. Sci.*, **28**(5), 739-744, doi:10. 3319/TAO.2016.12.05.01.

Wu, F.T., 1975: Gas well pressure fluctuations and earthquakes. *Nature*, **257**, 661-663.

Wu, F.T., and C.C. Feng, 1975: Gas well pressure fluctuation as an earthquake precursor. *Petrol. Geol. Taiwan*, **12**, 141-148.

Wu, K., M. Yue, H. Wu, X. Cao, H. Chen, W. Huang, K. Tian, and S. Lu, 1976: Certain characteristics of Haicheng earthquake (*M*=7.3) sequence. *Acta Geophys. Sinica*, **19**, 109-117.

Wu, Y.H., and C.C. Chen, 2007: Seismic reversal pattern for the 1999 Chi-Chi, Taiwan, M_w7.6 earthquake. *Tectonophys.*, **429**, 125-132, doi:10.1016/j.tecto.2006.09.015.

Wu, Y.H., C.C. Chen, and J.B. Rundle, 2008: Precursory seismic activation of the Pingtung (Taiwan) offshore doublet earthquakes on December 26, 2006: a pattern informatics analysis. *Terr. Atmos. Ocean. Sci.*, **19**(6), 743-749.

Wu, Y.H., C.c. Chen, J.B. Rundle, and J.H. Wang, 2012: Regional dependence of seismic migration pattern. *Terr. Atmos. Ocean. Sci.*, **23**(2), 161-170.

Wu, Y.M., and L.Y. Chiao, 2006: Seismic quiescence before the 1999 Chi-Chi, Taiwan M_w7.6 earthquake. *Bull. Seism. Soc. Am.*, **96**, 321-327.

Wu, Y.M., Y.J. Hsu, C.H. Chang, L.S.y. Teng, and M. Nakamura, 2010: Temporal and spatial variation of stress field in Taiwan from 1991 to 2007: Insights from comprehensive first motion focal mechanism catalog. *Earth Planet. Sci. Letts.*, **298**, 306-316.

Xia, Y., J.Y. Liu, X. Cui, J. Li, W. Chen, and C. Liu, 2011: Abnormal infrasound signals before 92 $M \geq 7.0$ worldwide earthquakes during 2002–2008. *J. Asian Earth*

Sci., **41**, 434-441, doi:10.1016/j.jseaes.2010.04.015.

Yang, T.F., V. Walia, L.L. Chyi, C.C. Fu, C.H. Chen, T.K. Liu, S.R. Song, C.Y. Lee, and M. Lee, 2005: Variations of soil radon and thoron concentrations in a fault zone and prospective earthquakes in SW Taiwan. *Radiat. Meas.*, **40**, 496-502.

Yang, T.F., C.C. Fu, V. Walia, C.H. Chen, L.L. Chyi, T.K. Liu, S.R. Song, M. Lee, C.W. Lin, and C.C. Lin, 2006: Seismo-geochemical variations in SW Taiwan: multi-parameter automatic gas monitoring results. *Pure Appl. Geophys.*, **163**(4), 693-709.

Yeh, Y.H., Y.B. Tsai, and T.L. Teng, 1981: Investigations of geomagnetic total intensity in Taiwan from 1979 to 1981. *Bull. Inst. Earth Sci., Acad. Sin.*, **1**, 157-188.

Yen, H.Y., C.H., Chen, and J.Y. Liu, 2004: Geomagnetic fluctuations during the 1999 Chi-Chi earthquake in Taiwan. *Earth Planets Space*, **56**, 39-45.

Yu, G.K., and B.J. Mitchell, 1988: A study of the non-tectonic influences on groundwater level fluctuations. *Proc. Geol. Soc. China*, **31**, 111-124.

Table 1. Precursory times, *T*, of long-term, intermediate-term, short-term, and imminent precursors for earthquakes occurring in Taiwan. In the table, M_L is the local magnitude determined by the CWB.

Types	Precursors	*T*	Remarks
Long-term	Mechanical Precursors		
	Stress Orientation Changes	9 years (M_L=7.3)	Wu et al. (2010); Hsu et al. (2010)
	Changes of seismicity patterns	3−6 years (M_L=7.1, 7.3)	Wu and Chen (2007); Wu et al. (2008)
	Variation in *b*-values	3−6 years (M_L=6.4−7.3)	Chen and Wang (1984); Chen et al. (1990);
	Changes in *P*-wave travel-time residual	6 years (M_L=7.3)	Tsai et al. (2006); Wu et al. (2008)
			Lee and Tsai (2004)
Intermediate-term	Mechanical Precursors		
	Surface deformations	3 years (M_L=7.3)	Tsai et al. (2006)
	Seismic quiescence	9−21 months (M_L=7.1, 7.3)	Wu and Chen (2007); Wu and Chiao (2006); Kawamura and Chen (2013, 2014)
	Groundwater level changes	250 days (M_L=7.3)	Chen et al. (2013b, 2015)
	Foreruners	8 months (M_L=6.4)	Chen and Wang (1984); Chen et al. (1990)
	EM Precursors		
	Geomagnetic annual changing rate	2 years (M_L=7.3)	Chen et al. (2004)
	Geochemical precursors	7 months (M_L=7.3)	Song et al. (2003)
Short-term	Mechanical Precursors		
	Crustal extension rate	4 months (M_L=6.4)	Fu et al. (2017b)
	Aseismic crustal strain	2.5−3 months (M_L=5.4−6.4)	Kuo et al. (2010)
	Variation in b-value	1 month (M_L=5.2)	Lin (2010)
	Variation in Q_p	2 months (M_L=6.2)	Wen et al. (2015)
	Groundwater level changes	10 days (M_L=6.2)	Yu and Mitchell (1988)
	Subsurface deformations	≤8 days (M_L≥5.0)	Chen et al. (2011b, 2013a)
	Gas well pressure change	9 days (M_L=7.3)	Wu (1975); Wu and Feng (1975)

	EM Precursor		
	ULF signals		
	Geomagnetic anomalies	2 months (M_L=7.3)	Akinaga et al. (2001)
		1.1 months (M_L=7.3)	Yen et al. (2004)
		1 month (M_L≥5.0)	Liu et al. (2006)
		10 days (M_L≥4.0)	Chen et al. (2009)
	Geoelectric field anomalies	5−80 days (M_L≥5.0)	Chen and Chen (2016, 2017)
	Thermal infrared radiation	1−25 days (M_L=**6.0**−7.3)	Pulinets and Dunajeck (2007); Pulinets and Ouzounov (2011); Genzano et al. (2015); Fu et al. (2020)
	Lightning	1−30 days (M_L≥5.0)	Liu et al (2015)
	Geochemical precursor	0.1−28.1 days (M_L=4.1−6.7)	Yang et al. (2006); Walia et al. (2013)
	Chemical compositions	54−171 days (M_L=5.0−6.4)	Kuo et al. (2006a,b, 2010, 2017, 2018, 2019)
	Radon concentration	21 and 60 days (M_L=5.9 and 6.4)	Fu et al. (2017b)
		4−51 days (M_L=4.6−5.8)	Liu et al. (1984)
		1−23 days (M_L≥4.0)	Fu et al. (2019)
		0.2−17.4 days (M_L=3.2−6.8)	Fu et al. (2017a)
		0.49−14.2 days (M_L=3.7−6.7)	Chyi et al. (2001, 2005); Yang et al. (2005);
			Fu et al. (2017c)
			Fu et al. (2009)
	γ-ray emissions	few days	Fu et al. (2015, 2019)
		2−20 days (M_L=2.8−6.7)	
	Animal anomalies (for some animals)	>7 days (M_L=7.3)	Chen et al. (2000)
Imminent	Mechanical precursors		
	Foreshocks	5 days (M_L=5.0−6.5)	Lin (2009)
		4 days (M_L=6.4)	Chen and Wang (1984); Chen et al. (1984)
		2 days (M_L=6.2)	Chan et al. (2019)
		0.3−few hours (M_L=5.2)	Lin (2012)
	Slow slip	5 days (M_L=7.3)	Lin (2012)
	Infrasound	3 days (M_L=7.3)	Xia et al. (2011)
	Duration ratio	4 days (M_L=6.4)	Wang (1988)
	EM precursors		
	TEC and f_oF_2	3−5 days (M_L=6.0−7.3)	Liu et al. (2001,2008, 2004a,b); Chuo et al. (2002)
	Geomagnetic anomalies	few days (M_L≥5.0)	Wen et al. (2012)
	Lightning	4 days (M_L=7.3)	Tsai et al. (2006); Liu et al.

	Atmospheric electric field ULF/ELF signals Earthquake light	2−4 days (M_L=6.8) 4 hours (M_L=7.3) few hours (M_L=7.3)	(2015) Kamogawa et al. (2004) Ohta et al. (2001) Chen et al. (2000)
	Geochemical precursor Chemical compositions	1− 5 days (M_L≥5.0)	Song et al. (2006); Walia et al. (2009)
	Animal anomalies (for some animals)	≤7 days (M_L=7.3)	Chen et al. (2000)

Table 2. The precursory times of anomalies of different animals before the 1999 Chi-Chi earthquake reported by Chen et al. (2000). (after Wang, 2021b)

Animals	Weeks	Days	Hours	Time Window
Ants	1 and 8−10	1 and 2−3		Short-term
Cicada	4−6			Short-term
Diplopods	1−2	1−2		Short-term
Earthwarms	1−2	1		Short-term
Fishes	1−2	1		Short-term
Birds	1	1−2		Imminent
Roach		3		Imminent
Dogs		1	1 and a few	Imminent
Cats		1		Imminent
Turtles		1		Imminent
Palm civet-like			a few	Imminent
Snakes			2	Imminent

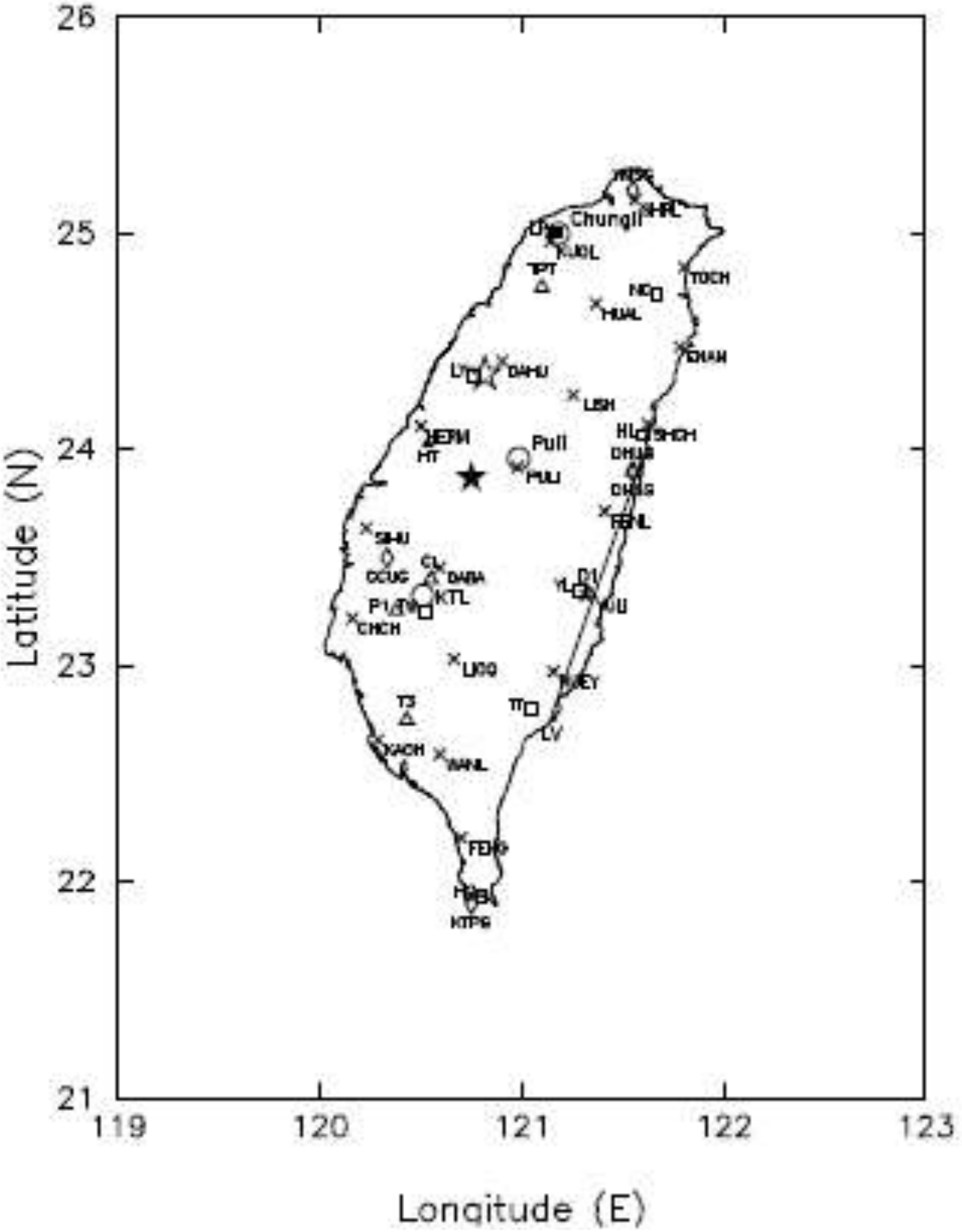

Figure 1. The figure shows the epicenter (in an open star) of the 1935 M_S7.2 Hsinchu-Taichung earthquake and that (in a solid star) of the 1999 M_w7.6 Chi-Chi earthquake. The geomagnetic LP station is denoted by a solid square and those at other seven stations are displayed by open squares. The groundwater HP station is shown by a solid triangle. The geochemical monitoring stations are shown by open triangles. The γ-ray monitoring stations are shown by open diamond symbols. The geoelectric field monitoring stations are shown by crosses. Three geographic places, i.e., Chungli, Puli, and Kuantzeling (KTL), are displayed by larger-sized open circles. A thin line marked with 'LV' in eastern Taiwan represents the Longitudinal Valley.

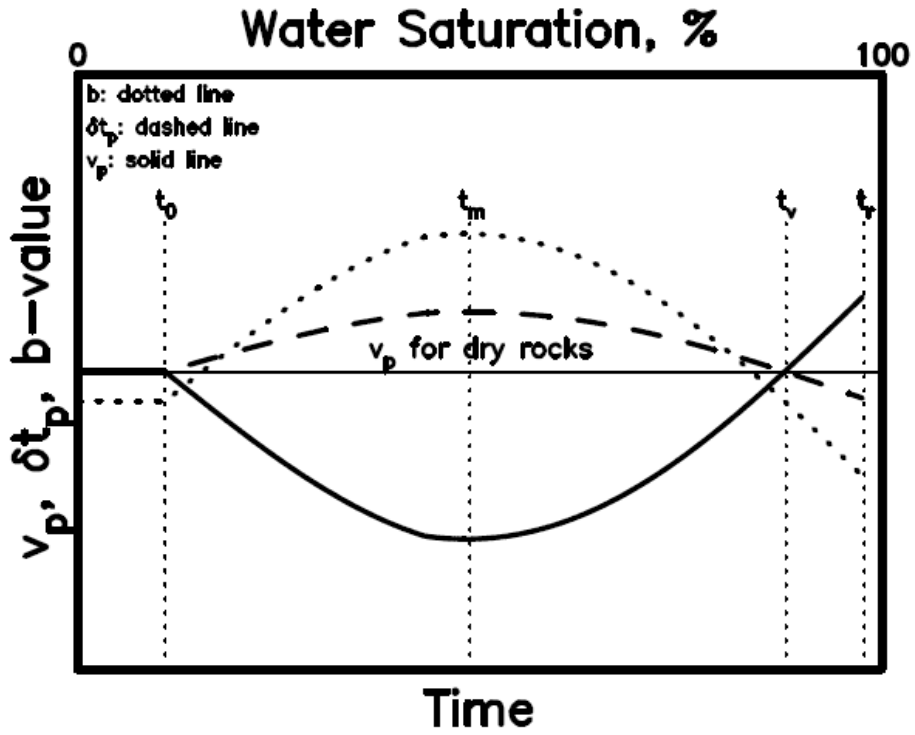

Figure 2. The temporal variations in water saturation, v_p, *P*-wave travel-time residue, δt_p, and *b*-value. The horizontal line denotes the v_p for dry rocks. The solid line, dashed line, and dotted line represent v_p, δt_p, and *b*-value, respectively. (modified from Wang, 2016)

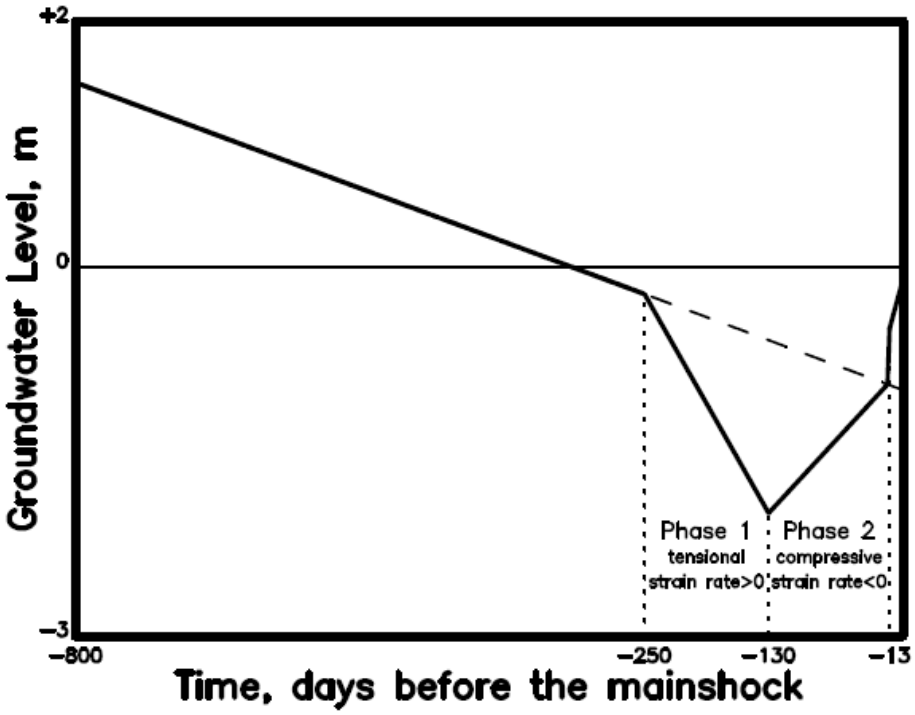

Figure 3. A temporal variation of groundwater level after air-pressure correction in the third aquifer at the HT station from July 1, 1997 to September 21, 1999. The dash line suggests that a decrease tendency of about -0.7 m/yr in the groundwater level. Phase 1 and Phase 2 represent, respectively, the fall and rise in the groundwater level prior to the Chi-Chi earthquake. (after Wang, 2021)

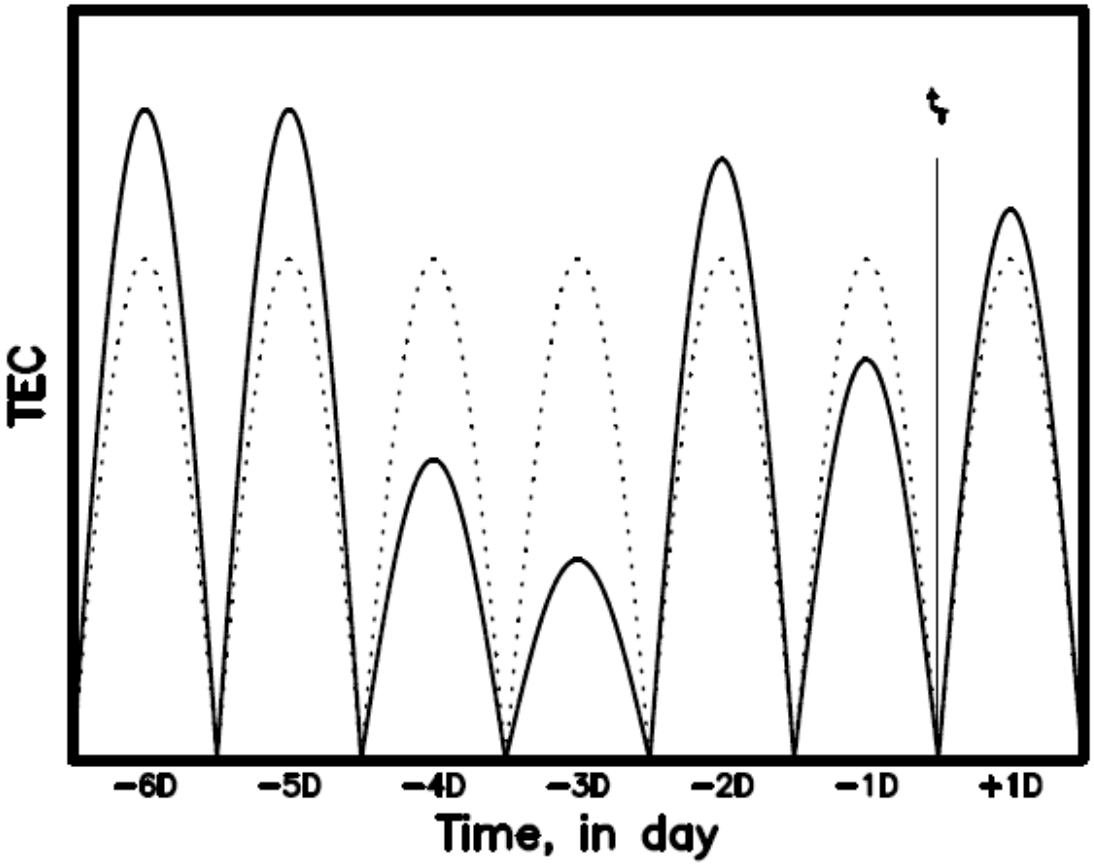

Figure 4. A simplified figure to show the time variations in TEC anomalies (in a solid line) and the reference data (in a dotted line) from six days before and one day after the mainshock, which occurred at time t_r, observed by Liu et al. (2001). (modified from Wang, 2021)